PHILOSOPHICAL TRANSACTIONS OF THE ROYAL SOCIETY A MATHEMATICAL, PHYSICAL & ENGINEERING SCIENCES

High-Temperature Properties of Silicate Liquids: Applications to the Equilibration and Ascent of Basic Magma [and Discussion]

I. S. E. Carmichael, J. Nicholls, F. J. Spera, B. J. Wood, S. A. Nelson, D. K. Bailey, J. V. Smith and M. J. O'Hara

Phil. Trans. R. Soc. Lond. A 1977 **286**, 373-431
doi: 10.1098/rsta.1977.0124

Phil. Trans. R. Soc. Lond. A. **286**, 373–431 (1977) [373]
Printed in Great Britain

High-temperature properties of silicate liquids: applications to the equilibration and ascent of basic magma

By I. S. E. Carmichael, J. Nicholls,† F. J. Spera, B. J. Wood,‡ and S. A. Nelson
Department of Geology and Geophysics, University of California, Berkeley, California 94720, *U.S.A.*
† *Department of Geology, University of Calgary, Alberta, Canada*
‡ *Department of Geology, University of Manchester*

High-temperature heat content measurements have been made on a series of silicate liquids, which in conjunction with published data, are used to derive partial molar heat capacities of SiO_2, TiO_2, Al_2O_3, Fe_2O_3, FeO, MgO, CaO, Na_2O and K_2O in the temperature range 1200–1650 K. Only Fe_2O_3 appears to be compositionally dependent, and the best evidence suggests that there is no excess heat capacity ($\bar{C}_{p,i} = C_p^\circ$). In combination with calorimetric data and the effect of pressure on the fusion temperature of solid compounds, a consistent set of enthalpy, entropy and volume data have been derived for the liquid compounds $CaMgSi_2O_6$, $NaAlSi_3O_8$, $KAlSi_3O_8$, Fe_2SiO_4 and TiO_2.

By using activities (relative to a liquid standard state) calculated at 1 bar for a range of lavas, the equilibration pressures and temperatures of lavas with a lherzolitic source material are calculated, and for basanites indicate 22–26 kbar and 1310–1360 °C. The regular solution formulation used in these calculations gives an estimated error of 40 °C and 5.7 kbar when compared to experimental equilibria. It is suggested that one of the thermal responses of ascending alkali basalt magma to engulfing cooler lherzolitic nodules could be the precipitation of megacrysts, and the calculated equilibration pressures and temperatures of the megacryst assemblage (16–20 kbar, 1220–1240 °C) is in accord with this.

The importance of viewing volcanic eruptions as the last stage in a sequence of chemical and thermomechanical instabilities is pointed out. Equations expressing the conservation of energy, mass and momentum on a macroscopic scale are given. The high Rayleigh numbers appropriate for even the relatively small magma volumes of erupted alkali basalts indicate turbulent flow-régimes with characteristic thermal convection velocities of the same order as nodule settling velocities. There is a significant partial melting effect in the mantle surrounding an ascending diapir if buoyancy is a significant force acting to drive the magma upwards. The effect of latent heat and convective heat losses on the thermal budget of a rising diapir has been calculated and shows the assumption of adiabaticity is often unwarranted – even for rapidly ascending magma. Finally, mass transfer rates due to convective diffusion have been calculated for all the major components in a basic silicate liquid. Integral mass exchange depends inversely on the ascent rate and is quite small for the rapidly ascending alkalic basalts.

Introduction

The liquid state is the essence of igneous petrogenesis, which broadly stated may be conceived of as the generation, ascent and cooling of a silicate liquid. Despite this central rôle, little is known of the thermodynamic properties of silicate liquids covering the range of composition of those found in nature. This paper, therefore, falls into three parts, the first dealing with measurements of the high temperature heat contents of silicate liquids, from which partial

molar heat capacities of the most abundant oxide components found in natural silicate liquids can be obtained. These heat capacity values can in turn be used to derive an internally consistent set of volume, enthalpy and entropy data for liquid silicate compounds based on published information on the effect of pressure on the fusion temperature of these compounds.

In the second part of the paper, these thermodynamic data are applied to naturally occurring silicate liquids or magmas, in order to calculate the equilibration conditions with a stipulated source material in the Earth's mantle. The ascent of basaltic magma, particularly through the upper mantle and lower crust is then considered in the third part, as an example of a segment of magma history which is all too often ignored in many of today's popular theories of magma genesis. One example will suffice: Mysen & Boettcher (1975) have suggested that almost the whole range of andesitic and basic magmas can be generated by partial fusion of peridotite containing both water and carbon dioxide. But in order to obtain these liquids on the surface of the Earth as lavas, an implicit assumption is that the ascent path must allow perhaps 15 mass % H_2O to be continuously exsolved, a diffusion controlled process, with approximately the same initial and final (eruption) temperature, without changing the composition of the silicate liquid. Such conditions, together with the marked increase in density and viscosity that exsolution would engender can be used to model the time-dependent ascent path, which as more data become available, will allow more constraints to be placed on theories of petrogenesis.

1. Calorimetric measurements

Many silicate liquids when cooled rapidly below their equilibrium melting point fail to crystallize and become supercooled liquids. Continued cooling of the supercooled liquid causes a discontinuity in the heat capacity (C_p) and the thermal expansion, and the temperature of this discontinuity is called the glass transformation temperature, T_g. In the glass industry, T_g is often defined operationally as the temperature at which the viscosity of the supercooled liquid exceeds 10^{13}P†. As the first-order thermodynamic properties, entropy, enthalpy and volume are continuous at T_g, the supercooled liquid–glass transition is usually accounted a second order transformation, although metastable with respect to the crystalline state. However, the temperature T_g is dependent on cooling rate, and very slow cooling will depress this temperature. For inorganic materials T_g is often close to the temperature at which the gram-atom‡ C_p attains the value of $3R$; thus T_g may be seen as the temperature at which appreciable translational mobility sets in. For organic polymers (Wrasidlo 1974), this temperature may frequently be less than 373 K, but few silicate compositions have such low temperatures (e.g. table 2; Bacon 1977).

High-temperature heat content measurements in the stable liquid region are available for only a few compositions so that a number of glasses were made of various compositions by repeated fusion of crystalline components at high temperatures. Each composition eventually became a homogeneous glass and was then analysed, with the results set down in table 1. Many of these compositions have been used by Bacon (1977) in his study of heat content and of the partial molar heat capacity of oxide components in the glass region (i.e. below T_g).

For measurement of heat content in the glass-supercooled liquid region, 7–9 g of glass (50–100 mesh) were loaded into Pt–10Rh capsules (2 cm diameter and 2.5 cm long), evacuated,

† $P = 10^{-1}$ Pa s.

‡ In this paper a gram formula mass divided by the number of atoms in the formula unit is called a gram atom; this conforms to the usage of the authors of the JANAF tables.

PHILOSOPHICAL TRANSACTIONS OF THE ROYAL SOCIETY A MATHEMATICAL, PHYSICAL & ENGINEERING SCIENCES

and sealed by arc-welding under 1 atmosphere of argon. The sample container was suspended by 0.25 mm Pt-10Rh wire in a vertical Pt-wound furnace. Temperature was measured with Pt/Pt–10Rh thermocouple placed just above the top of the container. The thermocouple was calibrated frequently at the melting temperature of Au (1063 °C), and the small corrections were assumed to be linear over the experimental temperature range (400–1650 K). Reported temperatures are believed to be accurate to ± 1 °C.

TABLE 1. ANALYSIS OF PREPARED COMPOSITIONS

	7	8	9	12	66	114	121
SiO_2	39.37	54.11	63.1	63.96	73.5	57.7	70.5
TiO_2	—	20.00	—	—	0.30	0.93	0.32
Al_2O_3	11.80	—	—	—	13.6	15.5	7.77
Fe_2O_3	1.61	—	—	—	1.92	9.99	9.14
FeO	41.39	—	—	—	—	—	—
MnO	0.03	—	—	—	0.02	0.18	0.24
MgO	—	—	14.0	10.58	0.32	3.50	0.03
CaO	5.99	—	—	—	1.24	6.91	0.35
Na_2O	—	25.45	22.9	—	4.04	3.99	6.88
K_2O	—	—	—	25.39	4.27	1.29	4.15
P_2O_5	—	—	—	—	0.03	0.26	0.01
MoO_3	—	—	—	—	0.02	0.24	0.35
gram formula mass	68.418	63.759	56.592	62.592	65.578	67.867	67.450
gram atom/formula mass	2.7052	3.0000	2.8034	2.8356	3.1726	3.1524	3.1753
gram atom/gram	0.03954	0.04705	0.04954	0.04530	0.04838	0.04645	0.04708

After the sample had reached thermal equilibrium in the furnace, two sets of gates shielding the bottom of the furnace and the top of the calorimeter were opened momentarily, and the sample dropped on its suspension wire in less than 1 s into the calorimeter well. The calorimeter consists of a copper tube with horizontal fins enclosed in a double-wall glass vessel immersed in a waterbath maintained at a constant temperature (± 0.001 K), slightly above the melting temperature of diphenyl ether (300.03 K). The space between the copper tube and the glass wall is filled with diphenyl ether, part of which is frozen into a crystalline mantle completely surrounding the horizontal fins. A pool of mercury in the bottom of the glass vessel connects with a calibrated horizontal capillary.

A hot sample introduced into the calorimeter melts some of the diphenyl ether, and forces mercury along the capillary, and the amount displaced is directly proportional to the heat content (H_T–H_{300}) of the sample at the instant it entered the calorimeter. The calorimeter constant is assumed to be 18.91 cal (79.2 J)/g mercury displaced (Jessup 1955).

The heat content of the Pt–10Rh container and suspension wire, and the heat lost during the drop, were accounted for by measuring the heat content of an empty container of similar size and shape, so that small differences in mass between containers could be corrected for by assuming that the heat content of an empty capsule is directly proportional to its mass, as all the Pt–10Rh components are similar.

For runs made from the stable liquid region (1200–1650 K), the mass of silicate material in the 2 × 2.5 cm containers was too large to recover glass and the sample partially devitrified while cooling in the calorimeter. Smaller containers of Pt–10Rh, 1 cm diameter and 2 cm long, were made for these high-temperature runs, and cooling in the calorimeter of the 1–1.5 g of

silicate material they contained was sufficiently rapid to recover the same glassy state, in terms of its heat content, as the glass which had been synthesized and used for experiments below and above T_g. Again the heat content of the empty small container was measured over a wide range of temperatures, but per unit mass was lower than for the large capsules.

Reproducibility of individual runs was generally within $\pm 0.3\,\%$ of the measured heat content, and a few runs were made on the National Bureau of Standards sapphire sample no. 720. Those runs made in the large containers matched those of Bacon (1977) which would suggest an accuracy of about $\pm 0.5\,\%$ in heat content and $\pm 1\,\%$ in heat capacity. Measurements of the heat content of sapphire in the small capsules were systematically low over a wide temperature range, and a small temperature-dependent correction was applied to all measurements made in the small capsules; this correction invariably produced excellent agreement with runs on the same composition made in the large containers over the same temperature range, i.e. just above T_g.

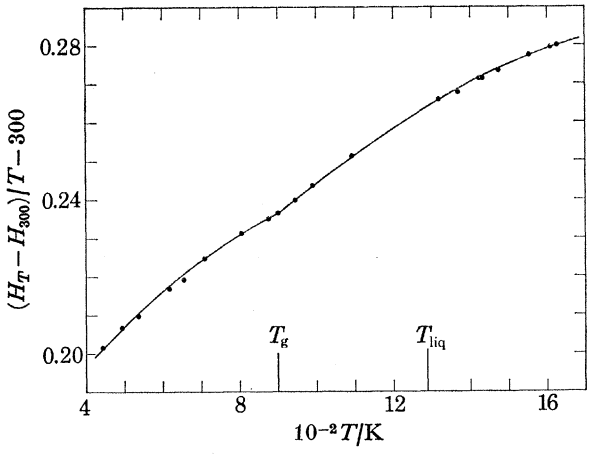

FIGURE 1. Values of mean specific heat, $(H_T - H_{300})/T - 300$, in cal/g for composition 12 plotted against T (K). Temperatures of the glass transformation, T_g, and the liquidus temperature are also shown.

Of the errors that could arise, the calculated contribution of the Ar gas to the measured heat content of the sample was so small that it was ignored. At high temperatures, Fe is soluble in Pt–10Rh and doubtless some of the Fe in the silicate liquid will dissolve in the containers, liberating oxygen. The FeO-rich sample (composition no. 7) was held for only a minimum time in the furnace before dropping; runs made at the end of the sequence of experiments, when presumably the solution of Fe in the container was more advanced, showed no detectable change in heat content.

The normal experimental procedure was initially to use the large capsules containing 7–9 g of the silicate composition, and measure the heat content of the sample at successively increasing temperatures (~ 50 K) until T_g was reached. This is most easily shown by plotting $(H_T - H_{300})/(T - 300)$ against T, and an example of this type of plot is shown in figure 1 for composition no. 12. There is a clear change in slope of the mean specific heat curve at T_g. Each run in the supercooled liquid region, i.e. above T_g, was followed by a run in the temperature range of the glass region to ensure that partial devitrification had not occurred, either in the furnace or in the calorimeter. The large capsules were abandoned once partial devitrification set in, and a set of measurements from the stable liquid region was made in small capsules, with a few runs made from the supercooled liquid region to ensure that the two sets of results were concordant.

TABLE 2. $H_T - H_{300}$ FOR COMPOSITIONS LISTED IN TABLE 1

(Data in calories per gram)

composition 8

run no.	T/K	$H_T - H_{300}$
glass region (T_g = 468 K)		
7	420.8	26.51
8	421.2	26.56
9	479.0	39.61
10	480.1	39.95
13	461.9	35.65
supercooled liquid region		
239	644.8	81.80
243	618.6	74.68
242	588.3	66.98
240	563.8	60.57
241	532.2	52.49
11	596.5	69.02
14	529.2	51.98
20	492.4	43.03
9	479.0	39.61
10	480.1	39.95
stable liquid region > 1150 K)		
230	1236.4	287.80
229	1456.6	364.94
228	1628.0	423.64
227	1265.1	297.88
226	1578.6	406.85
225	1312.4	315.36
224	1386.0	339.69
223	1522.1	387.38
221	1434.9	357.47

composition 7

run no.	T/K	$H_T - H_{300}$
stable liquid region (> 1375 K)		
258	1482.3	327.23
266	1430.1	313.18
265	1457.6	320.93
264	1500.5	333.12
263	1499.4	331.96
262	1407.1	306.51
261	1595.3	361.65
260	1541.8	346.99
259	1655.7	380.99

composition 9

run no.	T/K	$H_T - H_{300}$
glass region (T_g = 496 K)		
32	480.0	40.93
33	466.6	37.77
37	455.9	35.29
39	451.1	34.17
supercooled liquid region		
248	645.3	86.46
244	618.8	78.49
247	584.4	68.51
246	557.3	60.87
245	528.6	53.23
34	512.4	49.10
35	575.3	66.17
stable liquid region (> 1200 K)		
219	1479.0	377.85
218	1423.1	356.09
216	1262.9	297.06
214	1542.9	401.72
213	1351.5	328.96
212	1506.4	388.39
211	1320.8	318.47
209	1635.5	434.63
208	1507.6	389.06
207	1388.1	342.38

composition 66

run no.	T/K	$H_T - H_{300}$
stable liquid region (> 1300 K)		
274	1306.7	272.88
279	1345.6	285.40
278	1408.8	308.25
275	1482.7	332.30
277	1537.4	350.55
280	1590.7	366.72
276	1640.7	381.51

composition 12

run no.	T/K	$H_T - H_{300}$
glass region (T_g = 900 K)		
42	440.3	28.32
43	493.2	39.91
46	646.0	75.89
48	533.9	49.08
49	616.8	68.72
50	708.6	91.83
51	804.8	116.79
52	900.0	141.81
57	875.6	135.28
supercooled liquid region		
53	989.6	168.18
55	944.5	154.69
56	1090.3	198.67
stable liquid region (> 1286 K)		
206	1556.1	348.40
205	1430.6	306.84
204	1621.8	369.74
202	1609.8	365.81
201	1368.6	286.20
200	1319.4	271.04
198	1485.1	324.04
196	1422.1	304.44

composition 114

run no.	T/K	$H_T - H_{300}$
stable liquid region (> 1400 K)		
273	1663.0	405.41
272	1602.6	384.41
271	1431.3	324.42
270	1507.5	352.03
269	1545.8	365.25

composition 121

run no.	T/K	$H_T - H_{300}$
stable liquid region (> 1300 K)		
291	1436.1	330.60
290	1313.0	389.00
289	1544.0	368.09
288	1596.2	386.24
285	1637.6	400.38
283	1349.6	299.76
282	1542.2	366.82

All runs with numbers above 100 were made in small (1 cm dia × 2 cm length) containers; remainder in large containers.

PHILOSOPHICAL TRANSACTIONS OF THE ROYAL SOCIETY A MATHEMATICAL, PHYSICAL & ENGINEERING SCIENCES

For compositions of relatively low viscosity, and low values of T_g, there is a large temperature interval which is experimentally inaccessible between the last supercooled liquid run and the lowest temperature run from the stable liquid region. In this inaccessible region, devitrification or partial crystallization is prevalent, and cannot be prevented with the present experimenta conditions; for some compositions this interval is over 600 K (table 2).

The results for the seven compositions are given in table 2, but for compositions 7, 66, 121 and 114 only the stable liquid data are given, as Bacon (1977) has determined the heat contents of these four compositions in the glass and supercooled liquid region. However, we have ensured that in compositions 66, 121 and 114 all the FeO was oxidized to Fe_2O_3 by holding each composition open to the atmosphere at 800 K for 24 h followed by re-weighting the sample; the gain in mass was approximately what was expected. Thereafter the containers were crimped shut and weighed after each run to ensure that the composition remained constant.

TABLE 3. HEAT CONTENT $(H_T - H_{298.15})$ EQUATIONS FOR THE COMPOSITIONS INVESTIGATED

(data in cal/g)

composition	$H_T - H_{298.15}$	temp. range/K		mean % deviation
7	0.3000T – 116.235	1400–1655	stable liquid	0.22
8	0.3467T – 140.075	1236–1628	stable liquid	0.11
8	0.2527T – 81.188	470–645	supercooled liquid	0.39
9	0.3734T – 174.539	1260–1636	stable liquid	0.18
9	0.2813T – 95.513	512–645	supercooled liquid	0.49
12	0.3278T – 161.735	1319–1621	stable liquid	0.11
12	0.3018T – 130.122	990–1090	supercooled liquid	0.03
66	0.3278T – 154.308	1307–1641	stable liquid	0.30
121	0.3455T – 165.296	1313–1640	stable liquid	0.13
114	0.3483T – 173.217	1431–1663	stable liquid	0.11

The mean deviation is the average percentage deviation of the calculated (smoothed) heat content values from those measured.

Equations of heat content $(H_T - H_{298.15})$

The heat contents in the stable liquid region for the seven compositions given in table 2 can all be fitted by two-term equations to within $\pm 0.22\,\%$ or less (table 3) which is smaller than the experimental reproducibility. The only possible exception is composition 66, but although the fit is poorer than for all the other compositions, it is still within the experimental error. A small correction to the constant changes the reference temperature to 298.15 K.

Differentiation of the high-temperature heat content equations given in table 3 gives the specific heat capacity at constant pressure, C_p. Although within the experimental temperature range of 1200–1650 K, C_p is essentially independent of temperature, it is likely that over a larger temperature range, there will be a measurable temperature dependence of C_p, and it may be expected to decrease slightly,

Also shown in table 3 are fit equations for the heat content for the supercooled liquid region for the three compositions 8, 9 and 12. It is clear that C_p in the supercooled liquid region is quite different to that in the stable liquid region, so that all subsequent calculations have used only published data where it can be established that the heat content data is for the stable liquid region.

We wish to be able to express the molar heat capacity of any silicate liquid in terms of its component oxides so that

$$C_{p,\,\text{liquid}} = \sum_i X_i b_i$$

where b_i is the coefficient of the ith component, and X_i the mole fraction of i. As a first step, the compositions given in table 1 have to be recalculated onto a gram formula mass basis with the sum of the oxide components equal to unity. As an example, we may use the *composition* Fe_2SiO_4 for which we have:

	mass %	molecular proportions	molecular fraction	gram formula mass	gram atoms
SiO_2	29.49	0.4908	0.3334	$0.3334 \times 60.085 = 20.03$	$0.3334 \times 3 = 1.0000$
FeO	70.51	0.9814	0.6666	$0.6666 \times 71.846 = 47.89$	$0.6666 \times 2 = 1.3333$
				sum = 67.92	2.3333

and gram atoms/g of Fe_2SiO_4 = 2.3333/67.92 = 0.03436.

and the corresponding data for all the compositions are given in table 1. Note that the gram formula mass as expressed here is for $Fe_{\frac{2}{3}}Si_{\frac{1}{3}}O_{\frac{4}{3}}$ and not that conventionally given (Fe_2SiO_4) where the sum of the oxide components is equal to three rather than unity. All the measured specific heat capacities in table 3 require to be multiplied by the gram formula mass of each composition to put them on a comparable basis. The molecular masses we have used are given in table 4.

TABLE 4. MOLECULAR MASSES USED IN THE CALCULATION OF PARTIAL MOLAR HEAT CAPACITIES

SiO_2	60.0848	MgO	40.3044
TiO_2	79.8988	CaO	56.0794
Al_2O_3	101.9612	Na_2O	61.9790
Fe_2O_3	159.6922	K_2O	94.2034
FeO	71.8464	P_2O_5	141.9446
MnO	70.9374	MoO_3	143.9382

TABLE 5. PARTIAL MOLAR HEAT CAPACITIES (cal mol^{-1} K^{-1}) IN SILICATE LIQUIDS IN THE TEMPERATURE RANGE 1200–1650 K

	$\bar{C}_{p,i}$	σ	X_i
SiO_2	20.79	0.16	0.81 to 0.33
TiO_2	26.74	0.58	0.33 to 0.0
Al_2O_3	24.64	1.43	0.10 to 0.0
Fe_2O_3	78.64	3.53	0.04 to 0.0
FeO	18.34	0.18	0.67 to 0.0
MgO	21.62	0.54	0.20 to 0.0
CaO	19.32	0.64	0.33 to 0.0
Na_2O	22.00	0.33	0.50 to 0.0
K_2O	17.73	0.58	0.29 to 0.0

Note that the following values of partial liquid heat capacities have been assumed in the calculations: MnO = 19.08; P_2O_5 = 58.5; MoO_3 = 32.00.

Before the final calculation was performed, the appropriate amount for the contribution of MoO_3 (from the fusion crucible), P_2O_5 and MnO was subtracted from the gram formula mass heat capacity. The values used were MoO_3 (liquid) = 32.00; P_2O_5 (liquid) = 58.5 (Kelley 1960) and for $C_{p,\mathrm{MnO\,(liquid)}}$ we used a value of 19.08 cal mol^{-1} K^{-1} which was derived from Mah's (1960) data on liquid Mn_2SiO_4 and our data for SiO_2 (table 5).

In addition to the data of table 3, the heat capacities for liquid Fe_2SiO_4 (Orr 1953), liquid $CaTiSiO_5$ (King *et al.* 1954), liquid Na_2SiO_3 (Naylor 1945), liquid $K_2O.2.5SiO_2$, Wirtschaftsglas and $Na_2O.CaO.6SiO_2$ (Schweite & Zielger 1955) were also included and the whole array fitted by least-squares in an over determined matrix of 13 data sets to give values of $\bar{C}_{p,i}$, the partial molar heat capacities for each of the nine liquid oxide components.

PHILOSOPHICAL TRANSACTIONS OF THE ROYAL SOCIETY A MATHEMATICAL, PHYSICAL & ENGINEERING SCIENCES

These are listed in table 5 together with the calculated value of one standard deviation (σ) and the concentration range of each oxide component in the data set. By using these partial molar heat capacity values, the calculated values may be compared to the observed values for the data set together with the percentage difference and are given in table 6.

The magnitude of the standard deviation for each estimated value of $\bar{C}_{p,i}$ is clearly related to the range of concentration and each oxide component (table 5). The greatest uncertainties are for Al_2O_3 and Fe_2O_3, and both estimates for $\bar{C}_{p,i}$ require extensive extrapolation in terms of composition (e.g. for Fe_2O_3 from 0.04 to 1.00). It seems likely that $\overline{C_{p,\,Fe_2O_3}}$ is compositionally dependent, and as the concentration of Fe_2O_3 increases, the value would fall to an anticipated value close to $2.5\overline{C_{p,\,FeO}}$. Although the uncertainty in $\overline{C_{p,\,Fe_2O_3}}$ is very large, this is only of significance if this value is used to calculate the heat capacity of a liquid in which Fe_2O_3 is a major component; for natural silicate liquids with very small amounts of Fe_2O_3, the value in table 5 is appropriate for it was derived from such compositions.

TABLE 6. COMPARISON OF OBSERVED AND CALCULATED HEAT CAPACITIES

composition	observed C_p	calculated C_p	% difference
$\frac{2}{3}FeO.\frac{1}{3}SiO_2$	19.10	19.16	0.3
$\frac{1}{3}CaO.\frac{1}{3}TiO_2.\frac{1}{3}SiO_2$	22.27	22.29	0.1
$\frac{1}{2}Na_2O.\frac{1}{2}SiO_2$	21.41	21.40	0.05
7	20.52	20.42	0.5
8	22.11	22.06	0.2
9	21.13	21.21	0.4
12	20.52	20.41	0.5
66	21.48	21.54	0.3
121	23.21	23.16	0.2
114	23.50	23.54	0.2
$\frac{2}{7}K_2O.\frac{5}{7}SiO_2$	19.86	19.92	0.3
$\frac{1}{8}Na_2O.\frac{1}{8}CaO.\frac{3}{4}SiO_2$	20.84	20.76	0.4
Wirtschaftsglas	20.88	20.95	0.3

average deviation = 0.29%

With the possible exception of Fe_2O_3, the results in table 5 and table 6 show that within the composition range represented by the experimental compositions

$$\bar{C}_{p,i} = C^{\circ}_{p,i}$$

if i is taken as Fe_2SiO_4 or $CaTiSiO_5$; in other words, there is no excess heat capacity for these two components. If other components are chosen this conclusion is less easily substantiated, and possibly not experimentally capable of proof. For example, the measurement of the heat capacity of pure liquid $K_2O(C^{\circ}_{p,\,K_2O})$ is fraught with enormous difficulties so that it may be impossible ever to establish that

$$\bar{C}_{p,\,K_2O} = C^{\circ}_{p,\,K_2O}.$$

Similarly the heat capacity of pure liquid MgO had been calculated in the temperature range 3098–3873 K (Leu *et al.* 1975), and it would require only a small temperature dependence of $C^{\circ}_{p,MgO}$ ($\sim$ 23.81) to match $\bar{C}_{p,\,MgO}$ in the temperature range 1200–1650 K. Lastly, two sets of measurements of $C^{\circ}_{p,\,Al_2O_3}$ are available; one value is 34.623 (JANAF 1971) and a later value by Shpil'rain *et al.* (1972) shows that the heat capacity is temperature dependent in the range 2323–3100 K with a mean value near 46.03. Clearly the data on the pure liquid oxides, which are experimentally extremely difficult to obtain, can really not be used to show that $\bar{C}_{p,i} \neq C^{\circ}_{p,i}$,

PHILOSOPHICAL TRANSACTIONS OF THE ROYAL SOCIETY A MATHEMATICAL, PHYSICAL & ENGINEERING SCIENCES

and in what follows we shall assume that there is no excess heat capacity no matter which component is chosen, despite the fact that we have only been able to establish this for Fe_2SiO_4 and $CaTiSiO_5$.

The unwary reader may consider that it should be possible to use the individual heat content measurements (table 2) and from these derive partial molar heat contents for each oxide, and then by differentiation obtain the partial molar heat capacities. Such a procedure requires that the same reference state at 298.15 K, glass or crystals, be common to the data set; the two reference states cannot be mixed as the following equations illustrate. Cooling in the calorimeter liberates an amount of heat which is quite different depending on whether the sample is cooling to crystals or to glass. The heat liberated in cooling from T to glass reference state at 298.15 is given by

$$H_T - H_{T_g} + \int_{298}^{T_g} C_{p,\,\mathrm{glass}}\,\mathrm{d}T, \tag{1}$$

whereas the heat liberated in cooling from T to crystalline reference state at 298.15

$$= H_T - H_{T_m} + \Delta H_{\mathrm{crystal}} + \int_{298}^{T_m} C_{p,\,\mathrm{solid}}\,\mathrm{d}T, \tag{2}$$

where T_g, T_m and $\Delta H_{\mathrm{crystal}}$ refer to the glass transformation temperature, the equilibrium melting temperature and the heat of crystallization, respectively.

Until more data is available such a procedure has been rejected as it would require that the crystalline reference state data (e.g. Fe_2SiO_4, $CaTiSiO_5$) be ignored; thus we have of necessity focused on heat capacity and neglected the heat content data.

Thermodynamic data for liquid compounds

One use to which this liquid heat capacity data may be put is to derive an internally consistent set of enthalpy and volume data for liquid compounds if the equilibrium between solid and liquid is known as a function of pressure.

For the reaction solid $\rightleftharpoons$ liquid we may write at equilibrium along the fusion curve

$$\Delta G = 0 = \Delta H_{T_r} + \int_{T_r}^{T} (C_{p,\,\mathrm{liq}} - C_{p,\,\mathrm{solid}})\,\mathrm{d}T - T\left[\Delta S_{T_r} + \int_{T_r}^{T}\left(\frac{C_{p,\,\mathrm{liq}}}{T} - \frac{C_{p,\,\mathrm{solid}}}{T}\right)\mathrm{d}T\right] + \int_1^P \Delta V\,\mathrm{d}P, \tag{3}$$

where ΔH_{T_r} ΔS_{T_r}, ΔV are the enthalpy, entropy and volume of fusion of 1 mol of solid at the 1 bar melting temperature. The variation of the volume with P and T is conveniently expressed as

$$V_{\mathrm{solid}} = (a_s T + b_s)\,(1 - \beta P),$$

where β is the isothermal compressibility of the solid, and for the liquid

$$V_{\mathrm{liquid}} = (a_L T + b_L + c_L P),$$

where c_L is $\mathrm{d}V_{\mathrm{liquid}}/\mathrm{d}P$.

If the slope of the fusion curve is known at 1 bar then it is possible to estimate either the heat or volume of fusion from the Clapeyron relation

$$(\mathrm{d}T/\mathrm{d}P)_{1\ \mathrm{bar}} = \frac{T\Delta V_{\mathrm{fusion}}}{\Delta H_{\mathrm{fusion}}}.$$

We set out in table 7 the thermodynamic data on liquid compounds which have been derived using equation (3) coupled with the fusion curves.

PHILOSOPHICAL TRANSACTIONS OF THE ROYAL SOCIETY A MATHEMATICAL, PHYSICAL & ENGINEERING SCIENCES

TABLE 7. THERMODYNAMIC DATA FOR LIQUID COMPOUNDS

Precision and accuracy of the following data are not established and the number of decimal places is only given to avoid significant round-off errors.

Fe_2SiO_4

$C_{p,\,\text{liquid}} = 57.30$ (Orr 1953)

$C_{p,\,\text{solid}} = 36.51 + 9.36 \times 10^{-3} T - 6.70 \times 10^{5} T^{-2}$ (Kelley 1960)

$\Delta H_{\text{fusion}} = 22030$ cal (Orr 1953)

$T_{\text{fusion}} = 1490\,\text{K}$

$\Delta S_{\text{fusion}} = 14.785$ cal $\text{mol}^{-1}\,\text{K}^{-1}$

$V_{\text{solid}} = (31.43 \times 10^{-6} T + 1.0996)\,(1 - 0.91 \times 10^{-6} P)$ (Skinner 1966; Birch 1966)

$V_{\text{liquid}} = (101.75 \times 10^{-6} T + 1.0822 - 1.94 \times 10^{-6} P)$

where a_L and b_L are taken from Bottinga & Weill (1970) and c_L comes from fitting the fusion curve of Lindsley (1967). The calculated fusion curve in relation to the experimental curve is shown in figure 2.

$NaAlSi_3O_8$

$C_{p,\,\text{liquid}} = 85.69$ (table 5)

$C_{p,\,\text{solid}} = 61.70 + 13.90 \times 10^{-3} T - 15.01 \times 10^{5} T^{-2}$ (Kelley 1960)

$C_{p,\,\text{glass}} = 61.31 + 18.00 \times 10^{-3} T - 16.16 \times 10^{5} T^{-2}$ (Kelley 1960)

$T_{\text{fusion}} = 1391\,\text{K}$

for albite (crystals) → albite (glass), $\Delta H_{298} = 11904$ cal (Robie & Waldbaum 1968).

Given T_g at 1036 K (Arndt & Haberle 1973) then ΔH_{fusion} at 1391 K is found by integration of

$$\Delta H_{\text{fusion}} = \Delta H_{298} + \int_{298}^{1036} (C_{p,\,\text{glass}} - C_{p,\,c})\,\mathrm{d}T + \int_{1036}^{1391} (C_{p,\,\text{liq}} - C_{p,\,c})\,\mathrm{d}T$$

$= 16258$ cal,

$\Delta S_{\text{fusion}} = 11.688$ cal $\text{mol}^{-1}\,\text{K}^{-1}$

$V_{\text{solid}} = (67.66 \times 10^{-6} T + 2.377)\,(1 - 1.48 \times 10^{-6} P)$ (Skinner 1966; Birch 1966)

$V_{\text{liquid}} = (171.91 \times 10^{-6} T + 2.3727 - 7.49 \times 10^{-6} P)$ which comes from fitting the fusion curve of Boyd & England (1963).

The calculated fusion curve in relation to the experimental brackets is shown in figure 3.

$CaMgSi_2O_6$

$C_{p,\,\text{liquid}} = 82.52$ (table 5)

$C_{p,\,\text{solid}} = 52.87 + 7.84 \times 10^{-3} T - 15.74 \times 10^{5} T^{-2}$ (Kelley 1960)

$T_{\text{fusion}} = 1664$ K

$\Delta H_{\text{fusion}} = 31043$ cal obtained from density of liquid $CaMgSi_2O_6$ (Skinner 1966) and $\mathrm{d}P/\mathrm{d}T$ of fusion curve (Rosenhaum & Eggler 1975)

$\Delta S_{\text{fusion}} = 18.656$ cal $\text{mol}^{-1}\,\text{K}^{-1}$

$V_{\text{solid}} = (46.27 \times 10^{-6} T + 1.5644)\,(1 - 1.07 \times 10^{-6} P)$ Skinner 1966; Birch 1966)

$V_{\text{liquid}} = (178.25 \times 10^{-6} T + 1.6083 - 7.26 \times 10^{-6} P)$ which comes from fitting the fusion curve of Boyd & England (1963). The calculated value of ΔH_{fusion} is within the measured value (30700 ± 800 cal) of Ferrier (1970). The calculated fusion curve in relation to the experimental points is shown in figure 4.

$KAlSi_3O_8$

$C_{p,\,\text{liquid}} = 83.56$ (table 5)

$C_{p,\,\text{solid}} = 63.83 + 12.90 + 10^{-3} T - 17.05 \times 10^{5} T^{-2}$ (Kelley 1960)

$C_{p,\,\text{glass}} = 61.96 + 17.16 \times 10^{-3} T - 14.29 \times 10^{5} T^{-2}$ (Kelley 1960)

$T_{\text{fusion}} = 1473$ K

for sanidine (crystals) → sanidine (glass), $\Delta H_{298} = 11102$ cal (Robie & Waldbaum 1968).

PHILOSOPHICAL TRANSACTIONS OF THE ROYAL SOCIETY A MATHEMATICAL, PHYSICAL & ENGINEERING SCIENCES

TABLE 7 (*cont.*)

Given T_g = 1178 K (Arndt & Haberle 1973), then ΔH_{fusion} at 1473 K is found by integration of

$$\Delta H_{\text{fusion}} = \Delta H_{298} + \int_{298}^{1178} (C_{p,\,\text{glass}} - C_{p,\,c})\,\mathrm{d}T + \int_{1178}^{1473} (C_{p,\,\text{liq}} - C_{p,\,c})\,\mathrm{d}T$$

$$= 13980 \text{ cal}$$

$$\Delta S_{\text{fusion}} = 9.491 \text{ cal mol}^{-1}\text{ K}^{-1}$$

$$V_{\text{solid}} = (70.94 \times 10^{-6}T + 2.5795)\,(1 - 1.76 \times 10^{-6}P) \quad \text{(Skinner 1966, Birch 1966)}$$

$V_{\text{liquid}} = 78.03 \times 10^{-6}T + 2.7442 - 9.88 \times 10^{-6}P)$ which comes from fitting the three data points of Lindsley's (1966) fusion curve. The calculated fusion curve, metastable below 19.6 kbar, is shown in relation to the experimental brackets in figure 5.

TiO_2

$C_{p,\,\text{liquid}} = 26.74 - 1.25 \times 10^{-3}T$ (table 5 with a temperature dependence on C_p within the limits of table 5).

$C_{p,\,\text{solid}} = 17.97 + 0.28 \times 10^{-3}T - 4.35 \times 10^{5}T^{-2}$ (Kelley 1960)

T_{fusion} = 2103 K but JANAF (1975) give the stoichiometric melting temperature as 2130 K; the value here is taken from Robie & Waldbaum (1968).

ΔH_{fusion} = 10000 cal (estimated)

$\Delta S_{\text{fusion}} = 4.755 \text{ cal mol}^{-1}\text{ K}^{-1}$

$V_{\text{solid}} = (12.26 \times 10^{-6}T + 0.4460)\,(1 - 0.51 \times 10^{-6}P)$ (Skinner 1966; Birch 1966)

$V_{\text{liquid}} = (55.97 \times 10^{-6}T + 0.3887 - 1.04 \times 10^{-6}P)$ which is taken from fitting the fusion curve estimated from MacGregor (1969).

Al_2O_3

$C_{p,\,\text{liquid}} = 40.32$ (average of JANAF 1974 and Shpil'rain *et al.* 1972)

T_{fusion} = 2327 K

ΔH_{fusion} = 28000 cal (JANAF 1974)

$\Delta S_{\text{fusion}} = 12.033 \text{ cal mol}^{-1}\text{ K}^{-1}$.

$V_{\text{liquid}} = 330.99 \times 10^{-6}T + 0.03986 - 11.78 \times 10^{-6}P$ (Kirshenbaum & Cahill 1960. The value of $(\mathrm{d}V/\mathrm{d}P)_T$ is very uncertain in view of the range in the measured values of C_p of Al_2O_3 liquid, for it is derived from Slagle & Nelson's data (1970) on the adiabatic compressibility of Al_2O_3 liquid. Choosing the mean value of C_p (above), β_T becomes zero at 1944 K, which is impossible, so we have used the mean value in the experimental temperature range to obtain $(\mathrm{d}V/\mathrm{d}P)_T$.)

These data together with that of JANAF (1974) for solid Al_2O_3 (i.e. $\Delta H^\circ_{f,\,298} = -400500$ cal and $S^\circ_{298} = 12.18$ cal mol^{-1} K^{-1}) can be used to obtain $\Delta G^\circ_f/RT$ of Al_2O_3 liquid.

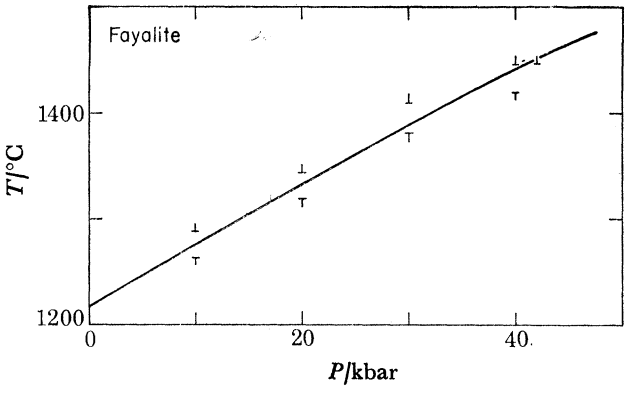

FIGURE 2. The experimental brackets for the fusion curve of Fe_2SiO_4 (Lindsley 1967) together with the calculated curve.

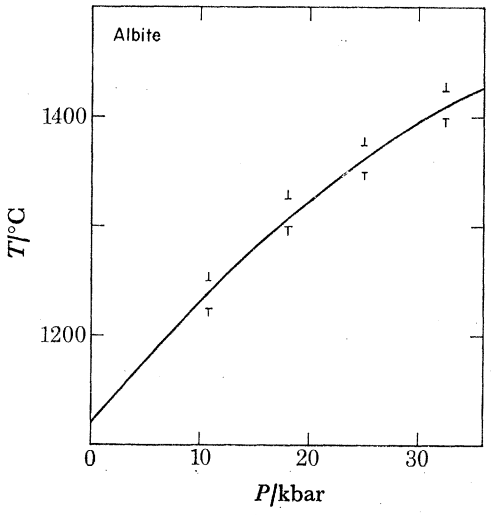

FIGURE 3. Experimental brackets on the $NaAlSi_3O_8$ fusion curve (Boyd & England 1963) and the calculated curve.

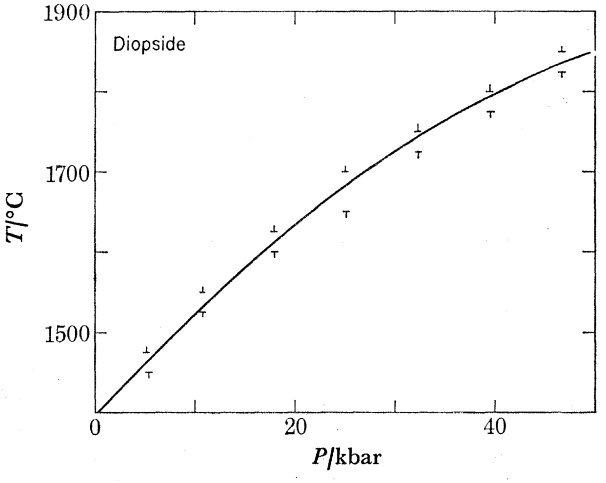

FIGURE 4. Experimental brackets on the $CaMgSi_2O_6$ fusion curve (Boyd & England 1963) and the calculated curve.

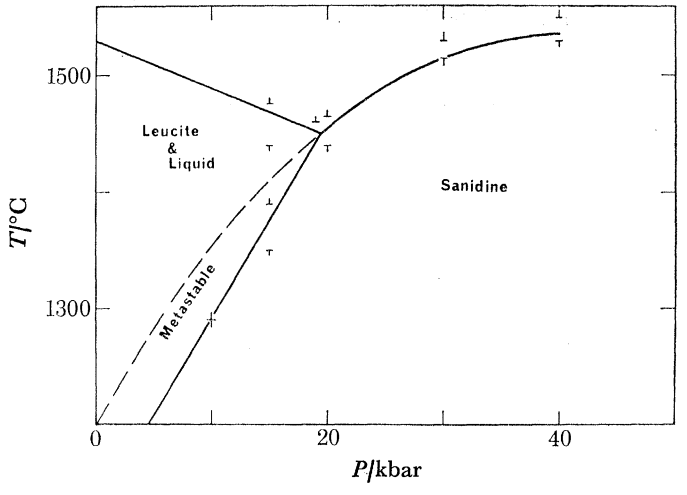

FIGURE 5. Experimental brackets on the $KAlSi_3O_8$ fusion curve (Lindsley 1966) and the calculated curve which is metastable below 19 kbar. The triangular area is the field of leucite plus liquid.

In the second part of this paper we wish to calculate the equilibration conditions in terms of pressure and temperature of a lava with a solid compound or with an assemblage of minerals. In table 8 we have listed the relevant thermodynamic data for these solids, which in conjunction with the heat capacity equations of Kelley (1960) suffice for the calculations.

TABLE 8. HEATS OF FORMATION ($\Delta H^\circ_{f,298}$), ENTROPIES, S°_{298}, VOLUMES ($a_s T + b_s$) AND COMPRESSIBILITIES OF SOLID COMPOUNDS USED IN EQUILIBRATION CALCULATIONS

			V (cal/bar)		
solid	$(\Delta H^\circ_f)_{298}$	S°_{298}	$10^{-6} \times a_s$	b_s	$10^{-6} \times \beta$
$MgAl_2O_4$ spinel	−551200	19.27	26.04	0.9408	0.41
$CaAl_2Si_2O_8$ anorthite	−1009300	48.45	—	—	—
$NaAlSi_2O_6$ jadeite	−719871	31.90	38.75	1.4314	0.75
Mg_2SiO_4 forsterite	−520300	22.75	35.78	1.0349	0.79
$MgSiO_3$ orthoenstatite	−370200	16.20	22.54	0.7444	1.01
$FeTiO_3$ ilmenite	−295560	25.30	—	—	—
Fe_2TiO_4 ulvospinel	−360992	40.36	61.51	1.1184	0.5
$CaMgSi_2O_8$ diopside	−765100	34.20	46.27	1.5644	1.07
$KAlSiO_4$ kaliophilite	−503926	31.85	86.72	1.4356	2.05
$KAlSi_3O_8$ sanidine	−944378	56.94	70.94	2.5795	1.76
$Ca_3Al_2Si_3O_{12}$ grossular	−1588393	57.70	70.46	2.9725	0.60
Ca_2SiO_4 calcium-olivine	−553973	28.80	—	—	—
SiO_2†β-quartz	−217725	9.00	−3.82	0.5703	1.776
SiO_2 glass	−215870	11.33	1.0559	0.6515	2.3
$CaAl_2SiO_6$ pyroxene	−786984	34.60	—	—	—
$KMg_3AlSi_3O_{10}(OH)_2$ hydroxy phlogopite	−1492800	76.40	117.69	3.5490	2.34

† Metastable at 298.15; extrapolated down to 298.15 from α–β transition.

Some recent results on the heats of solution of enstatite, forsterite and quartz (Charlu *et al.* 1975) indicate substantial differences for $\Delta H^\circ_{f,298}$ to those listed above, in particular for enstatite. However, this new data shows that forsterite and β-quartz, and forsterite and cristobalite, would be stable above about 1060 °C. As this is most unlikely, we have retained the older data for enstatite which is more compatible with the known instability of quartz and forsterite. Data taken from Robie & Waldbaum (1968), Pankratz (1968), JANAF (1971) Helgeson (pers. commun. 1974), Verhoogen (1962), Skinner (1966), Birch (1966).

2. APPLICATION TO PETROGENESIS

A large amount of effort has been invested in the experimental exploration of basic liquids formed by partial fusion of garnet–lherzolite, eclogite, pyrolite and other model mantle materials. This type of investigation, with or without water as an additional component, has been summarized by Green (1970) who has shown on a P–T grid the conditions under which liquids, corresponding to almost all the principal lava types, could have been generated by partial fusion. This experimental approach is only of general utility as the results cannot, at present, be used to deduce the pressure–temperature conditions of equilibration of a particular lava with a particular source material.

In the second part of this paper we consider one of the petrological-thermodynamic approaches available to the individual investigator who wishes to calculate the P–T conditions of equilibration of any basic lava with any stipulated source material, and who additionally desires to obtain some information on the composition of the solid residue.

The generation, ascent, eruption and crystallization of basic magma involves a sequence of time-dependent conditions which are difficult to quantify. Indeed the general petrological

approach to this dynamic system is to identify various 'static' stages in the evolution of a basic magma, and assume that for a particular segment of the life cycle of the magma, these conditions were typical of the whole. This difficulty can be illustrated by the crystallization of a basic lava on the Earth's surface. Among the minerals which precipitate are the iron–titanium oxides whose composition can be used to derive both the temperature and oxygen fugacity of their equilibration. This temperature is presumably the temperature at which the reaction rate effectively became zero, and this may, or may not, be the temperature at which the reaction rates for the coexisting minerals also became zero. At best it represents one point in the life cycle of the magma, and it is a petrological necessity to determine the properties of the coexisting minerals at this same point. Therefore we have to make the assumption that the iron–titanium equilibration temperature, hereafter called the quench temperature for brevity, applied to the whole groundmass assemblage. General petrological experience would suggest that this is rarely the case, for some of the minerals are strongly zoned. Often, however, the average bulk composition of a particular mineral comes close to that found in slowly cooled intrusions.

Similarly the thermodynamic estimates of pressure and temperature made in the later part of this paper refer to a 'static' segment in the life cycle, and thus in a dynamic magma régime to a smeared average of conditions which the techniques used here are unable yet to resolve further.

In what follows we in effect reverse the P–T path that a lava took in its ascent from source to surface, and in so doing we assume that the concentrations of all the components which determined the mineralogical composition of the lava as it crystallized on the surface remain unchanged in the inverse path to the source. In many lavas this assumption may be difficult to sustain, but in those alkali–olivine–basalt lavas which bring up ultrabasic mantle fragments (ρ = 3.3–3.4) 2 cm or more in diameter (up to 150 cm have been recorded) crystal settling is obviously not an operational method of changing the composition of the lava for that segment of its ascent path since the fragments were included. Until more is known of the rates of ascent of all varieties of magma, other than alkali-basalts containing nodules, it is difficult to make any statement of the viability of crystal fractionation changing the composition of the liquid during its ascent.

The volatile components, particularly H_2O, CO_2 and SO_2 would be expelled as the lava erupted and crystallized on the Earth's surface. Initially we will ignore any increase in the concentration of water in the inverse path, but later we relax this constraint and consider the effect of variable water concentration as far as the experimental and thermodynamic data will allow.

This second part will consider several topics: (i) a thermodynamic approach to the calculation of P–T equilibration with any stipulated source material, (ii) the thermal response of magma to engulfing cooler ultrabasic nodules and (iii) the concentration of water in lavas; we defer to the third part heat and mass transfer rates for ascending basaltic magma.

The thermodynamic treatment here is substantially that of Nicholls & Carmichael (1972), except that the assumptions of that paper are tested here against experimental liquid–solid equilibria, and are also modified to consider more complicated components than simple oxides.

At equilibrium at some pressure and temperature between a lava and its source material we may write

$$\mu_i^{\text{liquid}} = \mu_i^{\text{solid}}, \tag{4}$$

PHILOSOPHICAL TRANSACTIONS OF THE ROYAL SOCIETY A MATHEMATICAL, PHYSICAL & ENGINEERING SCIENCES

where i is a component in the superscript phase. There is no theoretical restriction to the components that may be chosen, except that $\sum_i X_i = 1$ where X_i is the mole fraction of i. In practice it is difficult either to define the activities of many components in a lava, or obtain thermodynamic data for the chosen components. In this paper we use liquid $NaAlSi_3O_8$, $KAlSi_3O_8$, $CaMgSi_2O_6$, Fe_2SiO_4, Al_2O_3, TiO_2 but SiO_2 glass for which the standard state thermodynamic data have been given earlier (table 7).

It is convenient to consider the lava first, as the relations here are more complicated, and involve several digressions into the thermodynamic treatment of solutions.

The lava and activities at 1 bar†

Basic lavas are quenched on the surface of the earth ($P = 1$ bar)† to an assemblage of minerals which typically include plagioclase, calcium-rich pyroxene, olivine, iron–titanium oxides and sometimes a calcium-poor pyroxene. If the temperature of the lava can be obtained, most conveniently from the compostion of the coexisting iron–titanium oxides using the calibration curves of Buddington & Lindsley (1964), then with analyses of the groundmass minerals, the activities of several components can be calculated at the quench temperature. With an assemblage of olivine and magnetite solid solutions $a^{\text{lava}}_{SiO_2}$ can be calculated from the reaction

$$\underset{\text{solid}}{\tfrac{2}{3}Fe_3O_4} + \underset{\text{glass}}{SiO_2} = \underset{\text{solid}}{Fe_2SiO_4} + \underset{\text{gas}}{\tfrac{1}{3}O_2} \qquad (5)$$

which gives $$\ln a^{\text{lava}}_{SiO_2} = \Delta G^\circ_5/RT + \ln a^{\text{olivine}}_{Fe_2SiO_4} + \tfrac{1}{3}\ln f_{O_2} - \tfrac{2}{3}\ln a^{\text{magnetite}}_{Fe_3O_4},$$

for which over the temperature range 900–1300 K (Wones & Gilbert 1969)

$$\Delta G^\circ_5/RT = 19042/T - 6.47,$$

and the method of treating the activity–composition relations of the solids will be considered in detail below.

The general form of $\Delta G^\circ/RT$ is given by

$$\frac{\Delta G^\circ}{RT} = [-a(\ln T - 1) - \tfrac{1}{2}bT + (\Delta H_{T_r} - aT_r + cT_r^{-1} - \tfrac{1}{2}bT_r^2)\ T^{-1} - \tfrac{1}{2}cT^{-2} + (-\Delta S_{T_r} + a\ln T_r + bT_r - \tfrac{1}{2}c\ T_r^{-2})]\ 1/R,$$

where ΔH_{T_r}, ΔS_{T_r} represent the standard state enthalpy and entropy change at a reference temperature T_r, and a, b, c are the coefficients of the Maier–Kelley heat capacity equation of the products less the reactants. We have given in table 9 the values of $\Delta G^\circ/RT$ for other reactions to calculate the activity of a component on a liquid standard state. In what follows we have used the superscript *lava* to denote conditions at 1 bar and the quench temperature, whereas the superscript *liquid* is used to refer to conditions at elevated P and T.

Activity–composition relations; solid solutions

It is often convenient, for petrological purposes, to assume that all but one of the solid solutions used to define the activity of a particular component are ideal, especially over small composition ranges, and so let any actual departure from ideality of these become incorporated in the activity coefficient of the one designated solid solution. The standard state free-energy change of reaction (5) has been experimentally determined by Wones & Gilbert (1969), and

† 1 bar = 10^5 Pa.

TABLE 9. REACTIONS WHICH DEFINE THE ACTIVITY OF A COMPONENT IN THE LAVA AND THE CONSTANTS IN THE EXPRESSION FOR THE STANDARD STATE FREE-ENERGY CHANGE OF THE REACTION: $\Delta G^\circ/RT = A \ln (T-1) + BT + CT^{-1} + DT^{-2} + E$

reaction	A	$10^{-3}B$	C	$10^{-5}D$	E
(6) Fe_2SiO_4 (liquid) $\rightleftharpoons$ Fe_2SiO_4 (solid)	10.462	−2.335	−952.412	1.690	−61.9063
(7) $CaMgSi_2O_6$ (liquid) $\rightleftharpoons$ $CaMgSi_2O_6$ (solid)	14.920	0.6617	10562.0	3.960	−103.3363
(8) $NaAlSi_3O_8$ (liquid) $\rightleftharpoons$ $NaAlSi_3O_8$ (solid)	12.072	−3.497	1301.12	3.777	−71.5698
(9) $KAlSi_3O_8$ (liquid) $\rightleftharpoons$ $KAlSi_3O_8$ (sanidine)	9.928	−3.246	−35.2072	4.290	−57.8935
(10) $CaMgSi_2O_6$ (solid) + Al_2O_3 (liquid) + $\frac{1}{2}SiO_2$ (glass) $\rightleftharpoons$ $CaAl_2Si_2O_8$ (solid) + Mg_2SiO_4 (solid)	8.834	−1.834	339.197	0.9272	−59.5084
(11) TiO_2 (liquid) + Fe_2TiO_4 (solid) $\rightleftharpoons$ $2FeTiO_3$ (solid)	2.184	1.2857	−560.7506	1.5549	−16.6055
(12) TiO_2 (liquid) + $\frac{1}{2}Fe_2SiO_4$ (solid) $\rightleftharpoons$ $FeTiO_3$ (solid) + $\frac{1}{2}SiO_2$ (glass)	5.2511	−0.697	2399.8	0.7963	−35.2616
(13) TiO_2 (liquid) + Fe_2SiO_4 (solid) $\rightleftharpoons$ Fe_2TiO_4 (solid) + SiO_2 (glass)	8.318	−2.680	5360.4	0.377	−53.9176

so far as possible all the derived activity coefficients used in this paper are made internally consistent with this reaction.†

From reaction (5) it is apparent that for any lava which contains olivine, magnetite solid solution and quartz, which precipitated at a known pressure, temperature, and oxygen fugacity, the latter two variables being obtained from the iron–titanium oxides (Buddington & Lindsley 1964) it is possible to calculate the activity of Fe_3O_4 in the magnetite solid solution. However, the value obtained will depend on the mixing model used for the olivine solid–solution series. For the Fe–Mg olivine series Williams (1972) found small departures from ideality, but we have noted that the difference between the activity of Fe_2SiO_4 calculated according to his model, and that calculated on the assumption of ideal two-site mixing ($a_{Fe_2SiO_4} = X^2_{Fe_2SiO_4}$) (Kerrick & Darken 1975) often lies well within the uncertainty of estimating the composition of a compositionally zoned olivine in a lava. Thus we have assumed that the Fe–Mg olivines mix ideally, and therefore that the activity coefficient of either Fe_2SiO_4 or Mg_2SiO_4 is not a function of olivine composition.

Treating the mixing of Fe_3O_4 in a titanomagnetite solid solution is more complicated, as Fe_2TiO_4, Fe_3O_4 and $MgFe_2O_4$ are inverse spinels, e.g. $Fe^{3+}_{oct}(Fe^{2+}Fe^{3+})\ O^{2-}_{4,tet}$ while some of the other (dilute) components, such as $MgAl_2O_4$ are not. As there is no unambiguous method of recalculating a microprobe analysis of a titanomagnetic solid solution, and thus of assigning atoms to either the tetrahedral or octahedral sites, it is necessary to assume that $a_{Fe_3O_4} = X_{Fe_3O_4}$. It has been demonstrated that within the limits of error of the standard state thermodynamic data, $\gamma_{Fe_3O_4}$ is unity in the temperature range 835–1035 °C, and in the composition range 0.425–0.226 Fe_2TiO_4, for naturally occurring titanomagnetite (Heming & Carmichael 1973).

† Their mineral assemblage contained solid SiO_2 as the standard state of SiO_2, so that their measured values have been changed to a standard state of SiO_2 glass.

PHILOSOPHICAL TRANSACTIONS OF THE ROYAL SOCIETY A MATHEMATICAL, PHYSICAL & ENGINEERING SCIENCES

Moreover Nicholls *et al.* (1971) were able to show a parallel internal consistency of thermodynamic data based on this assumption for a ugandite lava, where $a_{SiO_2}^{lava}$ could be calculated both from equation (5) and from the coexistence of kalsilite and leucite.

In the pyroxenes there are two octahedral cation sites, an $m2$ site and a smaller $m1$ site together with the tetrahedral t sites. The activity can be written as

$$a_{CaMgSi_2O_6}^{pyroxene} = (X_{Ca}\gamma_{Ca})_{m2}\,(X_{Mg}\gamma_{Mg})_{m1}\,(X_{Si}^2\gamma_{Si})_t,$$

and we have assumed $\gamma_{Ca}\gamma_{Mg}\gamma_{Si} = 1$,

$$\text{where } X_{Ca} = n_{Ca}/(n_{Ca}+n_{Mn}+n_{Na}+n_{Mg^1}+n_{Fe^1}),$$

$$X_{Mg} = n_{Mg}/(n_{Mg^1}+n_{Fe^1}+n_{Al}+n_{Ti}+n_{Cr}),$$

$$X_{Si} = n_{Si}/(n_{Si}+n_{Al}),$$

where n_{Ca}, etc. is the number of atoms in the 6 oxygen pyroxene formula; note that n_{Mg^1} and n_{Fe^1} represent the amount of Mg and Fe required to equalize the number of cations in the $m1$ and $m2$ sites, and they are allotted in proportion to the Fe/Mg ratio of the pyroxene.

Similar reasoning and assumptions would give for orthopyroxene

$$a_{MgSiO_3}^{orthopyroxene} = [(X_{Mg})_{m2}\,(X_{Mg})_{m1}\,(X_{Si}^2)_t]^{\frac{1}{2}},$$

so that for typical aluminous orthopyroxenes of $Mg/Mg+Fe \approx 0.88$, the calculated $a_{MgSiO_3} \approx 0.73$. The interpretation of the experimental results on the mixing of the Fe–Mg pyroxenes is conflicting. Navrotsky (1971) has concluded that the orthopyroxenes are essentially ideal at temperatures above 1000 °C; Nafziger (1973) came to essentially the same conclusion for monoclinic pyroxenes in equilibrium with spinels. However, Williams (1971), dealing with much the same temperature range as Nafziger, optically identified his pyroxenes as orthorhombic on the basis of their straight extinction, and used a regular solution mixing model to represent their departure from ideality. Wood & Strens (1971) have used the two-site mixing model for orthopyroxene, and their calculated Fe/Mg ratio for pyroxenes in equilibrium with olivine agrees closely with the experimental results of Smith (1970).

An ideal multi-site mixing model is used for spinel in the source region, namely

$$a_{MgAl_2O_4}^{spinel} = (X_{Mg}\gamma_{Mg})\,(X_{Al}^2\gamma_{Al}) \quad \text{where } \gamma_{Mg}\gamma_{Al} = 1,$$

for these spinels contain only small amounts of spinel components with inverse structures, so that the activity of $MgAl_2O_4$ may be approximated by ideal ionic mixing in the octahedral and tetrahedral sites. For grossular garnet we have used the activity coefficient determined by Hensen *et al.* (1975) and we have also assumed ideal mixing of $NaAlSi_3O_8$ and $CaAlSi_2O_8$ in high temperature plagioclase.

Henceforth we use these activity–composition relations consistently throughout the remainder of this paper, noting that as we are calculating $a_{CaMgSi_2O_6}$ in the lava from the activity of $CaMgSi_2O_6$ in the groundmass augite, and later considering the equilibration of that lava with an augite in the mantle, then provided that we formulate the activity of $CaMgSi_2O_6$ in the same way for both, any errors will tend to cancel.

PHILOSOPHICAL TRANSACTIONS OF THE ROYAL SOCIETY A MATHEMATICAL, PHYSICAL & ENGINEERING SCIENCES

Values of $RT \ln \gamma^{\text{pyroxene}}_{NaAlSi_2O_6}$ *and* $RT \ln \gamma^{\text{pyroxene}}_{CaAl_2SiO_6}$

In basic lavas which contain a groundmass assemblage of plagioclase, olivine, calcium-rich pyroxene and iron–titanium oxides, the following reaction may be used to obtain the activity coefficient of $NaAlSi_2O_6$ in the augite pyroxene,

$$\underset{\text{solid}}{NaAlSi_2O_6} + \underset{\text{glass}}{SiO_2} = \underset{\text{solid}}{NaAlSi_3O_8}. \tag{14}$$

If the ideal contribution to the activity of $NaAlSi_2O_6$ (jd) in the pyroxene is expressed as

$$\hat{X}_{jd} = (X_{Na})_{m2}\,(X_{Al})_{m1}\,(X^2_{Si})_t,$$

then by using the temperature obtained from the coexisting iron–titanium oxides, and the activity of SiO_2 calculated from equation (5), the activity coefficient of jadeite can be calculated. Note that any errors in the standard state thermodynamic data, or in the assumption of ideal mixing in the feldspar are incorporated in this activity coefficient. As an example, we have set down the pertinent information for a basanite lava (Bacon & Carmichael 1973)

	T/K	$X^{\text{plagioclase}}_{NaAlSi_3O_8}$	$\ln a^{\text{lava}}_{SiO_2}$	$\hat{X}_{jd}$	$RT \ln \gamma_{jd}$
CSQ-3	1278	0.443	−1.9844	1.851×10^{-3}	5020 cal.†

The average value of $RT \ln \gamma_{jd}$ calculated from ten lavas, spanning the composition range of high alumina basalts, tholeiites and basanites, and the temperature range 1253–1353 K is

$$RT \ln \gamma_{jd} = 5580 \text{ cal with a standard deviation of } 1820 \text{ cal.}$$

Much of the error will reside in the microprobe analysis of Na_2O in the pyroxene. Ganguly (1973) has shown that jadeite–diopside compositions are virtually ideal above 1100 °C, but below this temperature there is not ideal mixing, and he represented the low-temperature mixing by a quadratic solution model (Rowlinson 1969).

Approximating the pyroxene solution as a binary between jadeite and 'others' the activity coefficient of jadeite becomes:

$$\ln \gamma_{jd} = W(1-\hat{X}_{jd})^2/RT$$

for the quadratic model. In the limit as $\hat{X}_{jd} \to 0$ (i.e. in the range appropriate for an infinite dilution approximation) we have

$$RT \ln \gamma_{jd} = W \quad \text{(a constant)}$$

in agreement with the formulation given above.

A similar approach on the same lavas has been used to determine $\gamma_{CaAl_2SiO_6}$ by using the reaction

$$\underset{\text{solid}}{CaAl_2SiO_6} + \underset{\text{glass}}{SiO_2} = \underset{\text{solid}}{CaAl_2Si_2O_8}. \tag{15}$$

If the ideal contribution to the activity of $CaAl_2SiO_6$ (cats) is expressed as

$$\hat{X}_{cats} = (X_{Ca})_{m2}\,(X_{Al})_{m1}\,4(X_{Al}X_{Si})_t,$$

then
$$\ln \gamma^{pyx}_{cats} = \Delta G^\circ/RT + \ln a^{\text{plagioclase}}_{CaAl_2Si_2O_8} - \ln X^{pyx}_{cats} + \ln a^{\text{lava}}_{SiO_2}$$

and the average value of $RT \ln \gamma^{pyx}_{cats}$ for the same ten lavas is

$$RT \ln \gamma^{pyx}_{cats} = 6700 \text{ cal} \quad \text{with a standard deviation of } 1730 \text{ cal.}$$

† 1 cal = 4.184 J.

PHILOSOPHICAL TRANSACTIONS OF THE ROYAL SOCIETY A MATHEMATICAL, PHYSICAL & ENGINEERING SCIENCES

Calculation of $RT \ln \gamma^{\text{olivine}}_{Ca_2SiO_4}$

Stormer (1973) has shown that calcium content of olivine in a magma is a function of silica activity, temperature and pressure, and it is appropriate to calculate the activity coefficient of Ca_2SiO_4 in groundmass olivine (1 bar) for lavas which have crystallized at known temperatures. By representing the mineralogical assemblage by

$$\underset{\text{Ca-olivine}}{\tfrac{1}{2}Ca_2SiO_4} + \underset{\text{forsterite}}{\tfrac{1}{2}Mg_2SiO_4} + \underset{\text{fayalite}}{Fe_2SiO_4} + \underset{\text{gas}}{\tfrac{1}{3}O_2} = \underset{\text{diopside}}{CaMgSi_2O_6} + \underset{\text{magnetite}}{\tfrac{2}{3}Fe_3O_4} \qquad (16)$$

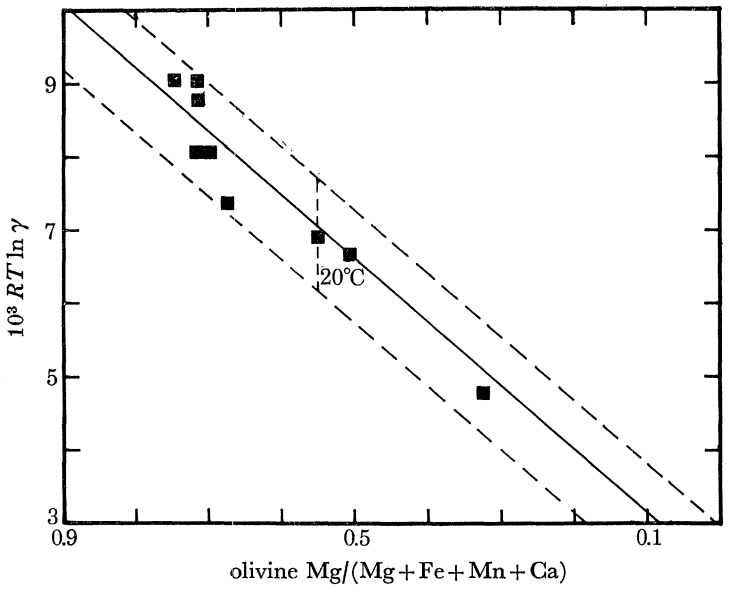

FIGURE 6. Plot of $RT \ln \gamma^{\text{olivine}}_{Ca_2SiO_4}$ at 1 bar against olivine composition using analyses of groundmass olivine in a variety of basalts. The limits of 20 °C variation in temperature are shown for one point. The equation of the least squares lines is given in the text.

for which $\Delta G^\circ/RT = -25223/T + 7.967$ in the temperature range 1100–1500 K. By rearrangement

$$\ln a^{\text{olivine}}_{Ca_2SiO_4} = \Delta G^\circ/RT + \ln \frac{a^{\text{pyroxene}}_{CaMgSi_2O_6} \cdot (a^{\text{titanomagnetite}}_{Fe_3O_4})^{\frac{2}{3}}}{(a^{\text{olivine}}_{Mg_2SiO_4})^{\frac{1}{2}} \cdot a^{\text{olivine}}_{Fe_2SiO_4} \cdot f_{O_2}^{\frac{1}{3}}},$$

and as $$a_{Ca_2SiO_4} = X^2_{Ca_2SiO_4} \gamma^2_{Ca_2SiO_4},$$

then $$\tfrac{1}{2}RT \ln a^{\text{olivine}}_{Ca_2SiO_4} = RT \ln X^{\text{olivine}}_{Ca_2SiO_4} + RT \ln \gamma^{\text{olivine}}_{Ca_2SiO_4}$$

and $RT \ln \gamma^{\text{olivine}}_{Ca_2SiO_4}$ for nine lavas, basanites and tholeiites, is plotted as a function of olivine composition in figure 6. Although there is some scatter, presumably arising from errors in both temperature and Ca determinations the line of best fit is

$$RT \ln \gamma^{\text{olivine}}_{Ca_2SiO_4} = 8651 X_{Mg} + 2286 \qquad (17)$$

with a correlation coefficient of 0.92.

This line is in accord with regular solution theory, for in a ternary regular solution of Ca_2SiO_4, Fe_2SiO_4 and Mg_2SiO_4 (Prigogine & Defay 1954, p. 257)

$$RT \ln \gamma_{Ca_2SiO_4} = (X_{Fe_2SiO_4})^2 W_{Fe\text{–}Ca} + (X_{Mg_2SiO_4})^2 W_{Mg\text{–}Ca} + (X_{Fe_2SiO_4} X_{Mg_2SiO_4})(W_{Fe\text{–}Ca} - W_{Fe\text{–}Mg} + W_{Mg\text{–}Ca}), \qquad (18)$$

where W represents the interaction between the subscript components, and is a constant for each interaction. If Mg–Fe exchange in olivines is assumed to be ideal, then $W_{\mathrm{Fe-Mg}} = 0$, and since the amount of Ca_2SiO_4 in these olivines is small ($X_{Ca_2SiO_4} = 0.0051$–0.0092), they can be considered as a binary Fe–Mg solid solution. Thus

$$X_{Fe_2SiO_4} = (1 - X_{Mg_2SiO_4}) \tag{19}$$

and by substituting equation (19) into (18) we find that

$$RT \ln \gamma^{\mathrm{olivine}}_{Ca_2SiO_4} = X_{Fe_2SiO_4} W_{\mathrm{Fe-Ca}} + X_{Mg_2SiO_4} W_{\mathrm{Mg-Ca}},$$

which is a straight line in agreement with the results in figure 6.

With a knowledge of $RT \ln \gamma^{\mathrm{olivine}}_{Ca_2SiO_4}$, the activity of silica can be calculated in those lavas without iron–titanium oxides, and other combinations of phases to define silica activity. The appropriate reaction is

$$\underset{\text{Ca-olivine}}{\tfrac{1}{2}Ca_2SiO_4} + \underset{\text{forsterite}}{\tfrac{1}{2}Mg_2SiO_4} + \underset{\text{glass}}{SiO_2} = \underset{\text{diopside}}{CaMgSi_2O_6}. \tag{20}$$

As the leucite–basanites from Vesuvius do not contain a groundmass mineral assemblage which conveniently define silica activity, the coexisting olivine and pyroxene using equation (20) and the appropriate value for $RT \ln \gamma_{Ca_2SiO_4}$ from equation (17) are used to calculate their activities of silica.

The discussion so far has treated the activity–composition relations of various solid solutions in a rather empirical way, either making plausible assumptions of ideal multi-site mixing, or obtaining activity coefficients from standard-state free energy data coupled with ideal mixing of the solid solution used to define the activity of the chosen component. For liquids the situation is more difficult, as there is far less experimental work to indicate the appropriate mixing model. For this reason the thermodynamics of solutions are considered in more detail, although they apply to all solutions, liquid or solid.

Activity–composition relations: liquids

Before examining the pressure and temperature dependence of the activity coefficients in the liquid, so as to take account of both increasing pressure and temperature in the inverse path of the lava, it is necessary to digress into how γ_i is calculated given that a_i is known. This requires that the ideal contribution to the activity of i, $\hat{X}_i$, be known, or formulated.

Calculation of $\ln \hat{X}_i^{\mathrm{liquid}}$

In order to obtain a value for $\ln \gamma_i^{\mathrm{liquid}}$, given that

$$\ln \gamma_i^{\mathrm{liquid}} = \ln a_i^{\mathrm{liquid}} - \ln \hat{X}_i^{\mathrm{liquid}},$$

some method must be found for calculating the ideal contribution to the activity of the multi-oxide compounds that we use here. It is clear that $\hat{X}_{SiO_2}$ and $\hat{X}_{Al_2O_3}$ could be represented by the mole fractions of the two oxides reported in the chemical analysis of the lava. However, $\hat{X}_{CaMgSi_2O_6}$, the ideal contribution to the activity, is not so obviously calculated, and we have used the following method which has been borrowed from aqueous electrolyte chemistry (Klotz 1964, p. 391). Consider for example a pure $CaMgSi_2O_6$ liquid for which we may write

$$\underset{\text{liquid}}{CaO} + \underset{\text{liquid}}{MgO} + \underset{\text{liquid}}{2SiO_2} = \underset{\text{liquid}}{CaMgSi_2O_6}.$$

Since it is pure liquid, then $\hat{X}^{\text{liquid}}_{CaMgSi_2O_6} = 1$. But we wish to use the simple liquid oxides, as components so that we define

$$\hat{X}^{\text{liquid}}_{CaMgSi_2O_6} = 1 = [(X^{\text{liq}}_{SiO_2})^2\, X^{\text{liq}}_{CaO}\, X^{\text{liq}}_{MgO}]\, \lambda^*$$

and thus

$$\hat{X}^{\text{liquid}}_{CaMgSi_2O_6} = (\tfrac{1}{2})^2\, \tfrac{1}{4}\, \tfrac{1}{4}\, \lambda^* = 1,$$

so that $\lambda^* = 64$ and λ^* is a factor which depends on stoichiometry and will make $\hat{X} = 1$ for the pure liquid compound. Similar reasoning gives for:

$$\hat{X}^{\text{liquid}}_{Fe_2SiO_4} = \lambda^* [(X^{\text{liq}}_{FeO})^2\, X^{\text{liq}}_{SiO_2}] \quad \text{where } \lambda^* = 6.75,$$

$$\hat{X}^{\text{liquid}}_{NaAlSi_3O_8} = \lambda^* [(X^{\text{liq}}_{Na_2O})^{\frac{1}{2}}\, (X^{\text{liq}}_{Al_2O_3})^{\frac{1}{2}}\, (X^{\text{liq}}_{SiO_2})^3] \quad \text{where } \lambda^* = 18.963.$$

The pressure and temperature dependence of activity coefficients

Although experiments can be devised to determine the temperature dependence of the Gibbs free-energy of a multi-component silicate liquid, natural silicate liquids have such a large range of composition that the experimental effort required would be enormous. It is far more practical at this stage to thermodynamically model the temperature dependence of the activity coefficients, which are related to the Gibbs free energy of the solution by

$$G = \sum_i n_i \mu_i$$

from which the excess Gibbs free energy (G^{xs}) is given by the relation $G = G^\circ + G^{\text{ideal}} + G^{xs}$ and so

$$G^{xs} = RT \sum_i n_i \ln \gamma_i.$$

If this equation is differentiated at constant temperature and pressure we obtain

$$\mathrm{d}G^{xs} = RT \sum_i n_i \mathrm{d} \ln \gamma_i + RT \sum_i \ln \gamma_i \mathrm{d}n_i,$$

so that under the stated constraints, the first term on the right is zero as required by the Gibbs–Duhem equation, and

$$(\partial G^{xs}/\partial n_i)_{T,P,nj} = \mu_i^{xs} = RT \ln \gamma_i.$$

Using the partial molar quantities, we have

$$V_i = V_i^\circ + RT\, (\partial \ln \gamma_i/\partial P)_{T,nj}, \tag{21}$$

$$S_i = S_i^\circ - R \ln a_i - RT (\partial \ln \gamma_i/\partial T)_{P,nj}, \tag{22}$$

$$H_i = H_i^\circ - RT^2\, (\partial \ln \gamma_i/\partial T)_{P,nj}, \tag{23}$$

$$C_{p,i} = C_{p,i}^\circ - 2RT\, (\partial \ln \gamma_i/\partial T)_{P,nj} - RT^2\, (\partial^2 \ln \gamma_i/\partial T^2)_{P,nj}. \tag{24}$$

The other excess partial functions can be obtained by subtraction of the ideal quantities.

It has been shown above that the activity (relative to a liquid standard state) of several components in the lava can be calculated from the composition of the solid assemblage. It is now necessary to determine how these liquid activity coefficients change with P and T in the absence of solids, as the original P–T path of the magma from its source is inverted. The liquid is assumed to be of constant composition for reasons discussed in the beginning of this paper.

PHILOSOPHICAL TRANSACTIONS OF THE ROYAL SOCIETY A MATHEMATICAL, PHYSICAL & ENGINEERING SCIENCES

The pressure dependence of γ_i. From equation (21), the pressure dependence of γ_i can be obtained if values of $\bar{V}_i$ and V_i° are known as a function of pressure and temperature. The partial molar volumes, $\bar{V}_i$ for several oxide components in silicate liquids at 1 bar have been calculated by Bottinga & Weill (1970); a least-squares fit to their data is given in table 10. As there is no simple way to define the properties of a stoichiometric compound when it is dissolved in a non-stoichiometric liquid, we have assumed that, for example,

$$\bar{V}_{Fe_2SiO_4} = 2\bar{V}_{FeO} + \bar{V}_{SiO_2} \text{ and } \bar{V}_{NaAlSi_3O_8} = \tfrac{1}{2}\bar{V}_{Na_2O} + \tfrac{1}{2}\bar{V}_{Al_2O_3} + 3\bar{V}_{SiO_2}.$$

TABLE 10. LEAST SQUARED VALUES OF $\bar{V}$ AFTER BOTTINGA & WEILL (1970). ALSO SHOWN ARE $\bar{V} - V^\circ$ FOR THE LIQUID COMPOUNDS USED IN THIS PAPER (UNITS OF cal/bar)

	$10^6 \times \bar{a}_L$	$\bar{b}_L$
SiO_2	6.15	0.6304
TiO_2	64.65	0.3937
Al_2O_3	24.37	0.8664
FeO	47.80	0.2259
MgO	64.65	0.1683
CaO	71.70	0.2744
Na_2O	164.33	0.4157
K_2O	329.51	0.5482

	$\bar{V} - V^0$ in the form of $aT + b + cP + dPT$			
	$10^6 \times a_L^\circ$	b_L°	$10^6 \times c_L^\circ$	$10^{12} \times d_L^\circ$
SiO_2	5.09	−0.02110	−1.162	2.429
Fe_2SiO_4	0	0	0	0
$KAlSi_3O_8$	117.36	−0.1457	0	0
$NaAlSi_3O_8$	−59.10	0.1595	0	0
$CaMgSi_2O_6$	−29.60	0.0952	0	0
TiO_2	8.68	0.0050	0	0
Al_2O_3	−306.62	0.8265	0	0

As we have expressed the variation of the volume of the liquid compounds (table 7) as

$$V^\circ = a_L^\circ T + b_L^\circ + c_L^\circ P,$$

then by subtraction of this expression for V° from $\bar{V}$ gives $\bar{V} - V^\circ$. We find

$$\bar{V} - V^\circ = (\overline{a_L} - a_L^\circ)\ T + (\overline{b_L} - b_L^\circ) + (\overline{c_L} - c_L^\circ)\ P,$$

but as there are no data available on $\overline{c_L}$, we have assumed that $\overline{c_L} = c_L^\circ$ or in other words that $\bar{V} - V^\circ$ is independent of pressure. Only for SiO_2 is this not the case, for V° refers to the standard state of SiO_2 glass, whereas $\bar{V}$ refers to SiO_2 in the liquid solution. It is well known that β for liquids is greater than for the corresponding glasses and we have used the value $(\overline{c_L})_{SiO_2} = (\partial \bar{V}/\partial P)_T = -2.66 \times 10^{-6}$ which is the mean value of the extrapolation of the compressibility of Na_2O–SiO_2 liquids and K_2O–SiO_2 liquids (Janz 1967) to pure SiO_2.

Thus with the exception of SiO_2, the integration of $\bar{V} - V^\circ$ in equation (21) can be assumed to be independent of pressure, so that between the limits of 1 and P bars

$$(\ln a_i^{liq})_T = (\ln a_i^{lava})_T^{1\,bar} + \frac{\bar{V} - V^\circ}{RT}(P - 1). \qquad (25)$$

The temperature dependence of γ_i. There are few data on multicomponent silicate liquids, corresponding to lavas, to indicate the form of the temperature dependence of γ_i, although

PHILOSOPHICAL TRANSACTIONS OF THE ROYAL SOCIETY A MATHEMATICAL, PHYSICAL & ENGINEERING SCIENCES

Burnham (1975) has suggested that with the appropriate choice of components, signifying polymerization of SiO_2 and $NaAlSi_3O_8$, natural silicate liquids saturated with H_2O, may mix ideally ($\gamma = 1$), a conclusion also reached by Flood & Knapp (1968) for anhydrous binary systems of SiO_2 and the feldspar components. Until vapour pressure measurements have been made of the components in equilibrium with silicate liquids, it is not possible to predict what polymer arrangements are present in multicomponent silicate liquids, and no consistent group of polymeric components can yet be chosen that will allow their activity coefficients to become unity. As the data to support any chosen mixing model are sparse, a simple model has obvious advantages, provided that it can reproduce liquid–solid phase equilibria.

One such is the quadratic solution model (Rowlinson 1969) and in a binary system, the excess free-energy per mole of this solution is given by

$$G^{xs} = X_1 X_2 W,$$

which satisfies the requirement that G^{xs} should be zero for pure X_1 or X_2. By differentiation

$$(\partial G^{xs}/\partial n_i)_{\rho, T, nj} = \mu_i^{xs} = (1 - X_i)^2 W, \tag{26}$$

so that

$$\mu_i = \mu_i^{\circ} + RT \ln X_i + (1 - X_i)^2 W, \tag{27}$$

or

$$\ln a_i = \ln X_i + \frac{(1 - X_i)^2 W}{RT},$$

where W is called an interaction parameter, with units of cal mol^{-1}. From equation (26) we obtain

$$\left(\frac{\partial \mu^{xs}}{\partial T}\right)_{P, nj} = (1 - X_i)^2 \left(\frac{\partial W}{\partial T}\right)_{P, nj} = -\bar{S}_i^{xs} \tag{28}$$

and

$$T\left(\frac{\partial S^{xs}}{\partial T}\right)_{P, nj} = (1 - X_i)^2 \left(-\frac{\partial^2 W}{\partial T^2}\right)_{P, nj} = \bar{C}_{Pi}^{xs}. \tag{29}$$

If $(\partial W/\partial T)_P$ is zero, then a quadratic solution is called a regular solution, which has therefore as its necessary conditions that $(\partial RT \ln \gamma_i/\partial T)_P = 0$ (equation (22)) and $C_P^{xs} = 0$ which has been established in the first part of this paper.

Several investigators have shown that a regular solution model will account for the observed behaviour of the activity coefficient in silicate liquids; thus Lumsden (1961) was able to treat the liquids of the system FeO–Fe_2O_3–SiO_2, over a temperature range of 200 °C, as a ternary regular solution, Somerville *et al.* (1973) similarly modelled liquids of the four component system $FeO + MnO + AlO_{1.5} + SiO_2$ at 1550 °C, and Nicholls & Carmichael (1972) showed that liquids saturated with corundum in the system Na_2O–Al_2O_3–SiO_2 behaved as regular solutions.

The approach taken in this paper also uses the regular solution model for lavas, following the lead of Kudo & Weill (1970), but with the added restriction that the composition of the lava remains constant. Nicholls & Carmichael (1972) used the following formulation

$$\ln a_i = \ln X_i + \phi_i/T, \tag{30}$$

so that from equation (27)

$$\frac{\phi_i}{T} = \frac{(1 - X_i)^2 W}{RT} = \ln \gamma_i \tag{31}$$

for a binary solution; note that for a liquid of constant composition $(1 - X_i)^2 W/R$ is a constant.

By combining equation (30) with (25) we obtain

$$(\ln a_i^{\mathrm{liq}})^{P,T} = \ln X_i + \frac{\phi_i}{T} + \frac{\bar{V} - V^\circ}{RT}(P-1), \tag{32}$$

which gives the temperature and pressure dependence of the activity of i in a liquid of constant composition.

If instead of treating equilibrium between a pure liquid and a pure solid compound as in equation 3, we retain the $\ln K$ term to account for both liquid and solid solutions, we have

$$(\ln a_i^{\mathrm{liq}})^{P,T} = \frac{1}{RT}\Big\{\Delta H_{T_r} + \int_{T_r}^{T} (C_{p,\,\mathrm{solid}} - C_{p,\,\mathrm{liq}})\,\mathrm{d}T - T\Big[\Delta S_{T_r} + \int_{T_r}^{T}\Big(\frac{C_{p,\,\mathrm{solid}}}{T} - \frac{C_{p,\,\mathrm{liq}}}{T}\Big)\,\mathrm{d}T\Big] + \int_1^P (V_{\mathrm{solid}} - V_{\mathrm{liq}})\,\mathrm{d}P + RT\ln a_i^{\mathrm{solid}}\Big\}.$$

If this equation is now combined with equation (32), we obtain

$$\ln X_i + \phi_i/T + (\bar{V}_i - V_i^\circ)\,(P-1)/RT = \Big[\Delta H^\circ_{T_r} + \int_{T_r}^{T} \Delta C_p^\circ\,\mathrm{d}T - T\Big(\Delta S^\circ_{T_r} + \int_T^T \frac{\Delta Cp\,\mathrm{d}T}{T}\Big) + \int_1^P \Delta V^\circ\,\mathrm{d}P + RT\ln \Pi a_i^{\mathrm{solid}}\Big]\frac{1}{RT}, \tag{33}$$

in which the left hand side gives the variation of $\ln a_i$ with P and T in the silicate liquid equivalent to the lava, and the right hand side incorporates a term ($RT\ln \Pi a_i^{\mathrm{solid}}$) for the composition of the single solid, or an assemblage of solids, which define the activity of i at P and T. In the integration of the standard state volume change of the reaction, both the thermal expansion, or rather $\mathrm{d}V/\mathrm{d}T$ (table 8) and compressibility are included, and are both assumed to be independent of temperature and pressure respectively. Equation (33) is the general equation used in this paper to calculate the condition of equilibration of a liquid with a solid, and is solved on a computer for P as a function of T.

The regular solution formulation applied to experimental equilibria

By using ϕ_i, calculated at 1 bar† and the lava quench temperature, the $P-T$ conditions of equilibration of a lava with olivine, or any other phase, may be compared to experimental results. Those of Bultitude & Green (1971) are used here, as these authors provide considerable information on the composition of the solids in equilibrium with liquid, and of their experimental compositions, the picrite–nephelinite has the most abundant information on olivine. On the assumption that the liquidus of this lava at 1 bar is 1400 °C, and the composition of the olivine Fa_9, then the calculated P–T curves of equilibration with olivine of varied composition are shown in figure 7.

If in addition to the results shown in figure 7, the remainder of Bultitude & Green's experiments are used, we find that the average difference between observed and calculated conditions for 27 data points for olivine and liquid is 0.84 % Fe_2SiO_4 in the composition of the olivine, 39.8 °C in temperature and 5.7 kbar in pressure. For 5 data points involving augite and liquid,

† The procedure to do this has been set out in detail by Nicholls & Carmichael (1972) and by Carmichael *et al.* (1974) (pp. 111–118) and thus need not be repeated here.

PHILOSOPHICAL TRANSACTIONS OF THE ROYAL SOCIETY A MATHEMATICAL, PHYSICAL & ENGINEERING SCIENCES

the average difference between observed and calculated conditions is 0.003 in the mole fraction of $CaMgSi_2O_6$ in the augite, 29 °C in temperature and 3.0 kbar in pressure. These errors are believed to be typical of using a regular solution model for the calculation of P–T equilibration conditions, but of necessity we have ignored any errors in composition, temperature and pressure in Bultitude & Green's results.

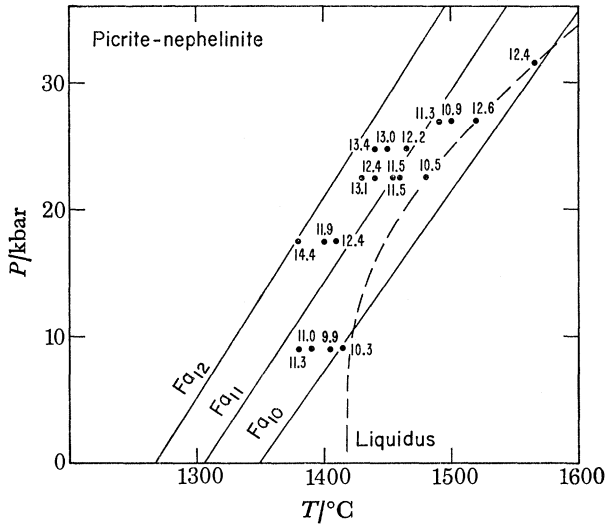

FIGURE 7. Compositions of near liquidus olivine given as % Fa for a picritic–nephelinite (Bultitude & Green 1971). The calculated lines of equilibration of this lava with various olivine compositions are shown. The liquidus of this lava is also shown.

Equilibration of basic lavas with stipulated source material

The composition of the solid residue with which we calculate the equilibration conditions of various lava types is augite ($a_{CaMgSi_2O_6} = 0.4$; $\hat{X}_{NaAlSi_2O_6} = 0.03$), spinel ($a_{MgAl_2O_4} = 0.614$), garnet ($X_{Ca_3Al_2Si_3O_{12}} = 0.18$) together with olivine ($X_{Mg_2SiO_4} = 0.90$) and orthopyroxene ($a_{MgSiO_3} = 0.73$). These minerals represent a typical solid residue judging from the composition of lherzolite nodules and relevant experimental equilibria (Aoki & Shiba 1973; Boyd 1969; Binns *et al.* 1970; Bacon & Carmichael 1973; Green 1973*a*).

By using equations (6) and (7) (table 8) for Fe_2SiO_4 and $CaMgSi_2O_6$ put in the form of equation (33), P–T lines of equilibration of the lava with the stated mineral compositions can be obtained. In addition, the activities of the SiO_2 and Al_2O_3 components will be defined in the solid residue by

$$\underset{\text{forsterite}}{Mg_2SiO_4} + \underset{\text{glass}}{SiO_2} = \underset{\text{orthoenstatite}}{2MgSiO_3} \tag{34}$$

and then at P and T

$$(\ln a_{SiO_2}^{\text{liquid}})^{P,T} = \Delta G^\circ_{34}/RT + \int_1^P \frac{\Delta V^\circ}{RT}\,dP + \ln \frac{(a_{MgSiO_3}^{\text{pyroxene}})^2}{a_{Mg_2SiO_4}^{\text{olivine}}}$$

and for the Al_2O_3 component

$$\underset{\text{forsterite}}{Mg_2SiO_4} + \underset{\text{liquid}}{Al_2O_3} = \underset{\text{orthoenstatite}}{MgSiO_3} + \underset{\text{spinel}}{MgAl_2O_4}, \tag{35}$$

and

$$\underset{\text{diopside}}{3CaMgSi_2O_6} + \underset{\text{liquid}}{Al_2O_3} = \underset{\text{garnet}}{Ca_3Al_2Si_3O_{12}} + \underset{\text{orthoenstatite}}{3MgSiO_3}, \tag{36}$$

PHILOSOPHICAL TRANSACTIONS OF THE ROYAL SOCIETY A MATHEMATICAL, PHYSICAL & ENGINEERING SCIENCES

and for the $NaAlSi_3O_8$ component

$$\underset{\text{liquid}}{NaAlSi_3O_8} + \underset{\text{forsterite}}{Mg_2SiO_4} = \underset{\text{orthoenstatite}}{2MgSiO_3} + \underset{\text{jadeite}}{NaAlSi_2O_6}, \tag{37}$$

and for the TiO_2 component

$$\underset{\text{liquid}}{TiO_2} + \underset{\text{forsterite}}{Mg_2SiO_4} + \underset{\text{fayalite}}{Fe_2SiO_4} = \underset{\text{orthoenstatite}}{2MgSiO_3} + \underset{\text{ulvospinel}}{Fe_2TiO_4}. \tag{38}$$

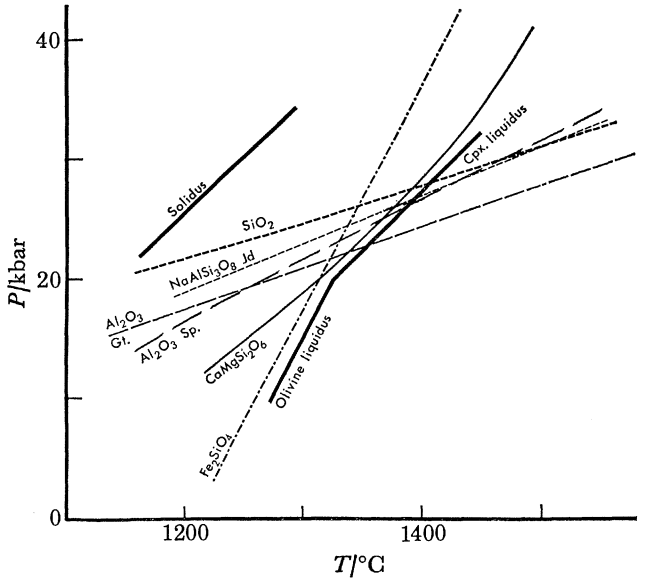

FIGURE 8. Plot of calculated equilibration lines for a basanite lava CSQ-3 for various components with a stipulated solid residue. Thus SiO_2 refers to equilibration of the SiO_2 component in the lava with olivine + orthopyroxene; Al_2O_3 Gt. to the component Al_2O_3 in the lava with garnet etc (reaction (36)); Al_2O_3 Sp. to the component Al_2O_3 in the lava with spinel, etc. (reaction (35)); $NaAlSi_3O_8$ Jd to the $NaAlSi_3O_8$ in the lava with jadeite, etc. (reaction (37)); $CaMgSi_2O_6$ and Fe_2SiO_4 in the lava with solid $CaMgSi_2O_6$ ($a = 0.4$) and olivine (Fa_{15}) respectively. The solidus, olivine–liquidus and augite (cpx)–liquidus are taken from Arculus (1975) for a basanite of similar composition.

Typical results for a basanite lava are shown in figure 8, in which it can be seen that the calculated olivine–liquid equilibration has a slope almost identical to that segment of the olivine liquidus of a similar basanitic lava (Arculus 1975); the calculated augite–liquid equilibration also matches closely the segment of the pyroxene liquidus found by Arculus. However, the composition of the olivine is Fa_{15} rather than Fa_{10} which is the typical olivine composition of lherzolite nodules; perhaps the olivine stable at depth in these basanitic lavas is more Fe-rich and the cause of this may lie in the small water content of these lavas at depth. Note that in figure 8 the calculated P–T equilibration lines extend into the unstable region, i.e. both above the experimental liquidus and below the solidus, so that it behoves one to check that the calculated P–T equilibration conditions do lie in the stable liquid region of the lava.

The calculated equilibration values for a variety of lava types are given in table 11, and for all, the same composition of solid residue is assumed, with the exception of the olivine–tholeiites and the potassic lava ugandite.

Olivine–tholeiites

The two Icelandic olivine–tholeiites equilibrate with a postulated mantle residue at relatively low pressures and temperatures, close to the transition plagioclase-spinel in pyrolite (figure 9; Green 1970); accordingly garnet as a phase was omitted from the calculations. It is satisfying to find that these two lavas plot above the anhydrous pyrolite solidus, and in the spinel field, for O'Nions & Grönvold (1973) have shown that Icelandic olivine–tholeiites do not have an Eu anomaly. Thus plagioclase was either completely consumed in their generation, or the ambient oxygen fugacity suppressed the Eu anomaly (Weill & Drake 1973), or plagioclase was not a phase contributing to these partial melts.

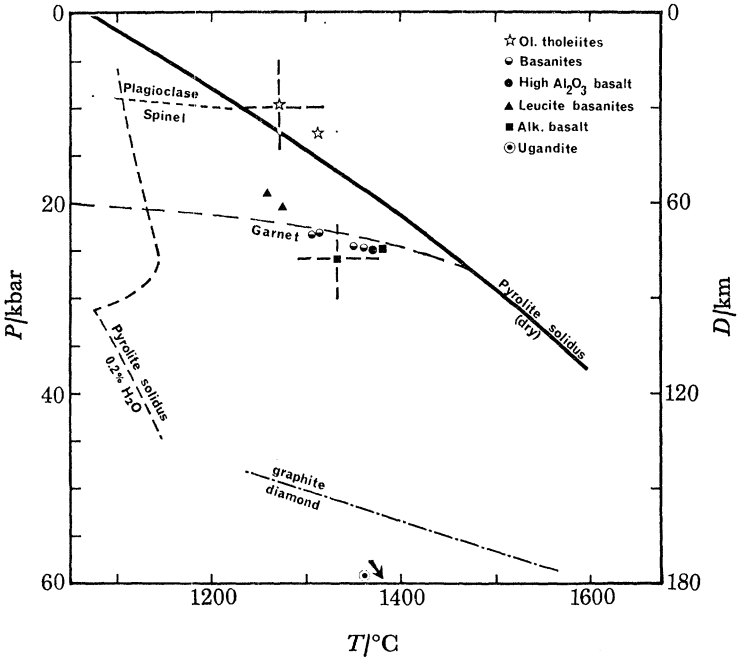

FIGURE 9. Calculated equilibration pressures and temperatures (table 11) plotted in relation to the melting temperatures of pyrolite. The dry and wet pyrolite solidus curves are taken from Green (1973), the plagioclase–spinel boundary from Green (1970) and the spinel–garnet boundary from O'Hara *et al.* (1971). Typical errors (±40°; ±5.7 kbar) are shown for two lava types.

Basanites and alkali-basalts

The basanites and alkali-basalts all plot in an area in figure 9 which suggests that they were in equilibrium with a solid residue at temperatures below the anhydrous pyrolite solidus. The solid residue in this case includes garnet and spinel, and although these two minerals may be antipathetic in simple silicate systems, with spinel transforming to garnet with increasing pressure, a spinel phase is found in many garnet-lherzolites, and also as an inclusion in diamond (Meyer & Boyd 1972), which suggests that it is stable as a Cr-rich variety to very high pressures. The calculated activity of Fe_2TiO_4 in the spinel at the equilibration conditions is significantly smaller ($a_{Fe_2TiO_4} \approx 0.005$) than for the tholeiites.

Green (1973*b*) has determined the liquidus relations, with and without water, of a basanitic

liquid, and his results are depicted in figure 10, together with the calculated P–T values of the lavas taken from table 11. If the small stability field of orthopyroxene is appropriate to all these lavas, then each should fall at the junction of the orthopyroxene field with garnet, olivine and augite, the stipulated solid residue. As the effect of water has not been taken account of explicitly in the calculations, either by assuming the effect of diluting the components without any specific interaction with an individual component, or by assuming a specific interaction, the lack of correspondence of the plotted points with the anhydrous pyrolite solidus could be the result of errors in the thermodynamic data.

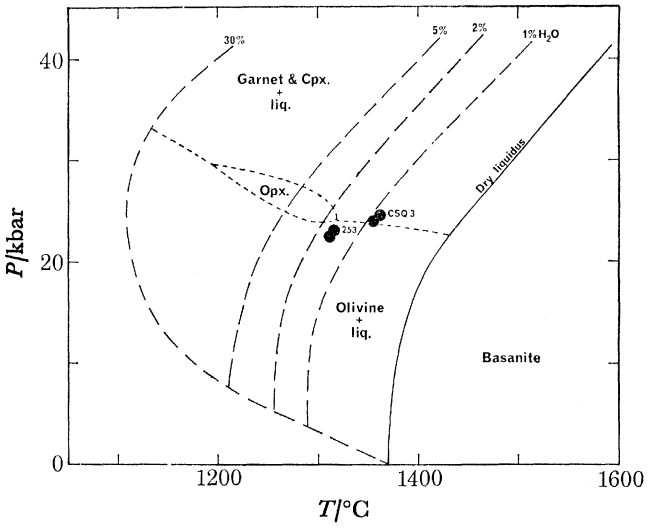

FIGURE 10. Experimental liquidus temperatures and stability fields for various amounts of water (weight percent) for a basanite lava (Green 1973). The four basanites of table 11 are plotted, and indicate water contents of less than 2%.

The concentrations of trace-elements, particularly their enrichment in the light rare-earths, have suggested that basanite liquids were in equilibrium with garnet at depth (Gast 1968; Kay & Gast 1973); the writers, while not suggesting otherwise, are reticent to accept any melting model of source material which excludes apatite, in which the light rare-earths are strongly enriched (Carmichael 1967*a*), especially as basanitic lavas show a correlation between the concentration of phosphorous and rare-earths (see, for example, Arculus & Shimizu 1974).

High-alumina basalt

The calculated equilibration conditions of this lava type with the solid residue fall in the spinel stability field of pyrolite in accord with the subdued rare-earth pattern of this lava type (Gast 1968), which suggests that garnet was not a residual phase.

Highly potassic lavas

Ugandite lavas and cinder cones in the African Rift valley (Brown 1971) are geographically associated with sporadic diamonds (Reece 1961) which would suggest that the source region of this magma type is in the diamond stability field (figure 9). However, it was impossible to obtain the types of intersection shown in figure 8 unless pyroxene with a high activity of the $CaMgSi_2O_6$ component was used. Thus the calculated equilibration conditions are very uncertain (table 11),

but fall in the diamond field. However, small amounts of CO_2 dissolved in the magma would tend to raise the activity of silica, as CO_2 causes the precipitation of enstatite in the system Mg_2SiO_4–Ca_2SiO_4 (Eggler 1975) and would thus reduce both the calculated temperature and pressure.

TABLE 11. CALCULATED EQUILIBRATION PRESSURES AND TEMPERATURES WITH SOLID RESIDUE DEFINED IN THE TEXT. THE CALCULATED ACTIVITIES OF Fe_2TiO_4 IN THIS RESIDUE ARE GIVEN FOR THE AVERAGE EQUILIBRATION CONDITIONS. THE ERRORS ARE DISCUSSED IN THE TEXT AND ARE CONSIDERED TO BE $\pm 40°$ AND ± 5.7 kbar

lava-type basanites	pressure/kbar	temperature/°C	$a_{Fe_2TiO_4}$
253	22.8	1314	0.0049
256	22.4	1311	0.0052
CSQ-3	24.7	1361	0.0049
CSQ-28	24.1	1356	0.0050
alkali-basalts of Lake Rudolph, Kenya			
SIC-3	26.2	1335	0.0055
SSC-7	24.1	1412	0.0058
high-alumina basalt, Hat Creek, California			
Cal 63	24.1	1393	0.0046
leucite-basanites of Vesuvius			
1760 AD flow 94–14	17.6	1261	—
1631 AD flow 94–18	20.8	1274	—
olivine tholeiites, Thingmuli, Iceland			
H-128	12.6	1311	0.014
H-6	9.8	1272	0.015
Makaopuhi Lava Lake, Hawaii	6.5	1280	—
ugandite, African Rift Valley, Uganda			
U-111	> 60.0	> 1350	

Data on the lavas taken from Bacon & Carmichael (1973), Brown & Carmichael (1971), Brown (1971), Smith & Carmichael (1968, 1969), Carmichael (1964, 1967*a*, *b*), Wright and Weiblen (1967), and unpublished data on the leucite-basanites of Vesuvius.

It should be apparent that the calculated equilibration conditions for all the various lava types depend completely upon the choice made for the composition of the minerals in the solid residue. Perhaps a more fruitful approach would be to reiterate the calculations by changing the composition of the solid solutions until all the curves intersected at a point in P–T space. As temperature shows such a sensitive response to change in composition (cf. figure 7), the calculated conditions may not be very different to those shown in table 11.

Ultrabasic nodules, basanites and their megacrysts

The occurrence of ultrabasic nodules, often well rounded, is a distinctive feature of basanite lavas both on the continents and on the continental side of island arcs. Very often these nodules display internal equilibration temperatures (MacGregor & Basu 1974) which are much lower than those of the lava at any point in its ascent. Although the internal equilibration temperatures and pressures are based essentially on the extrapolation of the $CaMgSi_2O_6$–$MgSiO_3$ solvus (Boyd 1973; Mercier & Carter 1975) to natural pyroxenes, there is a great range even within one nodule

PHILOSOPHICAL TRANSACTIONS OF THE ROYAL SOCIETY A MATHEMATICAL, PHYSICAL & ENGINEERING SCIENCES

(Wilshire & Jackson 1974), and the inferred conditions seem highly uncertain. This evidence, coupled with the Sr isotopic data (Stueber & Ikramuddin 1974), suggests that many nodules are foreign to the lavas in which they are found and it seems unlikely that any of the nodules represent crystalline source material expelled with the lava. However, if ultrabasic nodules, representing an internal equilibration range of 800–1100 °C and approximately 3–30 kbar (MacGregor & Basu 1974) become engulfed in the lava on its ascent to the surface, there must be a thermal response of the hot magma (1200–1350 °C) to the cooler nodules. One such response could be the precipitation of crystals, namely the megacrysts that are commonly found in nodule-containing basanite lavas.

As the ultrabasic nodules can only be incorporated from the mantle, at depths roughly speaking in excess of 35 km for the continental basanites, the equilibration of the megacryst assemblage should indicate pressures greater than this, and temperatures appropriate to the lava liquidus. One of the curious features of megacrysts (Bacon & Carmichael 1973) is that they are almost unzoned compositionally, but there may be several different compositional populations of the same phase. These populations often show only a small range in composition.

Binns *et al.* (1970) provide abundant analytical data on the composition of the megacrysts found in an Armidale (N.S.W.) basanite. The phases present as large crystals are augite, olivine, orthopyroxene, feldspar, spinel and zircon. By using the relevant activity coefficients noted above, the following solid–solid reactions can be plotted as curves in P–T space on the assumption that the assemblage of megacrysts are in equilibrium:

$$\underset{\text{solid}}{CaMgSi_2O_6} + \underset{\text{orthoenstatite}}{MgSiO_3} + \underset{\text{solid}}{MgAl_2O_4} = \underset{\text{solid}}{CaAl_2Si_2O_8} + \underset{\text{solid}}{Mg_2SiO_4}, \tag{39}$$

$$\underset{\text{solid}}{NaAlSi_2O_6} + \underset{\text{orthoenstatite}}{2MgSiO_3} = \underset{\text{solid}}{NaAlSi_3O_8} + \underset{\text{solid}}{Mg_2SiO_4}, \tag{40}$$

and

$$\underset{\text{solid}}{ZrO_2} + \underset{\text{orthoenstatite}}{2MgSiO_3} = \underset{\text{solid}}{Mg_2SiO_4} + \underset{\text{solid}}{ZrSiO_4}. \tag{41}$$

Note that as ZrO_2 is absent among the megacryst assemblage, the equilibration conditions have to be confined to the olivine–zircon field.

If the composition of the lava containing the megacrysts is also known (including the composition of all the mineral phases), then by using equation (33), the P–T lines of equilibration can be plotted for the lava with each type of megacryst. For the two basanites from San Quintin, Baja California (Bacon & Carmichael 1973), the megacrysts are assumed to be common to both, and the following results are obtained:

		P/kbar	T/°C
Armidale basanite		20.0	1225
San Quintin basanites	CSQ-3	17.3 ± 2	1236 ± 45
	CSQ-28	16.0 ± 2	1234 ± 45

These results are plotted in figure 11 and show that for any reasonable depth of mantle, the megacryst assemblage, assumed to be in equilibrium, corresponds to mantle pressures. Green & Hibberson (1970) were able to duplicate experimentally the composition of the pyroxene

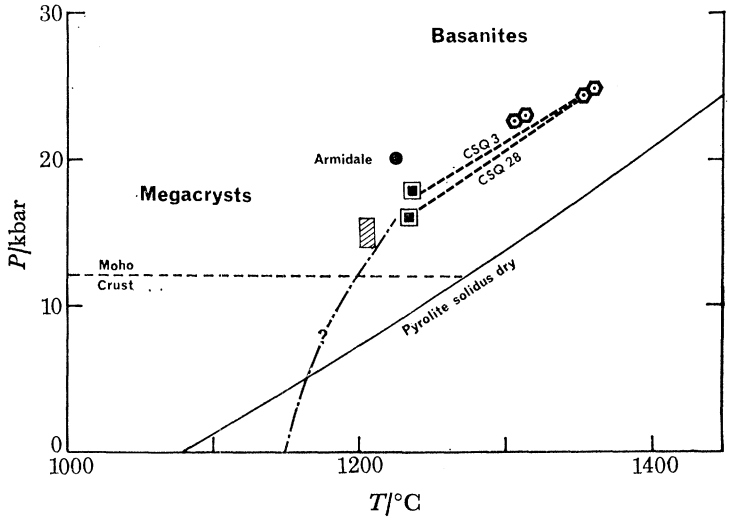

FIGURE 11. The calculated equilibration conditions of the megacryst assemblage of the San Quentin basanites are plotted, and connected by dashed lines to their lavas (table 11). The dot labelled Armidale refers to the megacrysts described by Binns *et al.* (1970), and the shaded area to the experimental conditions required to duplicate the composition of the pyroxene megacrysts in an alkali basalt (Green & Hibberson 1970).

megacrysts found in an alkali-basalt, and with approximately 2 % H_2O in the liquid, the required conditions were 1200 °C and 14–16 kbar (figure 11). However, a sodium-rich feldspar was not recorded in these experiments, and has not been found experimentally at high pressures near the liquidus (Green & Ringwood, 1967; Irving 1974). The very common occurrence of virtually unzoned feldspar megacrysts in nodule-bearing alkali basalt is difficult to reconcile with the present hydrous experimental data, and recent strontium isotopic evidence is ambiguous, for in the Ross Island basanites of Antarctica (Stuckless & Ericksen 1976) the megacrysts of tianiferous augite, kaersutite and anorthoclase are all in isotopic equilibrium with the host basalts, but in the basanites of southeastern Australia, only the augite megacrysts are in equilibrium (Stuckless & Irving 1976).

As the megacrysts from the Mexican basanites are unzoned, we may speculate that they precipitated and grew so quickly that their composition was unaffected by any change of P and T in the upward trajectory of the magma. Let it arbitrarily be taken that a change of less than 1 kbar ($\equiv$ 3 km) is without detectable effect on the composition of the crystals. Thus in the time taken to traverse this distance, approximately 6×10^3 s (ω = 50 cm s^{-1}), the feldspar crystals must nucleate and grow to a length of 2 cm or so, which necessitates a growth rate of 3.3×10^{-4} cm/s. This is a factor of 2 greater than the maximum growth rate (120° below the liquidus) for feldspar in lunar liquids (Scherer *et al.* 1972), but slower than the growth rate of anorthite in $CaAl_2Si_2O_8$ liquid 25 °C below the liquidus temperature (Klein & Uhlmann 1974). As the motion of rapidly ascending magma would ensure a plentiful supply of nutrients for the growing crystal, comparison with a growth rate determined for crystals growing from liquids of their own composition may be appropriate.

Water in basaltic source regions

Of the estimates of the pristine water content of basaltic magma, those by Moore (1970) are the most elegant and satisfying. In round numbers, tholeiitic basalts of Kilauea type contain

0.5 % by mass, whereas more alkali-rich basalts contain 0.9 %. The relation found by him between the concentration of water (H_2O^+) and P_2O_5 suggests that basanites contain approximately 1–1.4 %, which is in general conformity to the position of the equilibration points shown in figure 10.

In general terms, the experimental results on basaltic lavas show that the addition of H_2O lowers silica activity compared to the anhydrous liquids; in a Paricutin andesite orthopyroxene is stable in the absence of water, but with the addition of small amounts of water equivalent to a vapour pressure of 300 bar, olivine becomes stable (Eggler 1972). Nicholls & Ringwood (1973) have also remarked on the effect of increasing water concentration promoting the stability of olivine in tholeiitic liquids; Mysen & Boettcher (1975) so reduced the activity of silica in an andesite liquid by the addition of water that they were able to equilibrate the andesite with a peridotitic crystalline residue. These results necessitate (at constant temperature) an increase in pressure for the equilibration of a hydrous basaltic magma, compared to an anhydrous magma, with a solid residue of orthopyroxene and olivine. The effect of pressure on all solid assemblages which could define silica activity of the source regions is to lower the silica activity (Nicholls *et al.* 1971), and if that of the magma, or partial melt, is reduced by addition of water, then the equilibration pressure for the same solid residue must be greater compared to an anhydrous partial melt.

One way in which the addition of water in the inverse path can be taken into account in the calculations is to assume that water acts only to dilute the other components in the magma; this is a corollary of Burnham's (1975) claim that water mixes ideally in basaltic magmas. If it is assumed that 1 %, 2 %, or 4 % H_2O was present, then new values of X_i and ϕ_i for each lava are calculated, and the whole procedure repeated of plotting P–T lines of equilibration (figure 8) for each concentration of H_2O. The calculated P–T equilibration conditions are unaffected by such a non-specific dilution.

Basaltic lavas with between 1–2 % H_2O would only be saturated with H_2O at depths of a kilometre or less (Hamilton *et al.* 1964), and at all greater depths would be unsaturated. The possibility arises that during their ascent water was able to diffuse out of the magma into the surrounding mantle. This will be calculated in the next part of this paper as the time of ascent is known within limits, and the diffusion rate of water in basaltic magma may be approximated by Shaw's (1974) measurements on diffusion of H_2O in obsidian.

Water as a thermodynamic component

Water in the mantle resides either in hydrous phases such as phlogopitic mica or pargasitic amphibole, both perhaps containing significant amounts of fluorine (Holloway 1973) or in some combination of fluid inclusions, crystallographic vacancies and defects or as a chemisorbed hydroxylated surface layer.† To illustrate a calculation which takes explicit account of the specific thermodynamic properties of water as a component we consider a mantle assemblage containing phlogopitic mica. This is not an unreasonable choice for alkalic basalts in general

† There are, in general, two sorts of adsorption. Physically adsorbed water is water rather loosely held on a surface layer by van der Waals type forces (bond energies of order 2–5 kcal mol^{-1}) and can be several tens or hundreds of water molecules thick. Chemisorbed water is held by actual chemical reaction of water with the surface of the adsorbent probably to form OH^- groups, presumably in the same manner as H_2O reacts with silicate liquids at low H_2O concentration (Burnham & Davis 1974). Chemisorbed water, by necessity is one molecular layer thick and is the dominant form of sorption at high temperatures since it is characterized by somewhat larger bond energies (12–20 kcal) than physical adsorption.

PHILOSOPHICAL TRANSACTIONS OF THE ROYAL SOCIETY A MATHEMATICAL, PHYSICAL & ENGINEERING SCIENCES

and for highly potassic lavas in particular since potash must be present in the source regions. We assume that the fugacity of water is buffered by phlogopite and write the following reaction:

$$\underset{\text{phlogopite}}{KMg_3AlSi_3O_{10}(OH)_2} + \underset{\text{orthoenstatite}}{3MgSiO_3} \rightleftarrows \underset{\text{forsterite}}{3Mg_2SiO_4} + \underset{\text{liquid}}{KAlSi_3O_8} + \underset{\text{steam}}{H_2O}. \tag{42}$$

Since we are interested in predicting water contents we need as auxiliary information free energy data for the reaction

$$\underset{\text{in silicate liquid}}{H_2O} \rightleftarrows \underset{\text{steam}}{H_2O}. \tag{43}$$

Spera & Hildreth (1974) have considered this problem and have calculated the temperature dependence of the Henry's law constant for reaction (43) by numerically determining limiting Henry's law ($\gamma^{\text{liq}}_{H_2O} \to 1$ as $X^{\text{liq}}_{H_2O} \to 0$) slopes on $f^{\text{v}}_{H_2O}$ (fugacity of H_2O in vapour phase) against $(X^{\text{liq}}_{H_2O})^2$ (square of mole fraction H_2O in liquid) curves for a series of rock-water systems in which R (Lacey 1955), the ratio of oxygen to network forming cations, ranged from about 2 to 2.4. Burnham (1975) concluded that deviations from ideality generally were insignificant (i.e. $\gamma^{\text{liq}}_{H_2O} = 1$) in $NaAlSi_3O_8$ liquids with less than about 6 mass % H_2O.

The equilibrium constant calculated by these methods for reaction (43) becomes

$$\ln K = \ln f^{\text{v}}_{H_2O} - \ln a^{\text{liq}}_{H_2O} = -\frac{\Delta G^{\circ}_{43}}{RT} = -\frac{2854}{T} + 12.361, \tag{44}$$

where a solute standard state has been adopted (i.e. $\gamma^{\text{liq}}_{H_2O} \to 1$ as $X^{\text{liq}}_{H_2O} \to 0$) and where the activity of water in the liquid with respect to a sliding reference state in P and T becomes

$$a^{\text{liq}}_{H_2O} = (X^{\text{liq}}_{H_2O})^2. \tag{45}$$

The original polybaric and isothermal data apply strictly in the range from about 800 to 1200 °C but the simple nature of the ln K expression allows extrapolation to higher temperature without eccentric behaviour. Equation (44) pertains to systems under a total pressure (P_t) of 1 bar. In order to use (44) at mantle pressures we need partial molar volume data for H_2O in silicate melts so that we may determine the effect of P_{total} (P_t) on the free energy of H_2O in the liquid

$$\mu^{\text{liq}}_{H_2O}(P, T_0) - \mu^{\text{liq}}_{H_2O}(P_0, T_0) = \int_{P_0}^{P} \bar{V}^{\text{liq}}_{H_2O}\, dP. \tag{46}$$

Burnham & Davis (1971, 1974) have presented $P - \bar{V}_{H_2O} - T$ data for $NaAlSi_3O_8$ liquids ($R = 2$) and have shown that $\bar{V}^{\text{liq}}_{H_2O}$ is independent of composition. In the calculations which follow we have used their data for $P_t \leqslant 10$ kbar. For $P_t > 10$ kbar we have adopted a simple first order Taylor expansion equation of state for $\bar{V}^{\text{liq}}_{H_2O}$ given by

$$\bar{V}^{\text{liq}}_{H_2O} = (1 + \alpha(T\text{-}1273) - \beta(P\text{-}10000)) \tag{47}$$

where

$$\alpha \equiv \frac{1}{\bar{V}_{H_2O}} \left(\frac{\partial \bar{V}_{H_2O}}{\partial T}\right)_P, \tag{48}$$

the isobaric expansivity and

$$\beta \equiv \frac{-1}{\bar{V}^{\text{liq}}_{H_2O}} \left(\frac{\partial \bar{V}^{\text{liq}}_{H_2O}}{\partial P}\right)_T, \tag{49}$$

the isothermal compressibility and both are calculated from Burnham's (1975) $\overline{V}^{\text{liq}}_{H_2O}$ equation Thus the equilibrium constant defining reaction (43) becomes

$$\ln K = \ln f_{H_2O} - \ln a^{\text{liq}}_{H_2O} = \frac{-2854}{T} + 12.631 + \int_0^{10000} \frac{\overline{V}^{\text{liq}}_{H_2O}}{RT} + \int_{10000}^{P} \frac{\overline{V}^{\text{liq}}_{H_2O}}{RT}\, dP, \tag{50}$$

where the first integral is based on the Burnham & Davis (1971, 1974) expression for $\overline{V}^{\text{liq}}_{H_2O}$ and the second on that given above.†

By adding reactions (42) and (43) and rearranging we can generate an expression which defines the activity of the component $KAlSi_3O_8$ on a liquid standard state as a function of P_t, T, $X^{\text{liq}}_{H_2O}$ and the activities of orthoenstatite, phlogopite and forsterite:

$$\ln a^{\text{liquid}}_{KAlSi_3O_8} = 3 \ln a^{\text{pyroxene}}_{MgSiO_3} - 3 \ln a^{\text{olivine}}_{Mg_2SiO_4} + \ln a^{\text{mica}}_{KMg_3AlSi_3O_{10}(OH)_2} - 2 \ln X^{\text{liq}}_{H_2O}$$

$$+ \frac{\Delta G^\circ_{43} - \Delta G^\circ_{42}}{RT} - \int_1^P \frac{\Delta V^\circ_{\text{solids}}}{RT}\, dP - \int_1^{10000} \frac{\overline{V}^{\text{liq}}_{H_2O}}{RT}\, dP - \int_{10000}^{P} \frac{\overline{V}^{\text{liq}}_{H_2O}}{RT}\, dP. \tag{53}$$

Since equation (53) gives the activity of $KAlSi_3O_8$ in the model mantle source assemblage, all that remains is to write an equation that expresses the activity of $KAlSi_3O_8$ in a liquid unbuffered by the presence of solids.

Calculation of X_{H_2O}

If an estimate of the activity of $KAlSi_3O_8$ in the lavas can be made (reaction (9)), then a value can be calculated for $X^{\text{liq}}_{H_2O}$ at the equilibration pressure and temperature (table 11) by equating (53) to (32) for the $KAlSi_3O_8$ component. We have used as an example two basanite lavas which contain alkali-feldspar in the groundmass (Smith & Carmichael 1968). However, in order to calculate $X^{\text{liq}}_{H_2O}$, it is necessary to estimate the activity of hydroxyphlogopite, and we have assumed that the mica has the same composition as the magnesium biotite of a Tanzanian peridotite nodule (Dawson *et al.* 1970) and for which we calculate by the ionic mixing–probability model described earlier $a^{\text{mica}}_{KMg_3AlSi_3O_{10}(OH)_2} = 0.21$. Flower (1971) has also analysed a phlogopitic mica from Jan Mayen in the North Atlantic and his composition gives a lower activity (0.10) since fluorine was included in his analysis. The activities of $MgSiO_3$ and Mg_2SiO_4 are taken as 0.73 and 0.81 respectively.

For the two basanites 253 and 256 we obtain the results shown in table 12.

The agreement between the calculated results and the values deduced from figure 10 for these two basanites seems satisfactory especially considering the uncertainty in the activity of

† Written out in full for $P_t \leqslant 10$ kbar we have

$$\ln K = -2854/T + 12.631 + P\,(0.10998/T + 4.432 \times 10^{-5} + 1.4048 \times 10^{-7} T$$
$$- 2.3935 \times 10^{-11} T^2) + P^2(7.3365 \times 10^{-8}/T - 1.1696 \times 10^{-8} - 9.5 \times 10^{-13} T)$$
$$+ P^3\,(1.876 \times 10^{-10}/T + 4.5863 \times 10^{-13}) + P^4(-1.191 \times 10^{-14}/T). \tag{51}$$

Written out in full, for $P_t > 10$ kbar we have

$$\ln K = -1948/T + 10.954 + 1.41 \times 10^{-4}\, P + 0.032\,(P/T) - 5.03 \times 10^{-7}\,(P^2/T)$$
$$+ 1.31 \times 10^{-3}\, T - 2.4 \times 10^{-7}\, T^2. \tag{52}$$

PHILOSOPHICAL TRANSACTIONS OF THE ROYAL SOCIETY A MATHEMATICAL, PHYSICAL & ENGINEERING SCIENCES

phlogopite which was used to calculate $X^{liq}_{H_2O}$. In principle, the P–T equilibration conditions should be redetermined using the newly calculated $X^{liq}_{H_2O}$ in order to calculate new ϕ_i values and the iteration continued until an internally consistent set of thermodynamic intensive variables are obtained. In practice, however, the effect of several percent H_2O will alter ϕ_i values insignificantly; the new PT equilibration values differ from the original anhydrous ones by amounts smaller than the estimated errors in determining P_t and T.

TABLE 12. CALCULATED WATER CONTENTS IN EQUILIBRIUM WITH PHLOGOPITIC MICA

sample	T_{quench} °C	$\phi_{KAlSi_3O_8}$ K	$a_{KMg_3AlSi_3O_{10}(OH)_2}$	P_t bar	T °C	f_{H_2O} bar	P_{H_2O}‡ bar	$X^{liq}_{H_2O}$	mass % H_2O†
253	980	1047	0.10	22800	1314	4807	804	0.044	1.27 ± 0.50
253	980	1047	0.21	22800	1314	10095	1687	0.064	1.87 ± 0.50
256	995	1130	0.10	22400	1311	4697	786	0.045	1.31 ± 0.50
256	995	1130	0.21	22400	1311	9863	1469	0.065	1.93 ± 0.50

† Calculated using mass % $H_2O = 1800\ X^{liq}_{H_2O}/(gfw + X^{liq}_{H_2O}(18 - gfw))$ where gfw (253) = 64.2 and gfw (256) = 64.9.

‡ Calculated using estimated $\gamma^{v}_{H_2O}$ values from Spera (1974).

3. IRREVERSIBLE EFFECTS IN MAGMA PRODUCTION

Up to this point we have dealt solely with equilibrium or reversible conceptual schemes. The calculation of the intensive variables (P_e, T_e and a_i, ... a_n for n component system) are all based on the idea of chemical equilibrium, a concept of great utility but also a concept that somewhat limits the scope of inquiry. We immediately recognize the fact that from a dynamic or mechanistic point of view the eruption of lava onto the surface of the Earth is one of the last of a long chain of evolutionary instabilities characteristic of virtually all complicated chemical and mechanical systems far from equilibrium (Nicolis *et al.* 1975; Prigogine & Lefever 1974). This is not to say that the results previously given in this paper are invalid; only that they must be viewed in the context of a dynamically non-linear system that is continuously evolving in time and space. As an example of the different scales and mechanical régimes that influence the final volcanic product consider the following somewhat naive and idealized sequence of instabilities that culminate in a volcanic eruption.

(i) In situ *production of liquid by partial fusion process*; perhaps due to a thermomechanical failure, e.g. the thermal feedback problem (Shaw 1969; Gruntfest 1963; Shaw 1973).

(ii) *Segregation of melt from isolated pockets to larger pools of liquid*; if viscous failure is indeed a significant mechanism operating to produce melt the two processes would be related in that the large strain rates necessary to generate melt would also serve to coalesce the magma bubbles into large pools (Shaw 1969; Wertman 1971, 1972). If the region of space where magma segregation occurs is not characterized by high effective strains then a model of melt segregation such as Sleep's (1974) based on the fluid dynamics of 2-phase flow with mechanical interaction (see Faizullaev (1969) for a detailed account of the assumptions underlying this solution) may be applicable.

(iii) *The relatively rapid ascent of coherent batches of magma.* Until this point the magma has stayed relatively close to the area where it was initially generated. Once larger bodies of melt have formed they can ascend relatively rapidly by any number of means. Two that come to

PHILOSOPHICAL TRANSACTIONS OF THE ROYAL SOCIETY A MATHEMATICAL, PHYSICAL & ENGINEERING SCIENCES

mind quickly are the elastic crack propagation model (Weertman 1971) or the viscous upwelling governed by a fluid buoyancy Rayleigh–Taylor type instability (Chandrasekkar 1961; Ramberg 1972; Whitehead & Luther 1975). In the latter case the buoyant mass detaches from the growing melt layer when the Stokes's law ascent rate becomes greater than the rate of growth of the viscous sphere. During this period in the life cycle of the magma a great deal of what can happen remains obscure. For one, it is during this phase that the possibility of mass transfer from rising magma to mantle or vice versa may occur. Rheologically speaking, the rising magma bodies 'see' a whole spectrum of mechanical behaviour patterns in the surrounding mantle as the pressure and temperature varies continuously along the path from source to surface.

(iv) *The storage of magma in high level chambers and final eruption.* During this phase a variety of chemical and physical properties of the melt may change. Fractional crystallization and heat losses due to cooling may influence the final T–P path the magma follows. Depending on the initial volatile content and the volatile mass transfer rate the melt may eventually come to a level where a gas phase can separate. When this happens the dynamic régime changes from a solid–liquid incompressible fluid flow problem to a highly complicated 3-phase compressible fluid problem. Again the paths the magma may take in intensive variable–velocity space are many and difficult to systematize (Bennett 1971) in terms of broad generalizations.

In the previous discussion we separated the life history of a typical eruption into a number of distinct phases. It goes without saying that we do this solely for conceptual reasons. In fact, there exists a delicate coupling between all states and it is the inherent feedback effects which dominate what we see at the surface. It is beyond the scope of this paper to report on all aspects of the various régimes briefly alluded to above. Instead we would like to look more closely at some aspects of the ascent history of magmatic bodies.

Evolution of basanitic magmas during ascent

We propose now to look at some of the thermal, mechanical and chemical features that control to some extent what we as petrologists see at the surface of the Earth when studying an alkali basalt flow. We begin by gleaning information obtained directly from the sizes of ultrabasic inclusions combined with some simple (non-convective) models of fluid flow. We then turn our attention to some theoretical studies of thermal buoyancy convection in tubes in an effort to determine possible dynamothermal régimes. Finally we develop expressions for the heat, mass and momentum transfer rates following a simple boundary layer approach and then use the various flux expressions to quantitatively estimate (in conjunction with the ascent rate data) integral heat and mass exchange values. It should be noted that the results of these studies tell us something not only about the magma body but also of the medium (e.g. the mantle) the melt travels through since it is the properties of the medium as well as the magma that control what we see upon eruption.

The behaviour of *spherical* particles in a fluid stream can be predicted with reasonable accuracy since the problem finds many direct applications in the fluid dynamic and engineering literature (McNown & Malaika 1950; Sutterby 1973). The restriction to spherical particles is not a necessity as there have been empirical studies which correlate particle shape with settling velocity. The interested reader is referred to McNown & Malaika (1950) for the engineering aspects and Shaw (1965) for a geological consideration of this problem. We will treat the particles as being spherical because often xenolithic ultramafic nodules are found to be nearly so. For a non-accelerating particle in a stream, a settling velocity

PHILOSOPHICAL TRANSACTIONS OF THE ROYAL SOCIETY A MATHEMATICAL, PHYSICAL & ENGINEERING SCIENCES

may be computed by balancing the buoyancy force against the viscous tractive force (frictional forces) always opposing the direction of motion. The force or drag on a sphere is generally given in terms of a drag coefficient

$$C_d = 8F/\rho_n \omega^2 D_n^2 \tag{54}$$

where F is the force acting on the sphere, and ρ_n, ω and D_n are the density, vertical velocity and nominal diameter of the equivalent spherical nodule. In the range of Reynolds numbers, $Re_n \lesssim 0.1$, where

$$Re_n = \frac{\rho_n D_n \omega}{\eta_L} \tag{55}$$

Stokes's law applies and

$$C_d = \frac{Re_n}{24}. \tag{56}$$

For larger values of Re an empirical formula given by Kay (1968) gives

$$C_d = 18.0\, Re^{-0.6}. \tag{57}$$

Equating buoyancy and frictional forces and rearranging gives

$$\omega = \left[\frac{4D_n(\rho_n - \rho_L)\, g}{3C_d\, \rho_L}\right]^{\frac{1}{2}} \tag{58}$$

where ρ_L is the fluid (magma) density and g the acceleration due to gravity (981 cm s^{-2}). In the Stokes's law range (58) reduces to the familiar equation

$$\omega = \frac{D_n^2(\rho_n - \rho_L)\, g}{18\, \eta_L}. \tag{59}$$

To compute the actual settling velocity in the dynamic régime where $Re > 0.1$, recourse may be made to an iterative solution to equations (54) and (58) to obtain an internally consistent set of parameters. As an example consider the settling velocity of an olivine–orthopyroxene nodule from Hualalai Volcano, Hawaii with a density of 3.45 g cm^{-3} and a diameter of 30 cm. Given a density and viscosity of Hualalai alkali basalt (MacDonald 1949, p. 78, no. 1) of 2.80 g cm^{-3} and 350 P† respectively, we calculate

$$\begin{aligned} Re &= 14.9, \\ C_d &= 3.55, \\ \omega &= 50.6 \text{ cm s}^{-1} \quad (1.8 \text{ km h}^{-1}). \end{aligned} \tag{60}$$

Using the simple Stokes's law formula one calculates

$$\omega = 91.1 \text{ cm s}^{-1} \quad (3.2 \text{ km h}^{-1}).$$

Because the low Re number approximation underestimates the total drag, velocities calculated with equation (59) are in error by a significant amount. The settling velocity calculated above

† Densities are calculated from the partial molar volume data of Bottinga & Weill (1970), and viscosities by Shaw's (1972) algorithm.

PHILOSOPHICAL TRANSACTIONS OF THE ROYAL SOCIETY A MATHEMATICAL, PHYSICAL & ENGINEERING SCIENCES

illustrates the fact that we are dealing with characteristic velocities of tens of centimetres per second, orders of magnitude greater than the characteristic velocities at which plates move about on the surface of the Earth. In fact, the settling velocities calculated in this manner are *minimum* magma ascent rates, since if magma was moving upwards at just this rate, a 30 cm nodule would remain at a fixed depth.

Some information regarding the geometry of an ascending magmatic body can be obtained from some simple volumetric considerations. Lamb (1945) considered the problem of the drag on a spherical drop of fluid of radius R and viscosity η_L moving under a gravity-induced buoyancy force in a fluid of viscosity η_m. For the drag we have

$$F = \frac{2\pi\eta_m R(2\eta_m + 3\eta_L)}{(\eta_m + \eta_L)}. \tag{61}$$

Note that $$\lim_{\eta_L \to \infty} F = 6\pi\omega\eta_m R \quad \text{(hard sphere in viscous medium)} \tag{62}$$

and that $$\lim_{\eta_L \to 0} F = 4\pi\omega\eta_m R \quad \text{(gas bubble in viscous medium)}. \tag{63}$$

For a batch of magma ($\eta_L \simeq 10^3$ P) rising through the mantle ($\eta_L \sim 10^{21}$) it is clear that equation (63) is applicable. Equating the buoyancy force on the magmatic sphere to the drag force we have after rearrangement for the radius of the sphere

$$\left[\frac{3\omega\eta_m}{g(\rho_m - \rho_L)}\right]^{\frac{1}{2}} = R, \tag{64}$$

taking $\omega = 50.0$ cm s^{-1}, $\eta_m = 10^{21}$ P and $\Delta\rho = 0.60$ g cm^{-3} we have $R = 1.58 \times 10^{10}$ cm, clearly an outrageously large number. This is because of the high value of the viscosity of the mantle used in the calculation and because we have neglected convection within the rising body. It may be argued, however, that there is a significant wall effect; that is the hot magma will heat a boundary layer envelope around the magma tube perhaps to temperatures high enough to begin partial fusion of the surrounding spinel or garnet peridotite thereby lowering the effective viscosity of the mantle (η_m). Let us explore this argument further by calculating from the volume of a typical nodule- and megacryst-bearing basanite flow the value of η_m necessary to allow the magma sphere to ascend at a typical nodule settling rate. Since viscosity is a strong function of melt fraction at temperatures between the peridotite solidus and liquidus it is informative to convert the viscosity decrement to a temperature interval and inquire into the mineralogical constitution of any residue of the 'shell melting' episode. Consider, as an example, a nodule-bearing flow from Black Rock Summit, Nye County, Nevada with an estimated volume of about 0.03 km^3. Converting this volume to an equivalent sphere we have

$$R = (3V/4\pi)^{\frac{1}{3}} = 1.93 \times 10^4 \text{ cm} \quad \text{(i.e. } \sim 200 \text{ m)}. \tag{65}$$

With $\omega = 15$ cm s^{-1}†, $\Delta\rho = 0.65$ g cm^{-3} and $g = 981$ cm s^{-2} we have from equation (64)

$$\eta_m = \frac{R^2 g\Delta\rho}{3\omega} = 5.3 \times 10^9 \text{ P}. \tag{66}$$

In several papers Shaw (1969, 1973) has developed from experimental measurements and theoretical considerations a simple exponential type relation for the effective Newtonian viscosity

† This corresponds to the settling rate of a 9 cm nodule.

PHILOSOPHICAL TRANSACTIONS OF THE ROYAL SOCIETY A MATHEMATICAL, PHYSICAL & ENGINEERING SCIENCES

in basaltic crystal–liquid systems at temperatures between the solidus and liquidus where the volume fraction of liquid (θ) values continuously between 0.0 and 1.0. Although the viscosity of a solid liquid falls with increasing temperature, the decrease is orders of magnitude greater in the melting range where the effect of decreasing concentration of suspended crystals is large. In the melting range Shaw (1969) has used the equation

$$\eta = \eta_s \, e^{-a(T-T_s)}, \tag{67}$$

where η_s is the viscosity at the solidus temperature, T_s. This can be converted to an equivalent melt fraction by assuming a linear dependence of volume melt fraction θ with temperature. In this approximation we have

$$a(T-T_s) = b\theta, \tag{68}$$

where both a and b are calibrated by reference to experimental data. The melting interval (ΔT_f^P) for a spinel bearing peridotite from St Paul's Rocks is nearly independent of pressure and is about 510 °C (Millhollen *et al.* 1974). From (68) we calculate

$$\frac{a}{b} = \frac{\Delta\theta^P}{\Delta T_f^P} = 1.961 \times 10^{-3}\ \mathrm{K}^{-1}. \tag{69}$$

Now, if we fix η such that $\eta = 5 \times 10^2$ P for $\theta^P = 1$ (i.e. all liquid) and $\eta = 10^{18}$ P for $\theta^P = 0$† we have

$$b = \ln (10^{18}/5 \times 10^2) = 35.23 \tag{70}$$

and

$$a = \left(\frac{\Delta\theta^P}{\Delta T_f^P}\right) b = 0.0691. \tag{71}$$

We determine the melt fraction necessary in the shell boundary layer to allow the viscous sphere to ascend at the required rate as

$$\theta^P = \frac{1}{b} \ln \left(\frac{10^{18}}{5.3 \times 10^9}\right) = 0.54. \tag{72}$$

Transforming this melt fraction into an equivalent temperature increment above the solidus we have

$$T - T_s = b\theta^P/a = 275\ ^\circ\mathrm{C}. \tag{73}$$

From figure 1 in Millhollen's paper (1974) one notes that at 275 °C above the peridotite solidus at 30 kbar garnet is no longer stable; calcic pyroxene, orthopyroxene and olivine are the phases remaining in the residue after the partial melting episode. Table 13 summarizes these results for a range of thermal and transport coefficients.

We can also perform a simple macroscopic energy balance and obtain information with regard to the ratio of original magma volume to the partially fused conduit wall material and an estimate of the temperature loss of the ascending magma due to the latent heat effects incurred during partial fusion of peridotitic wall material. The energy necessary to partially fuse an annular ring δr cm thick of radius r and length l is approximately given by

$$2\pi\hat{\rho}\left(C_{P,\mathrm{m}} + \frac{\Delta H_f^P}{\Delta T_f^P}\right) r\,\delta r\, l\,(T - T_s), \tag{74}$$

where we have assumed the thickness of the annular ring δr is much smaller than the radius of the magna body, r. In (74) $C_{P,\mathrm{m}}$ is the isobaric heat capacity for the mantle, $\hat{\rho}$ is the average

† This is an approximation of the effective Newtonian viscosity of crystalline mantle material close to its solidus temperature (T_s).

PHILOSOPHICAL TRANSACTIONS OF THE ROYAL SOCIETY A MATHEMATICAL, PHYSICAL & ENGINEERING SCIENCES

density of the crystal–liquid system, $T-T_s$ is the temperature increase necessary to decrease η_m to a value commensurate with the nodule (and magma) ascent velocity calculated earlier. The thermal energy lost from the original batch of fluid is given by

$$\tfrac{4}{3}\pi\hat{\rho}\left(C_{P,L}+\frac{\Delta H_f^L}{\Delta T_f^L}\right)r^3\,(T_e-T), \tag{75}$$

TABLE 13. VISCOSITY–TEMPERATURE–MELT FRACTION DATA FOR THIN SHELL MELTING EPISODE

$\eta\ (\theta^P=1)$ P	$\eta\ (\theta^P=0)$ P	a K^{-1}	b	θ^P volume melt fraction	$T-T_s$ for peridotite °C	phases present (Millhollen *et al.* 1974) 10 kbar	20 kbar	30 kbar
500	10^{18}	0.0691	55.23	0.54	275	spinel opx ol	opx ol	cpx opx ol
500	10^{21}	0.0826	42.14	0.62	314	ol	ol opx	ol opx
10^3	10^{18}	0.0677	34.54	0.55	281	opx ol	opx ol	opx ol
10^2	10^{18}	0.0722	36.84	0.52	364	spinel opx ol	opx ol	opx ol

The volume melt fraction (θ^P) and temperature decrements for the peridotitic wall material were calculated assuming an effective mantle viscosity (η_m) computed from equation (67) in the text, and ignoring heat of solution effects. To convert to a mass basis (i.e. mass melt fraction, W_L) one may use the formula $W_L=\dfrac{\rho_L\theta^P}{\rho_s+\theta^P(\rho_L-\rho_s)}$ where ρ_L is the density of the liquid, ρ_s the density of the solid, θ^P the volume fraction of melt and W_L the mass fraction of melt. For small θ^P we have $W_L\simeq(\rho_L/\rho_s)\theta^P$. The shell partial melting episode may play a significant rôle in the production of vertical zones of considerable extent of depleted ultramafic rocks in the mantle. This may have some bearing on the observation by many petrologists that the inferred (by pyroxene geothermometry) temperatures of many xenoliths are considerably lower than the estimated temperatures prevailing at the time of partial fusion (i.e. the equilibration temperature, T_e).

where ΔH_f^L is the latent heat of crystallization of the melt, ΔT_f^L is the melting interval for the magma and T_e is the equilibration temperature with the source. Equating (75) and (74) one may calculate the temperature drop experienced by the magma. The two effective heat capacity terms do not cancel because the melting interval for peridotite (ΔT_m^P) is considerably larger than for an alkali basalt (ΔT_m^L). Thus

$$T_e-T=\frac{3}{2}\left(\frac{C_{P,m}+\Delta H_f^P/\Delta T_m^P}{C_{P,L}+\Delta H_f^L/\Delta T_f^L}\right)\frac{\delta r l}{r^2}\,(T-T_s). \tag{76}$$

Before estimating temperature losses of the rising magma we calculate the thickness of the partially molten zone that develops in the mantle adjacent to the rising diapir. In general, the thickness of a conduction controlled boundary layer propagating into the surrounding mantle is given by an expression of the form (Meyers 1971)

$$\delta r=\sqrt{(\pi\kappa t)}, \tag{77}$$

where κ is the thermal diffusivity (taken as 10^{-2} cm^2 s^{-1}) and t the time in seconds. Now, if a

PHILOSOPHICAL TRANSACTIONS OF THE ROYAL SOCIETY A MATHEMATICAL, PHYSICAL & ENGINEERING SCIENCES

sphere of radius r moves upwards at a velocity ω, the time any portion of the mantle will be adjacent a hot wall is roughly given by

$$t = 2r/\omega \tag{78}$$

and so (77) becomes

$$\delta r = (2\pi\kappa r/\omega)^{\frac{1}{2}}. \tag{79}$$

TABLE 14. SUMMARY OF ENERGY BALANCE RESULTS CALCULATED BY EQUATIONS (76) AND (79)

If effective mantle viscosities (η_m) are lowered by the partial fusion mechanism discussed, the energy required for fusion would be supplied by the latent heat effect and heat capacity of the diapir. Thicknesses of the partially molten zone (δr) and temperature decrements sustained by the magma are calculated from equations (79) and (80) respectively as a function of the temperature increase in the peridotitic rind ($T - T_s$) and the radius of the equivalent magma sphere. $T_e - T$ values have been converted to volume fraction crystallized ($\zeta = 1-\theta$) where $\theta = (T_e - T)/\Delta T_f^L$ with ΔT_f^L set equal to 250 °C. Assumed constant throughout have been $C_{P,L} = 0.25$ cal g^{-1} K^{-1}, $\Delta H_f^P = \Delta H_f^L = 140$ cal g^{-1} (the heat of fusion of diopside at 1 bar and 1391°C), $\Delta T_f^P = 510$ °C, $l = 60$ km, $\kappa = 10^{-2}$ cm^{2}s^{-1}, $\omega = 30$ cm s^{-1}. Values in parentheses in columns 4 and 5 are with $\omega = 15$ cm s^{-1} (all other parameters identical)

$T - T_s$ for peridotite °C	r m	δr cm	$T_e - T$ for magma °C	$\zeta = 1-\theta$ volume fraction of melt crystallized
100	75	4.0	41 (58)	0.164 (0.232)
	100	4.6	27 (38)	0.108 (0.152)
	150	5.6	15 (21)	0.06 (0.084)
	200	6.5	10 (14)	0.04 (0.056)
	300	7.9	5 (7)	0.02 (0.028)
200	75	4.0	83 (117)	0.332 (0.468)
	100	4.6	54 (76)	0.216 (0.304)
	150	5.6	31 (44)	0.124 (0.176)
	200	6.5	21 (30)	0.084 (0.12)
	300	7.9	9 (13)	0.036 (0.052)
250	100	4.6	68 (96)	0.272 (0.384)
	200	6.5	26 (37)	0.104 (0.148)
	300	7.9	11 (16)	0.044 (0.064)
275	100	4.6	74 (105)	0.296 (0.420)
	200	6.5	29 (41)	0.116 (0.164)
	300	7.9	13 (18)	0.052 (0.072)
300	75	4.0	123 (174)	0.492 (0.696)
	100	4.6	81 (115)	0.324 (0.46)
	150	5.6	45 (64)	0.180 (0.256)
	200	6.5	32 (45)	0.128 (0.18)
	300	7.9	17 (24)	0.068 (0.096)

Replacing δr in (76) by (79) we have finally

$$(T_e - T) = \tfrac{3}{2}\sqrt{(2\pi)}\left(\frac{C_{P,m} + \Delta H_f^P/\Delta T_f^P}{C_{P,L} + \Delta H_f^L/\Delta T_f^L}\right)\left(\frac{\kappa}{\omega}\right)^{\frac{1}{2}}\frac{l}{r^{\frac{3}{2}}}(T - T_s). \tag{80}$$

With velocities on the order of several centimetres per second and r several hundreds of metres, δr the boundary layer thickness is of the order of several centimetres. Table 14 summarizes some of the specific numerical values implied by equations (76) and (79). It is important to note that equation (75) implicitly assumes magma temperatures are greater than the solidus of the surrounding peridotitic material. This condition will be met as long as the 1 bar solidus mantle temperature is less than or equal to about 1200 °C. The pyrolite solidus of Green & Ringwood (1967) gives a 1 bar intercept of about 1175 °C. However, some garnet lherzolites would project to a 1 bar solidus temperature of 1220 °C (Kushiro *et al.* 1972). For those bulk

PHILOSOPHICAL TRANSACTIONS OF THE ROYAL SOCIETY A MATHEMATICAL, PHYSICAL & ENGINEERING SCIENCES

compositions and/or initial H_2O contents where $T_s^{1\,bar} > 1200$ °C, the rising magma could not supply enough energy to partially fuse its perioditic envelope thereby lowering η_m. The point we wish to make is that at early times during any given melting episode significant energy losses must be sustained by the diapir perhaps causing it to freeze at depth. Equation (76) also does not allow for any superheat in the magma. If viscous heating is important there will be no crystallization of any near liquidus phases (megacrysts) since latent heat will not contribute to the energy balance. In that case, the values for ζ listed in columns 5 and 6 would be maximum values. The results summarized in table 14 show, as one might expect, that increasing the effective volume of a magma body serves to minimize energy losses. Also note that upon increasing ω, the ascent rate, the magma body sustains a smaller temperature drop. It seems likely that rather than one pulse of magma moving up and heating its boundaries sufficient to allow quick ascent, a whole series of such thermal pulses are responsible for the eventual 'softening' of the medium surrounding the diapirs which follow in time. These considerations highlight the fact that evolving magmatic systems must be viewed within the context of the geologic history of a region. Geochronological and eruptive volume data are the basic information needed to provide the crucial link between the chemistry of the lava and the dynamics of ascent.

TABLE 15. η_m VALUES CALCULATED ASSUMING THE BALANCE REPRESENTED BY EQUATION (82)

(For the physical parameters reported in the text $Re_n = 1.31$, $C_d = 15.34$ and $\omega = 13.5$ cm s^{-1}, $D_n = 10$ cm, $\Delta\rho$ is taken as 0.6 g cm^{-3} and $\rho_L = 2.8$ g cm^{-3}. The first value in the table is for $r = 300$ m and the value in parentheses is for $r = 200$ m. The Z value is the depth the nodule gets trapped by the rising magma body. Note that the values of the viscosity calculated are in reasonable agreement with those calculated earlier in the thermal budgetary calculation.)

Z depth/km	η_m effective mantle viscosity/P
30	1.51×10^8 (4.47×10^7)
40	1.13×10^8 (3.34×10^7)
50	9.07×10^7 (2.69×10^7)
60	7.56×10^7 (2.24×10^7)
70	6.48×10^7 (1.92×10^7)
80	5.67×10^7 (1.68×10^7)
90	5.04×10^7 (1.49×10^7)
100	4.54×10^7 (1.34×10^7)

A slightly different argument also supports the contention that effective mantle viscosities must be orders of magnitude smaller than 'nominal' isostatically derived values (if the motion is buoyancy induced). If a xenolith is to be erupted on the surface we reason that the time necessary for the nodule to settle the distance $2r$, where r is the equivalent radius of the magma bubble, is greater than the time the bubble of magma rises through the superincumbent mantle and crust. Stated mathematically the condition becomes

$$\frac{2r}{\omega} \geqslant \frac{Z}{U}, \tag{81}$$

where ω is the settling velocity of the xenolith (equations (54) and (56) or (57) depending on Re), Z the average depth of the magma body below the surface when the xenolith gets trapped

and U the ascent rate of the less viscous magma bubble in the more viscous surrounding mantle ($U = g\Delta\rho r^2/3\eta_m$, see equation (62)). Equation (81) becomes

$$\eta_m \leqslant \frac{r^3}{3Z}\left[\frac{3g(\rho_n - \rho_L)\, C_d \rho_L}{D_n}\right]^{\frac{1}{2}}. \tag{82}$$

As an example, table 15 gives maximum values of the effective viscosity of the mantle (η_m) through which the magma body rises with a 10 cm diameter nodule. The diameter of the magma body is taken to be 600 or 400 m.

We close this section of the paper with an illustrative ascent history model. Ignoring for the moment energy losses by convection (we consider convective régimes in the next section) and viscous heating effects we note that for a body rising as fast as is inferred by the high settling velocities (of order 10 cm s^{-1}) total heat losses by conduction are small and of order (Carslaw & Jaeger 1959)

$$Q = 4\pi r^2 \left(\frac{Z}{\omega}\right)^{\frac{1}{2}} \frac{k}{\sqrt{(\pi\kappa)}} \Delta T_f^L, \tag{83}$$

where k is the thermal conductivity (0.007 cal deg^{-1} s^{-1} cm^{-1}) and ΔT_f^L maximum difference in temperature across the body (*ca.* 200 °C). Temperature drops sustained by the body as a whole are of order

$$\frac{3Q}{4\rho_L \pi r^3 C_{P,L}} = (T_e - T)_{\text{conduction}}. \tag{84}$$

For the 200 m radius body we have used in our reference calculations one calculates, for an ascent rate of 10 cm s^{-1} and an initial depth (Z) of 75 km,

$$(T_e - T)_{\text{conduction}} \simeq 2\ ^\circ\text{C}.$$

One concludes from this that the significant energy sink is the latent heat involved in the partial fusion of the external boundary layer of peridotitic material. A 200 m radius sphere of magma moving upwards at a rate of several centimetres per second (as indicated by the nodule settling rate) from a depth of say 70 km, will partially fuse mantle material in a zone roughly 5–10 cm thick to the extent of about 20 % by volume producing ol–opx or ol–opx–cpx residue. The body will cool by about 30 °C. The effective viscosity of the sheath of mantle the body rises through is of the order 10^8 P. Heat losses incurred by molecular conduction will be small (e.g. not more than several degrees Celsius). The ratio of the mass added by partial fusion to the initial mass of the sphere is of order

$$3\delta r l\theta/2r^2 \simeq 0.06, \tag{85}$$

or about 6 % by mass. The composition of the liquid phase that results from this partial fusion episode is that of a mildly alkaline to tholeiitic basalt (Carmichael *et al.* 1974).

On the convective state of rising diapirs

In the discussion so far we have neglected internal convective régimes in the ascending magma body. Since it is our ultimate aim to evaluate the processes which govern the behaviour of evolving magmatic systems, we now seek to develop quantitative expressions expressing local heat, mass and momentum transfer rates. In the calculations which follow the convective velocities determined are those arising in response to the temperature difference between the cool walls and the hot interior of the magma body. We recognize, however, that superimposed

PHILOSOPHICAL TRANSACTIONS OF THE ROYAL SOCIETY A MATHEMATICAL, PHYSICAL & ENGINEERING SCIENCES

upon the thermal convection flow field will be a forced axisymmetric toroidal circulation pattern induced by the bulk translation of the liquid sphere at rate ω through the mantle.† Because the length scales of the two processes are very different and because of the inherent computational difficulties which arise in feedback problems we have ignored the possibility of coupling.

As the forced flow velocities are in the same direction (near the walls) as the free convection rates, one may simply add the ascent rate of the magma body (ω) to the boundary layer velocities (u) when calculating the heat and mass transfer values. This should take account (at least to first order) of the internal flow.

The two dimensionless variables which characterize the flow régime in naturally convecting systems are the Prandtl number

$$Pr = \nu/\kappa \tag{86}$$

and the Grashof number

$$Gr = \alpha g \Delta T r^3/\nu^2, \tag{87}$$

where ν is the kinematic viscosity, κ the thermal diffusivity, α the isobaric expansivity and ΔT and r a characteristic temperature difference and length respectively. The product $PrGr$ is yet another dimensionless number called the Rayleigh number,

$$Ra = PrGr. \tag{88}$$

The Pr number measures the relative rates at which momentum and energy are transferred by molecular diffusion through a given fluid. The Rayleigh number may be thought of as the ratio of buoyancy forces operating in a system (inducing flow) divided by the viscous forces acting to retard flow. Below a certain critical Ra number (about 10^3) viscous forces are effective in damping out any bulk flow and therefore heat is transported by molecular conduction and/or radiation. It is to a large extent, the balances amongst these various dimensionless numbers which (together with appropriate boundary conditions) determine the velocity and temperature profiles (and hence the various fluxes). The reader is referred to Shaw (1974, p. 157) for additional comments and insight into the concepts underlying the calculations which follow.

Geometrical and scale considerations

In what follows, we draw heavily upon the work of Lighthill (1953) who performed a thorough analysis of free convection in cylindrical tubes. Other workers who have contributed to this subject include Hallman (1955), Ostrach *et al.* (1956), Morton (1960) and Scheele *et al.* (1962). From the discussion in Lighthill (1953) and especially from his figures 7 and 10, it becomes apparent that for convection in a cylindrical tube of length l and radius r it is the product $(r/l)\ Ra$ where

$$Ra = \alpha g \Delta T r^3/\kappa\nu, \tag{89}$$

that characterizes the kind of flow to be expected. For example, at constant values of r and Ra as r/l goes from 1.0 to 1/100 flow régimes would change from the thin boundary layer‡ type (b.l. not filling tube) to a fully developed flow with the boundary layer completely filling the

† The interested reader is referred to Batchelor (1967, p. 237) or Lamb (1945, p. 600) for the equation of the stream function (ψ) for the internal toroidal flow discussed here. The tangential and radial components of the velocity may be easily computed from ψ.

‡ A boundary layer régime is one where temperature, velocity and concentration profiles are flat except in the neighbourhood of a surface or boundary. For the boundary layer approximations to the conservation equations to be valid it must be true that $\delta \ll h$ where δ is the thickness of the boundary layer and h a characteristic length of the body.

PHILOSOPHICAL TRANSACTIONS OF THE ROYAL SOCIETY A MATHEMATICAL, PHYSICAL & ENGINEERING SCIENCES

tube and finally to a flow geometry where a stagnant portion of fluid would lie above or below (depending on the geometry) the fully developed laminar boundary layer flow (see figure 12 in Shaw (1965); figures 2, 3, and 6 in Lighthill (1953)). Unfortunately it is difficult for us to obtain accurate r/l values for the 'tear-drop' streamlined diapirs of magma rising through the mantle. Using data from diapiric studies (Ramberg 1968) it would seem that r/l would perhaps not be much smaller than 1/20. In the calculations performed below it turns out that the dependence of the magnitude of fluxes on r/l is negligible. At high enough values of Ra, the heat, mass and momentum transfer rates all asymptotically approach the values of the limiting case – that of free convection from a vertical plate. $T_\infty - T_w$ is the driving force behind the convective system (T_∞ represents the temperature of the magma unaffected by the presence of the wall and T_w the temperature at the boundary). We realize of course that in fact ΔT is a function of time. For instance early in the ascent history we might expect temperature differences to be smaller and for ΔT to progressively grow larger with time as the magma rises into cooler and cooler surrounding. We have chosen $T_\infty - T_w$ values to maximize the various flux quantities. The important aspect to note, however, is that in the Ra number the temperature difference appears to only the first power whereas length appears to the third power. The importance of estimating flow volumes is made obvious by some simple calculations.

Free laminar boundary layer convection

Because Ra is generally so large, even for the relatively small eruptive volumes represented by alkalic basalts, the flow régime will be of the thin boundary layer character. The limiting case of laminar boundary layer flow régimes is free convection from a flat plate. This problem has been solved by Squire (quoted in Goldstein, 1938) for arbitrary Pr with the results quoted below. In forced convection problems the thermal and momentum boundary layers (δ_t and δ_m) are not of equal thickness. In fact, for flow over a flat plate $\delta_m = Pr^{\frac{1}{3}}\delta_t$ (Bird *et al.* 1960, p. 369). In free convection problems, since it is the temperature difference which creates the buoyancy force the fluid will tend to descend only in the region where there is a temperature deficiency so δ_t has been set equal to δ_m (see Goldstein 1938, p. 641). For combined flow problems we would expect δ_t/δ_m to lie somewhere between 1 and $Pr^{-\frac{1}{3}}$.

Now, the boundary layer thickness δ is given by

$$\delta/r = 3.93\, Ra^{-\frac{1}{4}}, \tag{90}$$

with the scale velocity being given by

$$u_r = 5.17\nu\, Pr^{-\frac{1}{2}} \left[\frac{g\alpha(T_\infty - T_w)}{\nu^2}\right]^{\frac{1}{2}} r^{\frac{1}{2}}. \tag{91}$$

The expressions for the vertical (anti-parallel gravity vector) velocity and temperature are (y is measured orthogonal to $\boldsymbol{g}$ and positive *into* the magma chamber):

$$u = u_r \frac{y}{\delta}\left(1 - \frac{y}{\delta}\right)^2, \tag{92}$$

$$\frac{T - T_\infty}{T_w - T_\infty} = \left(1 - \frac{y}{\delta}\right)^2. \tag{93}$$

From (93) we calculate for the heat flux

$$q = -k\frac{\partial T}{\partial y} = \frac{2k(T_w - T_\infty)}{\delta}\left(1 - \frac{y}{\delta}\right), \tag{94}$$

so that at the wall ($y = 0$)

$$q_w = -k \left.\frac{\partial T}{\partial y}\right|_{y=0} = \frac{2k(T_w - T_\infty)}{\delta}. \tag{95}$$

Finally, the Nusselt number defined as

$$Nu \equiv \frac{Qr}{kS(T_\infty - T_w)} = \frac{q_w r}{k\Delta T}, \tag{96}$$

where Q is the quantity of heat transferred per unit time from a body of surface S, characteristic length r and thermal conductivity k, depends on Ra in the following fashion:

$$Nu = 0.508\, Ra^{\frac{1}{4}}. \tag{97}$$

Gathered in table 16 are the summarized results calculated by means of equations (90) to (97).

Table 16

All entries calculated using a length scale defined by a right cylinder where $r/l = 1$ so that $r = (V/\pi)^{\frac{1}{3}}$ where V is the volume of the magma chamber. The y coordinate axis is taken as positive into the magma chamber. The following parameters are taken as constant throughout:

$\kappa = 10^{-2}$ cm^2 s^{-1} $\quad \rho_L = 2.70$ g cm^{-3}
$\alpha = 5 \times 10^{-5}$ K^{-1} $\quad C_{P,L} = 0.30$ cal g^{-1} K^{-1}
$g = 981$ cm^2 s^{-1} $\quad \omega = 10$ cm s^{-1}
$k = 0.007$ cal cm^{-1} K^{-1} s^{-1} $\quad T_\infty - T_w = 200$ K
$Z = 75$ km

For laminar flow note that u attains its maximum value at $y = \frac{1}{3}\delta$ where $u_{max} = \frac{4}{27}u_r$. In turbulence u_{max} occurs at $y = \delta/29$ where $u_{max} = 0.54u_r$ $(T_e - T)$ is calculated from the definition of Nu and the volume of the magma body by means of the expression

$$(T_e - T) = \frac{4\pi k r Z (T_\infty - T_w)\, Nu}{\rho_L C_{P,L} \omega V} \tag{T 16}$$

where Z is the depth at which ascent begins and ω the rate of ascent. $(T_e - T)$ does not include latent heat effects such as the partial fusion of wall rock material. For that contribution to the temperature drop see values of $(T_e - T)$ in table 14. Values in parentheses are calculated by the equations for turbulent flow (equations (99) to (105)). The inset to the table gives the value of δ_m/δ_t calculated from Kraichnan (1962) for turbulent flow and from Bird *et al.* (1961) for laminar flow over a horizontal plate.)

volume / km^3	kinematic viscosity / cm^2 s^{-1}	Prandtl number (Pr)	Rayleigh number (Ra)	Nusselt‡ number (Nu)	heat flux at boundary $q = -k\left.\frac{\partial T}{\partial y}\right\|_{y=0}$ / cal cm^{-2} s^{-1}	boundary layer thickness δ / cm	maximum boundary layer‡ velocity $u_m = \frac{4}{27}u_r$ at $y = \frac{1}{3}\delta$ (laminar) $u_m = 0.54u_r$ at $y = \frac{1}{29}\delta$ (turbulent) / cm s^{-1}	$(T_e - T)$‡ / °C
0.03	2×10^2	2×10^4	4.7×10^{13}	1330 (4691)	8.75×10^{-2} (31.0×10^{-2})	32 (13)	3.0 (15)	15 (53)
0.03	50	5×10^3	1.9×10^{14}	1881 (7474)	12.5×10^{-2} (49.0×10^{-2})	22 (18)	5.0 (25)	21 (86)
0.185†	2×10^2	2×10^4	2.9×10^{14}	2096 (8605)	7.56×10^{-2} (31.0×10^{-2})	37 (19)	3.0 (39)	7 (29)
0.185	50	5×10^3	1.2×10^{15}	2972 (13815)	10.7×10^{-2} (50.0×10^{-2})	26 (28)	7.0 (62)	10 (47)
0.03	5.0×10^2	5×10^4	1.9×10^{13}	1061 (3469)	7.0×10^{-2} (23.0×10^{-2})	40 (10)	2.6 (11)	12 (39)

† This is an estimate of the volume of the remarkable Kaupulehu flow of the 1801 eruption of Hualalai Volcano, Hawaii.
‡ Values for tubulent flow régime in parentheses.

Pr	$\frac{\delta_m}{\delta_t} = 3.2\, Pr^{\frac{1}{3}}$ (turbulent)§	$\frac{\delta_m}{\delta_t} = Pr^{\frac{1}{3}}$ (laminar)§
5×10^3	226	17
1×10^4	320	22
2.5×10^4	506	29
3.5×10^4	599	33
5×10^4	716	37

§ δ_m/δ_t for turbulent flow calculated from Kraichnan (1962); δ_m/δ_t (laminar) from Bird *et al.* (1961).

PHILOSOPHICAL TRANSACTIONS OF THE ROYAL SOCIETY A MATHEMATICAL, PHYSICAL & ENGINEERING SCIENCES

It should be noted that the Squire solution does not permit a vertical velocity outside the boundary layer and furthermore assumes

$$\delta_t = \delta_m. \tag{98}$$

Lighthill (1953) has in his classic paper lifted the former constraint. As the results of his calculations are not very different from those given here we will not treat his results in any detail.

Free turbulent boundary layer convection

Examination of figure 10 in Lighthill (1953) or figure 10 in Shaw (1965) indicates that for most choices of the governing parameters (e.g. α, g, ΔT, r, ν, κ and l) rising alkali basalt diapirs will lie in a turbulent convective dynamic régime. That is, for the most part, calculated values of Ra are greater than 10^{10}. Summarized below are the equations governing the temperature and velocity fields in turbulent régimes. These were derived by Eckert & Jackson (1950) from integral forms of the conservation equations and are quoted from Rohsenow & Choi (1962). The derivation assumes $\delta_t = \delta_m$. Calculations were also performed using the results from a mixing-length type formulation by Kraichnan (1962), which does not assume $\delta_m = \delta_t$. Calculated results from the two methods appeared broadly compatible. For the sake of brevity, table 16 lists the results of the integral theory only. This should facilitate comparison of results with the laminar theory since the assumptions about δ_t and δ_m are the same. The equations used to calculate the results in parentheses in table 16 are as follows (these are analogous to equations (90) to (97) in the laminar case):

$$\frac{\delta}{r} = 0.527\, Ra^{-\frac{1}{10}}\, Pr^{-\frac{11}{30}}, \tag{99}$$

$$u_r = \frac{1.69\nu}{r}\, Ra^{\frac{1}{2}}\, Pr^{-\frac{5}{6}}, \tag{100}$$

$$u = u_r \left(\frac{y}{\delta}\right)^{\frac{1}{7}} \left(1-\frac{y}{\delta}\right)^{4}, \tag{101}$$

$$\frac{T-T_\infty}{T_w-T_\infty} = 1-\left(\frac{y}{\delta}\right)^{\frac{1}{7}}, \tag{102}$$

$$q = -k\frac{\partial T}{\partial y} = \frac{k(T_w-T_\infty)}{7y}\left(\frac{y}{\delta}\right)^{\frac{1}{7}}, \tag{103}$$

$$q_w = -k\left.\frac{\partial T}{\partial y}\right|_{y=0} = \frac{k(T_w-T_\infty)}{r}\, Nu, \tag{104}$$

and finally

$$Nu = 0.13\, Ra^{\frac{1}{3}}. \tag{105}$$

Discussion

Several significant conclusions come from an analysis of the computational results tabulated in table 16. Firstly, Ra numbers seem to exceed the critical value of about 10^{10} (above which there is turbulence) in spite of the rather small flow volumes. Even reducing $(T_\infty - T_w)$ by a factor of 10 (e.g. $T_\infty - T_w = 20$ °C) will not alter the conclusion that magmas rising through the mantle should be fairly well mixed. This is especially true when they ascend through relatively cool volumes of mantle. In the case of turbulent mixing, energy losses may be large

PHILOSOPHICAL TRANSACTIONS OF THE ROYAL SOCIETY A MATHEMATICAL, PHYSICAL & ENGINEERING SCIENCES

enough to crystallize significant portions of the diapir thereby reducing buoyancy forces and effectively ending ascent. From a heat transfer point of view it is interesting to note that for constant *Ra* the convective heat losses sustained by a rising diapir are 3 to 5 times greater for turbulent flow than for laminar. The assumption of adiabatic rise is often made in petrologic arguments. As can be seen, however, this assumption can be in error even for the rapidly ascending bodies calculated in table 16. The velocities calculated (for turbulence) are of the same order as the Stokes nodule settling rates and so the balance used earlier (equation (82)) may not be totally appropriate for high *Ra* flow.

Mass transfer rates

We now turn to a calculation of the rate of mass transfer a rising diapir may be expected to experience in its ascent. In the source region of course the liquid is in chemical and thermal equilibrium with its surroundings. Once it separates from its residue, however, and begins to rise into a cooler environment chemical potential and thermal gradients will be established and hence the tendency for mass and energy exchange will exist. We have already calculated heat losses and have shown they can be important. Our aim is to develop quantitative expressions for the rate of mass transfer for the various components. The authors recognize the fact that in general, multicomponent diffusion can be a very complicated process with various species diffusing up their activity gradients; the only constraint on the system is that the total rate of entropy production be positive and a minimum if the classical linear phenomenological laws are being followed. In addition to these problems, the diffusion tensors for each component in silicate melts have not been determined; consequently a rigorous treatment of multicomponent diffusion is beyond our means at the present time. As an alternative we treat the multicomponent silicate systems as pseudobinary systems to at least obtain an estimate of what mass fluxes may be important.

The equation of continuity for component i is (assuming constant ρ and D_i where D_i is the mass diffusivity of component i in the silicate melt and ignoring the non-steady term):

$$u\frac{\partial W_i}{\partial Z} = D_i\frac{\partial^2 W_i}{\partial y^2}, \tag{106}$$

where W_i is the mass fraction of component i and u is the velocity in the boundary layer. Concentration boundary layers are much smaller then either δ_t or δ_m because typical D_i values are orders of magnitude smaller than either κ or ν. In fact it can be shown (Bird *et al.* 1960, p. 607) that $\delta_m = Sc^{\frac{1}{3}}\,\delta_c$ where Sc, the Schmidt number, is defined as

$$Sc = \nu/D. \tag{107}$$

A typical value for Sc is $ca.\ 10^2/10^{-7} \approx 10^9$.

Accordingly, we expect the diffusional front to lie entirely within the thermal and momentum boundary layers and therefore take (for laminar flow)

$$u = \frac{3u_{\max}}{\delta}y \tag{108}$$

in equation (106) and

$$u = \frac{29u_{\max}}{\delta}y \tag{109}$$

in equation (106) for turbulent flow. This is tantamount to assuming that velocities are linear

functions of the y spatial coordinate within the thin chemical boundary layer. The boundary conditions for equation (106) are

$$\text{b.c. 1} \quad W = W_\infty \quad \text{at} \quad y = \infty, \tag{110}$$

$$\text{b.c. 2} \quad W = W_\text{w} \quad \text{at} \quad y = 0, \tag{111}$$

$$\text{b.c. 3} \quad W = W_\infty \quad \text{at} \quad Z = 0. \tag{112}$$

The solution to equation (106) subject to the velocity distributions given by (108) and (109) and the boundary conditions (110) through (112) is given in the appendix. The results for the mass flux at the wall are:

$$j^l_\text{m} = 1.12\rho_\text{L} D_i (W_\text{w} - W_\infty) \left(\frac{u_\text{max}}{3\delta r D_i}\right)^{\frac{1}{3}} \quad \text{(laminar flow, } l\text{)} \tag{113}$$

$$j^t_\text{m} = 1.12\rho_\text{L} D_i (W_\text{w} - W_\infty) \left(\frac{29 u_\text{max}}{9 D_i \delta r}\right)^{\frac{1}{3}} \quad \text{(turbulent flow, } t\text{)}. \tag{114}$$

These local rates may be used to calculate integral quantities (e.g. total mass gain or loss) analogous to the temperature loss calculations previously performed. This procedure gives

$$m^t_{T,i} = \frac{SZ}{\omega} j^t_{\text{m},i}, \tag{115}$$

$$m^l_{T,i} = \frac{SZ}{\omega} j^l_{\text{m},i}, \tag{116}$$

where S is the total surface area (taken here as $4\pi r^2$) and Z and ω the ascent depth and rate respectively. Table 17 presents some quantitative estimates of the local rate and total mass flow for a number of silicate melt components. The diffusivity data has come from a number of sources, the reliability of which is difficult to estimate. Nevertheless we feel these data do give some idea of the approximate amount of mass transfer that might take place in the flow regimes discussed in this paper. The values for u_max and δ come from the equations given earlier in the heat transfer section and are the same values listed in table 16. Several features may be noted by an examination of table 17. Turbulent mass transfer rates tend to be higher by about a factor of 5 or so than the corresponding laminar values. There are three main reasons for this: (1) the maximum velocity in turbulent flow occurs closer to the boundary; (2) the turbulent boundary layer is thinner than the laminar one thereby reducing the effective distance a particle must travel to get into the well mixed zone and (3) turbulent velocities (at constant Ra, Pr and ν) are higher than laminar velocities. Integral values of mass exchange ($m^t_{T,i}$ or $m^l_{T,i}$) are small in comparison to the total mass of the ascending diapir. For the case given in table 17 for instance, the total amount of magma is of order 3×10^{14} g whereas the greatest integral value, the value of 4×10^{10} g for MgO, represents a gain of only 0.15 mass % MgO. It should be pointed out, however, that these calculations depend inversely on the ascent velocity. If ω was 10 times smaller, for instance, mass transfer rates and integral quantities would be 10 times higher. Note that for components in small amounts (such as certain radiogenic nuclides) advective diffusional mass transfer could play a significant rôle, especially if concentration differences were magnified for some reason. Although it appears that to first order the nodule-bearing alkali basalts rise too quickly for any significant mass exchange these same equations and processes might find application to other magmatic systems. Marsh (1974) for example, calculated by energy balance methods similar to those used here, typical ascent times of 10^4

PHILOSOPHICAL TRANSACTIONS OF THE ROYAL SOCIETY A MATHEMATICAL, PHYSICAL & ENGINEERING SCIENCES

years for kilometre sized (radius) 'andesitic' magma bodies rises from Benioff zones in island arc areas. A calculation of the u_{max} and δ from the dynamical equations and application of equations (A 17) and (A 18) shows that indeed there should be significant mass exchange; a little reflection makes the idea of relatively acid magmas ascending through something of the order of 100 km of peridotitic mantle with no compositional imprint seem a bit implausible.

TABLE 17. MASS TRANSFER RATES

Estimates of convection diffusive mass fluxes and total mass exchange values for a typical alkali basalt system are listed in the table. The rate and integral quantities are calculated using equations (A 17) and (A 18) and estimates of the effective binary diffusivities from Winchell (1969), Shaw (1974), Medford (1973), Hoffman (1974), Varshneya & Cooper (1968*a*, *b*), Cooper *et al.* (1967) and the present authors. $W_w - W_\infty$ is calculated by subtracting from the mass fractions of the various oxide components in pyrolite the corresponding quantity in CSQ-28. The diffusivities in column 3 are approximations to D_i at 1500 °C for the various components in basic silicate melts. All values listed were calculated using u_{max} and δ values calculated by the hydrodynamic equations cited earlier and tabulated in table 16. The parameters held constant are as follows:

$Ra = 1.2 \times 10^{15}$ $\quad \rho_L = 2.75$ gm cm^{-3}

$Pr = 5 \times 10^3$ $\quad Z = 75$ km

$\nu = 50$ cm^2 s^{-1} $\quad \omega = 10$ cm s^{-1}

$V = 0.185$ km^3

Total magma mass $= \rho_L V = 2.5 \times 10^{14}$ g.

Negative fluxes and integral mass quantities refer to movement out of the magma into the surroundings. Columns 5 and 7 computed using equation 115 in the text)

com-ponent	$W_w - W_\infty$ (mass fraction)	D_i / cm^2 s^{-1}	j_m^i / g cm^{-2} s^{-1}	m_T^l / g	j_m^t / g cm^{-2} s^{-1}	m_T^t / g
Si	−0.0142	8×10^{-7}	-5×10^{-8}	-7.1×10^8	-1.1×10^{-5}	3×10^9
Ti	−0.0187	7×10^{-7}	-6×10^{-8}	-8.5×10^8	-2.6×10^{-7}	-3.6×10^9
Al	−0.120	5×10^{-7}	-3×10^{-7}	-4.2×10^9	-1.3×10^{-6}	-1.8×10^{10}
Fe	−0.0163	9×10^{-7}	-6×10^{-8}	-8.5×10^8	-2.6×10^{-7}	-3.6×10^9
Mg	0.288	4×10^{-7}	6×10^{-7}	8.5×10^9	2.6×10^{-6}	3.6×10^{10}
Ca	−0.0588	5×10^{-7}	-2×10^{-7}	-2.8×10^9	-8.6×10^{-7}	-1.2×10^{10}
Na	−0.0322	4×10^{-6}	-3.3×10^{-7}	-4.7×10^9	-1.4×10^{-6}	-2×10^{10}
K	−0.0156	2×10^{-6}	-1×10^{-7}	-1.4×10^9	-4.3×10^{-6}	-6×10^{10}
H_2O	−0.0100	1×10^{-7}	-8.7×10^{-9}	-1.2×10^8	-3.7×10^{-8}	-5×10^8
Ni	0.002	9×10^{-7}	7.6×10^{-9}	1.1×10^8	3.2×10^{-8}	4.7×10^8
Sr	0.002	9×10^{-5}	1.6×10^{-7}	2.3×10^9	6.9×10^{-7}	9.8×10^9
Cs	0.002	2×10^{-6}	1.3×10^{-8}	1.8×10^8	5.6×10^{-8}	7.7×10^8

In order to summarize the conclusions of the previous few sections, we attempt here to reconstruct the temperature-depth history of a specific sample – CSQ-28. This sample has been chosen since the equilibration of CSQ-28 liquid and its megacryst assemblage has been calculated. There are three main contributions to the temperature loss the ascending alkalic basalt magma body sustains:

(i) latent heat effects (equation (80) and table 14);

(ii) convective heat loss through boundary layer flow (equations (90)–(97) for laminar flow; equations (99)–(105) for turbulent flow, equation (T 16) and table 16);

(iii) heat effect associated with work done by expansion as the magma rises to lower pressure environment (i.e. the adiabatic work term).

PHILOSOPHICAL TRANSACTIONS OF THE ROYAL SOCIETY A MATHEMATICAL, PHYSICAL & ENGINEERING SCIENCES

For CSQ-28 we take as the starting point or point of beginning ascent, the previously calculated equilibration conditions with spinel bearing peridotite of

$$T_e = 1356\ ^\circ\text{C},\ 1629\ \text{K},$$

$$P_e = 24.1\ \text{kbar}\ (Z_e = 77\ \text{km}).$$

The adiabatic temperature drop experienced by the magma body is given by

$$(\Delta T)^{\text{reversible}}_{\text{expansion}} = -T_e\,[1-\exp\,(-\alpha g(Z-Z_e)/C_{P,\,L})] \simeq -47\ ^\circ\text{C}.$$

Assuming the volume of magma to be 0.03 km^3 and ω, the ascent rate to be on the average 10 cm s^{-1} we calculate from equation (64) an effective mantle viscosity of $\eta_m \sim 7.3 \times 10^9$ P. Equations (72) and (73) then allows an estimate of $(T-T_s)$ for peridotite of 277 °C, the thickness of the partial melt zone being $\delta r \sim 12$ cm (equation (79)). The temperature loss incurred by the magma (equation (80)) is $(T_e-T)^{\text{latent}}_{\text{heat}} \simeq 54$ °C. Application of the turbulent hydrodynamic equations enables us to estimate the convective heat loss for the system. We have, after application of equations (99), (100), (105) and (T 16) (see legend of table 16) $(T_e-T)_{\text{convection}} \simeq 175°$. If these heat effects are distributed linearly over the ascent depth we estimate a total ΔT of -183 °C over a length of 77 km for a linear temperature gradient of -2.4 °C/km. We would predict a value of $T_e+(\Delta T)_{\text{heat loss}} = 1173$ °C for the temperature at which the lava is erupted. At the depth of megacryst precipitation (~ 50 km) we would predict a temperature of 1291 °C, about 57 °C higher than the calculated equilibration temperature. Considering the uncertainty in the thermodynamic and transport properties this discrepancy is not particularly unsettling.

Conclusions

We can think of no better statement to end this paper with than one written by H. R. Shaw in a paper published in 1965:

> In a sense, the preceding commentary may be construed as a catalogue of deficiencies in our knowledge of magmatic systems. These are perhaps about equally divided between insufficient quantitative data from the field and an inadequate foundation in theory and experiment for their interpretation. Many of the latter have been pointed out already, but it is the problem of quantitative measurements from the field that is perhaps the major obstacle in view of the difficulty and time required to carry out measurements in sufficient detail. The mechanistic approach to problems of magmatic evolution may seem to offer impossible goals, and consequently gathering data toward these ends may seem fruitless. Consider, however, that it is precisely the elucidation of the mechanical process by which an igneous rock is produced that is one of the chief aims, usually only by implication, of petrogenetic studies. The work that is needed most is to extend observations of a kind already made as a routine part of petrologic studies, that is, formulate on a more quantitative basis the description of an igneous rock body with regard to all chemical, mineralogical, and textural variations within a quantitatively described geologic setting. These results can provide us with several guides to an interpretation of the mechanical history of the rock body.

PHILOSOPHICAL TRANSACTIONS OF THE ROYAL SOCIETY A MATHEMATICAL, PHYSICAL & ENGINEERING SCIENCES

To these comments we would only like to emphasize the importance of viewing magmatic systems historically; that is as a succession of chemical and mechanical instabilities each operating with an appropriate time scale. The product of any given volcanic eruption is really the physical manifestation of the superposition of the various competing thermodynamic and thermomechanical processes operating in the Earth.

This research was supported by the National Science Foundation (EAR74-12782), the United States Energy Research and Development Administration, the Committee on Research of the University of California, the Penrose Fund of the Geological Society of America and the National Research Council of Canada (A7372). We are particularly indebted to Dr R. Hultgren for the use of his drop calorimeter and to Dr C. R. Bacon for instruction in its use. Dr H. R. Shaw provided guidance, criticism and continuous commentary.

Appendix

The equations we want to solve are

$$\frac{3u_{\mathrm{m}}}{\delta}\, y\, \frac{\partial W_i}{\partial Z} = D_i \frac{\partial^2 W_i}{\partial y^2} \quad \text{(laminar flow)}, \tag{A 1}$$

$$\frac{29u_{\mathrm{m}}}{\delta}\, y\, \frac{\partial W_i}{\partial Z} = D_i \frac{\partial^2 W_i}{\partial y^2} \quad \text{(turbulent flow)}, \tag{A 2}$$

subject to the boundary conditions

$$W = W_{\mathrm{w}} \quad \text{at} \quad y = 0,$$

$$W = W_{\infty} \quad \text{at} \quad y = \infty.$$

Now, let

$$\beta_l = \frac{D\delta}{3u_{\max}}, \quad \beta_t = \frac{D\delta}{29u_{\max}} \tag{A 3}$$

so that we have

$$y\, \frac{\partial W_i}{\partial Z} = \beta_l \frac{\partial^2 W_i}{\partial y^2} \tag{A 4}$$

and an equation with β_t instead of β_l for the turbulent case. In what follows we only deal with the laminar case; the turbulent results may be found by simply substituting β_t for β_l.

We define the following reduced variables

$$C = \frac{W - W_{\infty}}{W_{\mathrm{w}} - W_{\infty}} \quad \text{and} \quad \eta = y(9\beta z)^{-\frac{1}{3}}$$

and substituting these back into (A 4) we have after some reduction

$$\frac{\mathrm{d}^2 C}{\mathrm{d}\eta^2} + 3\eta^2 \frac{\mathrm{d}C}{\mathrm{d}\eta} = 0, \tag{A 6}$$

$$\left.\begin{aligned} &\text{b.c. 1.} \quad C = 0 \quad \text{as} \quad \eta \to \infty \\ &\text{b.c. 2.} \quad C = 1 \quad \text{at} \quad \eta = 0 \end{aligned}\right\}. \tag{A 7}$$

Integrating (A 6) once gives

$$\frac{\mathrm{d}C}{\mathrm{d}\eta} = B_1 \mathrm{e}^{-\eta^3}, \tag{A 8}$$

which may be integrated again to give

$$C = B_1 \int_0^{\eta} \mathrm{e}^{-\eta^3}\, \mathrm{d}\eta + B_2. \tag{A 9}$$

Applying the boundary conditions to (A 9) we solve for the constants B_1 and B_2. This gives

$$B_1 = 1 \quad \text{and} \tag{A 10}$$

$$B_2 = \left[-\int_0^\infty \mathrm{e}^{-\eta^3}\,\mathrm{d}\eta\right]^{-1}. \tag{A 11}$$

The definite integral is well known, being the value of the gamma function

$$\Gamma(\tfrac{4}{3}) = \tfrac{1}{3}\Gamma(\tfrac{1}{3}) = 0.893. \tag{A 12}$$

The final result for the mass distribution becomes

$$C = \frac{\int_0^\eta \mathrm{e}^{-\eta^3}\,\mathrm{d}\eta}{\int_0^\infty \mathrm{e}^{-\eta^3}\,\mathrm{d}\eta} + 1 = 1 - 1.12\int_0^\eta \mathrm{e}^{-\eta^3}\,\mathrm{d}\eta. \tag{A 13}$$

The mass flux at the wall entering the magma body is obtained as follows

$$j_{\mathrm{m},i} = -\rho_{\mathrm{L}} D_i \frac{\mathrm{d}W}{\mathrm{d}y} = -\rho D_i \frac{\partial W}{\partial c}\frac{\partial C}{\partial \eta}\frac{\partial \eta}{\partial y}, \tag{A 14}$$

$$= -\rho_{\mathrm{L}} D_i (W_{\mathrm{w}} - W_\infty)\frac{\eta}{y}\frac{\mathrm{d}c}{\mathrm{d}\eta}, \tag{A 15}$$

$$j_{\mathrm{m},i} = \frac{+\rho_{\mathrm{L}} D_i (W_{\mathrm{w}} - W_\infty)}{\Gamma(\frac{4}{3})}\left(\frac{u_{\max}}{3D_i \delta Z}\right)^{\frac{1}{3}} \exp\left[\frac{-u_{\max}\, y^3}{3\delta D_i Z}\right]. \tag{A 16}$$

At the wall, $y = 0$ (recall that y is positive *into* the magma) and letting r be the reference length scale we have

$$j^{\mathrm{l}}_{\mathrm{m},i} = 1.12\rho_{\mathrm{L}} D_i (W_{\mathrm{w}} - W_\infty)\left(\frac{u_{\max}}{3D_i \delta r}\right)^{\frac{1}{3}} \quad \text{(laminar flow)} \tag{A 17}$$

and

$$j^{t}_{\mathrm{m},i} = 1.12\rho_{\mathrm{L}} D_i (W_{\mathrm{w}} - W_\infty)\left(\frac{29u_{\max}}{9D_i \delta r}\right)^{\frac{1}{3}} \quad \text{(turbulent flow)}. \tag{A 18}$$

j_{m} is measured in g cm^{-2} s^{-1}.

References (Carmichael *et al.*)

Aoki, K. & Shiba, I. 1943 Pyroxenes from lherzolite inclusions of Itinomegata, Japan. *Lithos* **6**, 41–52.

Arculus, R. J. 1975 Melting behavior of two basanites in the range 10–35 kbar and the effect of TiO_2 on the olivine–diopside reactions at high pressures. *Carnegie Inst. Wash. Yb.* **74**, 512–515.

Arculus, R. J. & Shimizu, N. 1974 Rare earth elements in a suite of basanitoids and alkali olivine basalts from Grenada, Lesser Antilles. *Carnegie Inst. Wash. Yb.* **73**, 553–560.

Arndt, J. & Häberle, F. 1973 Thermal expansion and glass transition temperatures of synthetic glasses of plagioclase-like compositions. *Contr. Mineral. Petrol.* **39**, 175–183.

Bacon, C. R. 1977 High temperature heat content and heat capacity of silicate glasses: experimental determination and a model for calculation. *Am. J. Sci.* **277**, 109–135.

Bacon, C. R. & Carmichael, I. S. E. 1973 Stages in the P–T path of ascending basalt magma: An example from San Quentin, Baja California. *Contr. Mineral. Petrol.* **41**, 1–22.

Batchelor, G. K. 1967 *An introduction to fluid dynamics*. Cambridge University Press.

Bennett, F. D. 1971 Vaporization waves in explosive volcanism. *Nature, Lond.* **234**, 538–539.

Binns, R. A., Duggan, M. B. & Wilkinson, J. F. G. 1970 High-pressure megacrysts in alkaline lavas from north-eastern New South Wales. *Am. J. Sci.* **269**, 132–168.

Birch, F. 1966 Compressibility; elastic constants. In *Handbook of physical constants* (ed. S. P. Clark, Jr), pp. 97–173. Geol. Soc. Am. Mem.

Bird, R. B., Stewart, W. E. & Lightfoot, E. N. 1960 *Transport phenomena*. New York: John Wiley.

PHILOSOPHICAL TRANSACTIONS OF THE ROYAL SOCIETY A MATHEMATICAL, PHYSICAL & ENGINEERING SCIENCES

Bottinga, Y. A. & Weill, D. F. 1970 Densities of liquid silicate systems calculated from partial molar volumes of oxide components. *Am. J. Sci.* **269**, 169–182.
Boyd, F. R. 1969 Electron microprobe study of diopside inclusions from kimberlite. *Am. J. Sci.* **267** A, 50–69.
Boyd, F. R. 1973 A pyroxene geotherm. *Geochim. cosmochim. Acta* **37**, 2533–2546.
Boyd, F. R. & England, J. L. 1963 Effect of pressure on the melting of diopside, $CaMgSi_2O_6$, and albite, $NaAlSi_3O_8$, in the range up to 50 kilobars. *J. geophys. Res.* **68**, 311–323.
Brown, F. H. 1971 Volcanic petrology of the Toro-Ankole region, Western Uganda. Ph.D. Thesis, University of California, Berkeley, 152 pp.
Brown, F. H. & Carmichael, I. S.E. 1971 Quaternary volcanoes of the Lake Rudolf region: II. The lavas of North Island, South Island, and the Barrier. *Lithos* **4**, 305–323.
Buddington, A. F. & Lindsley, D. H. 1964 Iron–titanium oxide minerals and synthetic equivalents. *J. Petrol.* **5**, 310–357.
Bultitude, R. J. & Green, D. H. 1971 Experimental study of crystal–liquid relationships at high pressures in olivine nephelinite and basanite compositions. *J. Petrol.* **12**, 121–147.
Burnham, C. W. 1975 Water and magmas; a mixing model. *Geochim. cosmochim. Acta* **39**, 1077–1084.
Burnham, C. W. & Davis, N. F. 1971 The role of H_2O in silicate melts. I. P–V–T relations in the system $NaAlSi_3O_8$–H_2O to 10 kilobars and 1000 °C. *Am. J. Sci.* **270**, 54–79.
Burnham, C. W. & Davis, N. F. 1974 The role of H_2O in silicate melts. II. Thermodynamic and phase relations in the system $NaAlSi_3O_8$–H_2O to 10 kilobars, 700° to 1100 °C. *Am. J. Sci.* **274**, 902–940.
Carmichael, I. S. E. 1967*a* The mineralogy and petrology of the volcanic rocks from the Leucite Hills, Wyoming. *Contr. Mineral. Petrol.* **15**, 24–66.
Carmichael, I. S. E. 1967*b* The mineralogy of Thingmuli, a Tertiary volcano in Eastern Iceland. *Am. Miner.* **52**, 1815–1841.
Carmichael, I. S. E., Turner, F. J. & Verhoogen, J. 1974 *Igneous petrology*. New York: McGraw Hill.
Carslaw, H. S. & Jaeger, J. C. 1959 *Conduction of heat in solids*, 2nd ed. Oxford University Press.
Chandrasekkar, S. 1961 *Hydrodynamics and hydromagnetic stability*. Oxford University Press.
Charlu, T. V., Newton, R. C. & Kleppa, O. J. 1975 Enthalpies of formation at 970 K of compounds in the system MgO–Al_2O_3–SiO_2 from high temperature solution calorimetry. *Geochim. cosmochim. Acta* **39**, 1487–1497.
Cooper, A. R. & Varshenya, A. K. 1968 Diffusion in the system K_2O-SrO-SiO_2. I. Effective binary diffusion coefficients. *J. Am. Ceram. Soc.* **51**, 103–106.
Dawson, J. B., Powell, D. G. & Reid, A. M. 1970 Ultrabasic xenoliths and lava from the Lashaine Volcano, Northern Tanzania. *J. Petrol.* **11**, 519–548.
Eckert, E. G. & Jackson, T. W. 1950 *Nat. Advisory Comm. Aeronaut. Tech. Note* 2207.
Eggler, D. H. 1972 Water saturated and unsaturated melting relations in a Paricutin andesite and an estimate of water content in the natural magma. *Contr. Mineral. Petrol.* **34**, 261–271.
Faizullaev, D. 1969 *Laminar motion of multiphase media in conduits*. New York: Consultants Bureau.
Ferrier, A. 1970 Kristallisationswärme von diopsid. *Ber. Dt. Keram. Ges.* **47**, 64–67.
Flood, H. & Knapp, W. J. 1968 Structural characteristics of liquid mixtures of feldspars and silica. *J. Am. Ceram. Soc.* **51**, 259–263.
Flower, M. F. J. 1971 Evidence for the role of phlogopite in the genesis of alkali basalts. *Contr. Mineral. Petrol.* **32**, 126–137.
Ganguly, J. 1973 Activity-composition relation of jadeite in omphacite pyroxene: theoretical deductions. *Earth Planet. Sci. Lett.* **19**, 145–153.
Gast, P. W. 1968 Trace element fractionation and the origin of tholeiitic and alkaline magma types. *Geochim. cosmochim. Acta* **32**, 1057–1086.
Goldstein, S. 1938 *Modern developments in fluid mechanics*, vol. 2. Oxford: Clarendon Press.
Green, D. H. 1970 The origin of basaltic and nephelinitic magmas. *Trans. Leicester Lit. Phil. Soc.* **64**, 26–54.
Green, D. H. 1973*a* Conditions of melting of basanite magma from garnet peridotite. *Earth Planet. Sci. Lett.* **17**, 456–465.
Green, D. H. 1973*b* Experimental melting studies on a model upper mantle composition at high pressure under water-saturated and water-undersaturated conditions. *Earth Planet. Sci. Lett.* **19**, 37–53.
Green, D. H. & Hibberson, W. O. 1970 Experimental duplication of conditions of precipitation of high pressure phenocrysts in a basaltic magma. *Phys. Earth Planet. Int.* **3**, 247–254.
Green, D. H. & Ringwood, A. E. 1967 The genesis of basaltic magmas. *Contr. Mineral. Petrol.* **15**, 103–190.
Gruntfest, I. J. 1963 Thermal feedback in liquid flow; plane shear at constant stress. *Trans. Soc. Rheol.* **7**, 195–207.
Hallman, T. M. 1956 Combined forced and free-laminar transfer in vertical tubes with uniform internal heat generation. *Trans. A.S.M.E.* **78**, 1831–1840.
Hamilton, D. L., Burnham, C. W. & Osborn, E. F. 1964 The solubility of water and effects of oxygen fugacity and water content on crystallization in mafic magmas. *J. Petrol.* **5**, 21–39.
Heming, R. F. & Carmichael, I. S. E. 1973 High-temperature pumice flows from the Rabaul Caldera, Papua, New Guinea. *Contr. Mineral. Petrol.* **38**, 1–20.
Hensen, B. J., Schmid, R. & Wood, B. J. 1975 Activity–composition relationships for pyrope-grossular garnet. *Contr. Mineral. Petrol.* **51**, 161–166.

PHILOSOPHICAL TRANSACTIONS OF THE ROYAL SOCIETY A MATHEMATICAL, PHYSICAL & ENGINEERING SCIENCES

Hoffman, A. 1974 *Dept. Terrestrial Magnetism, Carnegie Inst. Wash. Yb.* **74**, 183.
Holloway, J. R. 1973 The system pargasite–H_2O–CO_2: a model for melting of a hydrous mineral with a mixed volatile fluid. I. Experimental results to 8 kbar. *Geochim. cosmochim. Acta* **37**, 651–666.
Irving, A. J. 1974 Megacrysts from the newer basalts and other basaltic rocks of southeastern Australia. *Geol. Soc. Am. Bull.* **85**, 1503–1514.
JANAF 1971 *JANAF Thermochemical Tables*, 2nd edn. Nat. Stand. Ref. Data Ser., Nat. Bur. Stand. (U.S.) **37**, 1141 pages.
JANAF 1974 Thermochemical Tables, 1974 Supplement. *J. Phys Chem. Ref. Data* **3**, 311–480.
JANAF 1975 Thermochemical Tables, 1975 Supplement. *J. Phys Chem. Ref. Data* **4**, 1–175.
Janz, G. J. 1967 *Molten salts handbook*. New York: Academic Press Inc.
Jessup, R. S. 1955 A new bunsen-type calorimeter. *J. Res. Nat. Bur. Stds.* **55**, 317–322.
Kay, J. M. 1968 *An introduction to fluid mechanics and heat transfer*, 2nd ed. Cambridge University Press.
Kay, R. W. & Gast, P. W. 1973 The rare earth content and origin of alkali-rich basalts. *J. Geol.* **18**, 653–682.
Kelley, K. K. 1960 Contributions to the data on theoretical metallurgy: pt. 13, high temperature heat content, heat capacity and entropy data for the elements and inorganic compounds. *U.S. Bur. Mines Bull.* **584**, 232 pp.
Kerrick, D. M. & Darken, L. S. 1975 Statistical thermodynamic models for ideal oxide and silicate solid solutions, with applications to plagioclase. *Geochim. cosmochim. Acta* **39**, 1431–1442.
King, E. G., Orr, R. L. & Bonnickson, K. R. 1954 Low temperature heat capacity, entropy at 298.16 °K., and high temperature heat content of sphene ($CaTiSiO_5$). *J. Am. Chem. Soc.* **76**, 4320–4321.
Kirshenbaum, A. D. & Cahill, J. A. 1960 The density of liquid aluminium oxide. *J. inorg. nucl. Chem.* **14**, 283–287
Klein, L. & Uhlman, D. R. 1974 Crystallization behavior of anorthite. *J. geophys. Res.* **79**, 4869–4874.
Klotz, I. R. 1964 *Chemical thermodynamics*, New York: W. A. Benjamin Inc.
Kraichnan, R. H. 1962 Turbulent thermal convection at arbitrary Prandtl number. *Phys. Fluids* **5**, 1374–1389.
Kudo, A. M. & Weill, D. F. 1970 An igneous plagioclase thermometer. *Contr. Mineral. Petrol.* **25**, 52–65.
Kushiro, I., Shimizu, N., Nakamura, Y. & Akimoto, S. 1972 Compositions of coexisting liquid and solid phases formed upon melting of natural garnet and spinel lherzolites at high presures: A preliminary report. *Earth Planet. Sci. Lett.* **14**, 19–25.
Lacy, E. D. 1955 Atomic packing in silicate glasses. In *The vitreous state*, pp. 23–46. University of Sheffield, England: Glass Delegacy.
Lamb, H. 1945 *Hydrodynamics*, 6th ed. New York: Dover Publications.
Leu, A., Ma, S. & Eyring, H. 1975 Properties of molten magnesium oxide. *Proc. Natn. Acad. Sci. U.S.A.* **72**, 1026–1030.
Lighthill, M. J. 1953 Theoretical considerations on free convection in tubes. *Q. J. Mech. appl. Math.* **6**, 398–439.
Lindsley, D. H. 1966 Melting relations of $KAlSi_3O_8$: effect of pressures up to 40 kilobars. *Am. Mineral.* **51**, 1793–1799.
Lindsley, D. H. 1967 Pressure–temperature relations in the system FeO-SiO_2. *Carnegie Inst. Wash. Yb.* **65**, 226–230.
Lumsden, J. 1961 The thermodynamics of liquid iron silicates, in Physical Chemistry of Process Metallurgy. *Metal. Soc. Conf.* **7**. New York: Interscience.
MacDonald, G. A. 1949 Petrography of the island of Hawaii. *U.S. Geol. Soc. Prof. Paper* **214**-D, 51–96.
MacGregor, I. D. 1969 The system MgO-SiO_2-TiO_2 and its bearing on the distribution of TiO_2 in basalts. *Am. J. Sci.* **267**-A, 342–363.
MacGregor, I. D. & Basu, A. R. 1974 Thermal structure of the lithosphere: a petrologic model. *Science, N.Y.* **185**, 1007–1011.
Mah, A. D. 1960 Thermodynamic properties of manganese and its compounds. *U.S. Bureau of Mines Report of Investigations* 5600, 34 pp.
Marsh, B. D. 1974 Aleutian island arc magmatism. Ph.D. Thesis, University of California, Berkeley.
McNown, J. S. & Malaika, J. 1950 Effects of particle shape on settling velocity at low Reynolds numbers. *Am. geophys. Un. Trans.* **31**, 74–82.
Medford, G. A. 1973 Calcium diffusion in a mugearite melt. *Can. J. Earth Sci.* **10**, 394–402.
Mercier, J. C. & Carter, N. L. 1975 Pyroxene geotherms. *J. geophys. Res.* **80**, 3349–3362.
Meyer, H. O. A. & Boyd, F. R. 1972 Composition and origin of crystalline inclusions in natural diamonds. *Geochim. cosmochim. Acta* **36**, 1255–1273.
Meyers, G. E. 1971 *Analytical methods in conduction heat transfer*. New York: McGraw-Hill.
Millhollen, G. L., Irving, A. J. & Wyllie, P. J. 1974 Melting interval of peridotite with 5.7 percent water to 30 kilobars. *J. Geol.* **82**, 575–587.
Moore, J. G. 1970 Water content of basalt erupted on the ocean floor. *Contr. Mineral. Petrol.* **28**, 272–279.
Morton, B. R. 1960 Laminar convection in uniformity heated vertical pipes. *J. Fluid Mech.* **8**, 227–240.
Mysen, B. & Boettcher, A. L. 1975 Melting of a hydrous mantle. II. Geochemistry of crystals and liquids formed by anatexis of mantle peridotite at high pressures and temperatures as a function of controlled activities of water, hydrogen, and carbon dioxide. *J. Petrol.* **16**, 549–593.
Nafziger, R. H. 1973 High-temperature activity composition relations of equilibrium spinels, olivines and pyroxenes in the system MgO-Fe-SiO_2. *Am. Mineral.* **58**, 457–465.

PHILOSOPHICAL TRANSACTIONS OF THE ROYAL SOCIETY A MATHEMATICAL, PHYSICAL & ENGINEERING SCIENCES

Navrotsky, A. 1971 The intracrystalline cation distribution and the thermodynamics of solid solution formation in the system $FeSiO_3$-$MgSiO_3$. *Am. Mineral* **56**, 201–211.
Naylor, B. F. 1945 High temperature heat contents of sodium metasilicate. *J. Am. Ceram. Soc.* **41**, 461–463.
Nehru, C. G. & Wyllie, P. J. 1974 Electron microprobe measurement of pyroxenes coexisting with H_2O-saturated liquid in the join $CaMgSi_2O_6$-$Mg_2Si_2O_6$ at 30 kilobars with application to geothermometry. *Contr. Mineral. Petrol.* **48**, 221–228.
Nicholls, I. A. & Ringwood, A. E. 1973 Effect of water on olivine stability in thoeliites and the production of silica-saturated magmas in the island arc environment. *J. Geol.* **81**, 285–300.
Nicholls, J. & Carmichael, I. S. E. 1972 The equilibration temperature and pressure of various lava types with spinel and garnet peridotite. *Am. Mineral.* **57**, 941–959.
Nicholls, J., Carmichael, I. S. E. & Stormer, J. 1971 Silica activity and P_{total} in igneous rocks. *Contr. Mineral. Petrol.* **33**, 1–20.
Nicolis, G., Prigogine, I. & Glansdorff 1975 On the mechanism of instabilities in nonlinear systems. *Adv. Chem. Phys.* **32**, 1–11.
O'Hara, M. J., Richardson, S. W. & Wilson, G. 1971 Garnet–peridotite stability and occurrence in crust and mantle. *Contr. Mineral. Petrol.* **32**, 48–68.
O'Nions, R. K. & Grönwold, K. 1973 Petrogenetic relationship of acid and basic rocks in Iceland: Sr isotopes and rare-earth elements in late and postglacial volcanics. *Earth Planet. Sci. Lett.* **19**, 397–409.
Orr, R. L. 1953 High-temperature heat contents of magnesium orthosilicate and ferrous orthosilicate. *J. Am. Chem. Soc.* **75**, 528–529.
Ostrach, S. & Thornton, P. R. 1958 On the stagnation of natural-convection flows in closed-end tubes. *Trans. A.S.M.E.* **80**, 363–366.
Pankratz, L. 1968 High temperature heat contents and entropies of dehydrated analcite, kaliophilite and leucite. *U.S. Bur. Mines Dept. Invest.* 7201.
Prigogine, I. & Defay, R. 1954 *Chemical thermodynamics* (trans. D. H. Everett). London: Longmans, Green and Co.
Prigogine, I. & Lefever, R. 1975 Stability and self-organization in open systems. *Adv chem. Phys.* **24**, 1–28.
Ramberg, H. 1968 Mantle diapirism and its tectonic and magmagenetic consequences. *Phys. Earth Planet. Interiors* **5**, 45–60.
Robie, R. A. & Waldbaum, D. R. 1968 Thermodynamic properties of minerals and related substances at 298.15 °K (25.0 °C) and one atmosphere (1.013 bars) pressure and at higher temperatures. *U.S.G.S. Bull. No.* 1259, 256 pp.
Rohsenow, W. M. & Choi, H. Y. 1962 *Heat, mass, and momentum transfer*. New Jersey: Prentice-Hall.
Rosenhauer, M. & Eggler, D. H. 1975 Solution of H_2O and CO_2 in diopside melt. *Carnegie Inst. Wash. Yb.* **74**, 474–479.
Rowlinson, J. S. 1969 *Liquids and liquid mixtures*, 2nd ed. London: Butterworth.
Scarfe, C. M. 1973 Water solubility in basic and ultrabasic magmas. *Nature Phys. Sci.* **246**, 9–11.
Scarfe, C. M., Luth, W. C. & Tuttle, O. F. 1966 An experimental study bearing on the absence of leucite in plutonic rocks. *Am. Mineral.* **51**, 726–735.
Scheele, G. F. & Hanratty, T. J. 1962 Effect of natural convection on stability of flow in a vertical pipe. *J. Fluid Mech.* **14**, 244–256.
Scherer, G., Hopper, R. W. & Uhlman, D. R. 1972 Crystallization behavior and glass formation of selected lunar compositions. *Proceedings of the Third Lunar Science Conference, Geochim. cosmochim. Acta Suppl.* **3**, 2627–2637.
Schweite, H. E. & Ziegler, G. 1955 Beitrag zur specifichen wärme der gläser. *Glastech Ber.* **28**, 137–146.
Shaw, H. R. 1965 Comments on viscosity, crystal settling, and convection in granitic systems. *Am. J. Sci.* **263**, 120–152.
Shaw, H. R. 1969 Rheology of basalt in the melting range. *J. Petrol.* **10**, 510–535.
Shaw, H. R. 1972 Viscosities of magmatic silicate liquids: an empirical method of prediction. *Am. J. Sci.* **272**, 870–893.
Shaw, H. R. 1973 Mantle convection and volcanic periodicity in the Pacific; evidence from Hawaii. *Geol. Soc. Am. Bull.* **84**, 1505–1527.
Shaw, H. R. 1974 Diffusion of H_2O in granitic liquids. Part 1, Experimental data; Part II, Mass transfer in magma chambers. In *Geochemical transport and kinetics*. Proceedings of a Conference held at Airlie House, Warrenton, Virginia, June 1973 (eds. A. W. Hoffmsn, B. J. Gilletti, H. S. Yoder & R. A. Gund), pp. 139–170. Washington: Carnegie Inst.
Shpil'rain, E. E., Kagan, D. N. & Barkhatov, L. S. 1972 Thermodynamic properties of the condensed phase of alumina near the melting point. *High Temperatures–High Pressures* **4**, 605–609.
Skinner, B. J. 1966 Thermal expansion. In *Handbook of physical constants* (ed. S. P. Clark, Jr.), pp. 75–96. Geol. Soc. Am. Mem.
Slagle, O. D. & Nelson, R. P. 1970 Adiabatic compressibility of molten alumina. *J. Am. Ceram. Soc.* **53**, 637–638.
Sleep, N. H. 1974 Segregation of magma from a mostly crystalline mush. *Geol. Soc. Am. Bull.* **85**, 1225–1232.
Smith, A. L. & Carmichael, I. S. E. 1968 Quaternary lavas from the southern Cascades, Western U.S.A. *Contr. Mineral. Petrol.* **19**, 212–238.

PHILOSOPHICAL TRANSACTIONS OF THE ROYAL SOCIETY A MATHEMATICAL, PHYSICAL & ENGINEERING SCIENCES

Smith, A. L. & Carmichael, I. S. E. 1969 Quaternary trachybasalts from Southeastern California. *Am. Mineral.* **54**, 909–923.
Smith, D. 1970 Stability of iron-rich orthopyroxene. *Carnegie Inst. Wash. Yb.* **68**, 229–231.
Sommerville, I. D., Ivanchev, I. & Bell, H. B. 1973 Quoted from: Richardson, F. D. 1974 *Physical chemistry of melts in metallurgy*, vol. 1, 289 pages. London: Academic Press.
Spera, F. J. 1974 A thermodynamic basis for predicting water solubilities in silicate melts and implications for the low velocity zone. *Contr. Mineral. Petrol.* **45**, 175–186.
Spera, F. J. & Hildreth, W. 1974 Activity of H_2O in undersaturated silicate liquids: petrogenetic implications. (Abs.) *Geol. Soc. Am. Abst. with Prog.* **6**, 964.
Stormer, J. C., Jr. 1973 Calcium zoning in olivine and its relationship to silica activity and pressure. *Geochim. cosmochim. Acta* **37**, 1815–1821.
Stuckless, J. S. & Erickson, R. L. 1976 Strontium isotopic geochemistry of the volcanic rocks and associated megacrysts and inclusions from Ross Island and vicinity, Antarctica. *Contr. Mineral. Petrol.* **58**, 111–126.
Stuckless, J. S. & Irving, A. J. 1976 Strontium isotope geochemistry of megacrysts and host basalts from Southeastern Australia. *Geochim. cosmochim. Acta* **40**, 209–213.
Stueber, A. M. & Ikramuddin, M. 1974 Rubidium, strontium and the isotopic composition of strontium in ultramafic nodule minerals and host basalts. *Geochim. cosmochim. Acta* **38**, 207–216.
Sutterby, J. L. 1973 Falling sphere viscometry. I. Wall and inertial corrections to Stokes' Law in long tubes. *Trans. Soc. Rheology* **17**, 559–573.
Varshenya, A. K. & Cooper, A. R. 1972*a* Diffusion in the system K_2O–SrO–SiO_2. II. Cation self-diffusion coefficients. *J. Am. Ceram. Soc.* **55**, 220–223.
Varshenya, A. K. & Cooper, A. R. 1972*b* Diffusion in the system K_2O–SrO–SiO_2. III. Interdiffusion coefficients. *J. Am. Ceram. Soc.* **55**, 312–317.
Verhoogen, J. 1962 Oxidation of iron–titanium oxides in igneous rocks. *J. Geol.* **70**, 168–181.
Weertman, J. 1971 Theory of water-filled crevices in glaciers applied to vertical magma transport beneath oceanic ridges. *J. geophys. Res.* **76**, 1171–1183.
Weill, D. F. & Drake, M. J. 1973 Europium anomaly in plagioclase feldspar: Experimental results and semi-quantitative model. *Science, N.Y.* **180**, 1059–1060.
Whitehead, J. A. & Luther, D. S. 1975 Dynamics of laboratory diapirs and plume models. *J. geophys. Res.* **80**, 705–717.
Williams, R. J. 1971 Reaction constants in the system Fe–MgO–SiO_2–O_2 at 1 atm. between 900 °C and 1300 °C: Experimental results. *Am. J. Sci.* **270**, 334–360.
Williams, R. J. 1972 Activity-composition relations in the fayalite-forsterite solid solution between 900 °C and 1300 °C at low pressure. *Earth Planet. Sci. Lett.* **15**, 296–300.
Wilshire, H. G. & Jackson, E. D. 1975 Problems in determining mantle geotherms from pyroxene compositions of ultramafic rocks. *J. Geol.* **83**, 313–329.
Winchell, P. 1969 The compensation law for diffusion in silicates. *High Temp. Sci.* **1**, 200–215.
Wones, D. R. & Gilbert, M. E. 1969 The fayalite–magnetite–quartz assemblage between 600 °C and 800 °C. *Am. J. Sci.* **267**-A, 480–488.
Wood, B. J. & Strens, R. G. J. 1971 The orthopyroxene geobarometer. *Earth Planet. Sci. Lett.* **11**, 1–6.
Wrasidlo, W. 1974 Thermal analysis of polymers. *Adv. Polymer Sci.* **13**, 99 pp. Berlin: Springer-Verlag.
Wright, T. L. & Weiblen, P. W. 1967 Mineral composition and paragenesis in tholeiitic basalt from Makaopulhi lava lake, Hawaii (abstract). *An. Mtg. Geol. Soc. Amer.* 1967, *Program, New Orleans*, 242 pp.

Discussion

D. K. Bailey (*Department of Geology, University of Reading*). Some experiments in recent years show that liquids which have been heated to high temperatures above the liquidus fail to renucleate in the expected times, on cooling below the liquidus. These results suggest that some important structural change may have taken place in the liquids when they are overheated. Is there anything in the calorimetry results to indicate any such change in the liquid structure, and would any such change affect the calculations presented in the paper?

J. V. Smith (*Dept. of the Geophysical Sciences, University of Chicago, Chicago, Illinois*, 60637, *U.S.A.*). You suggested in your important and provocative talk that heat transfer from uprising magma to cooler fragments of wall rock causes precipitation of abundant megacrysts. Several questions are pertinent: (*a*) is there a good correlation between the abundances of megacrysts and of xenoliths, (*b*) have you examined the surfaces of the xenoliths for evidence of reaction

PHILOSOPHICAL TRANSACTIONS OF THE ROYAL SOCIETY A MATHEMATICAL, PHYSICAL & ENGINEERING SCIENCES

with the magma, and (*c*) have you attempted to estimate the heat transfer into the xenoliths using a time estimated for a velocity high enough to lift the xenoliths; and if so, does the heat flow match that for the latent heat of crystallization of the megacrysts?

M. J. O'Hara (*Department of Geology, Edinburgh University*). What assumptions have you made about the effect of pressure and changes in the H_2O and CO_2 content of the silicate liquids upon the partial molar heat contents which you have presented? What uncertainties in the pressures and temperatures of the calculated equilibration with upper mantle minerals result from the cumulative experimental and computational errors?

It is an inherent assumption in the application of the technique which you have described that a lava identified at the surface is a primary magma, last equilibrated with an upper mantle mineralogy at a precisely defined pressure and temperature. One requires, therefore, a unique simultaneous solution to all the equations defining the activities of each oxide component in a lava, but in the way of things, there will be a complex envelope of closure in pressure–temperature space, due to imperfections in the thermodynamic measurements and assumptions. In the present state of the art, how big an envelope (expressed as a percentage of the calculated pressure and temperature) is it reasonable for us to ascribe to uncertainties in the thermodynamic calculations? To phrase the same question in a more positive way, what criteria have you built into your hypothesis by which you can say that a given error of closure exceeds that reasonably ascribable to known errors in the input data? Unless these limits are defined the validity of your initial hypothesis (that you are dealing with a primary magma) is untestable, or at least incapable of undergoing a negative test, a philosophical situation which Popper (1972) and Carmichael *et al.* (1974, p. 628) have previously considered undesirable.

The equations can be solved simultaneously to yield a unique solution, provided that the compositions of the putative minerals with which the liquid had equilibrated are allowed to vary. When you state that the use of this approach invariably yields an assemblage of plausible upper mantle minerals, what criteria do you use to define the limit between plausibility and implausibility of the mineral compositions? For example, olivine compositions in residual upper mantle rocks appear to be Fo_{92-94} (O'Hara *et al.* 1975); a solution which yields Fo_{88} is one which yields an answer 50–100 % too high (in terms of fayalite content of the olivine), and the discrepancy appears much more conspicuous numerically when it is translated into Fe/Mg ratios of the liquids which are, or would be, in equilibrium with these olivines.

The lunar samples are rocks which have been extensively investigated at low and high pressure, and which present fewer problems of reaction with their containers, or of indefinable changes of volatile contents, than any terrestrial samples. How successful is your technique at predicting the observed phase equilibria in such samples?

References

Carmichael, I. S. E., Turner, F. J. & Verhoogen, J. 1974 *Igneous Petrol.* New York: McGraw-Hill.
O'Hara, M. J., Mercy, E. L. P. & Saunders, M. R. 1975 Garnet–peridotite, primary ultrabasic magma and eclogites interpretation of upper mantle processes in kimberlite. *Phys. Chem. of the Earth* **9**, 571–604.
Popper, K. 1973 *Conjectures and refutations*, 4th ed. London: Routledge & Kegan Paul.

I. S. E. Carmichael. The authors are uncertain of the drift of Professor Bailey's statement and question. With the possible exception of 66, our heat content data show that there is no measurable structural change in the liquids over the temperature range investigated; and we depend on suppression of crystal nucleation (?re-nucleate) to obtain a reproducible reference state.

PHILOSOPHICAL TRANSACTIONS OF THE ROYAL SOCIETY A MATHEMATICAL, PHYSICAL & ENGINEERING SCIENCES

As Professor Smith suggests there should be a correlation between the relative masses of entrapped nodules and megacrysts, if the latter do represent the thermal response to the incorporation of the former. A simple energy balance can show the relation between them. Consider that a magma of mass M_L at superliquidus temperature T engulfs nodules of mass M_N at T_N and cooling from T to T_M precipitates crystals of mass M_{Xal} at T_M. Thus we have

$$M_L C_{P,L}(T - T_M) + \Delta H_{fusion} M_{Xal} = M_N C_{P,N}(T_M - T_N),$$

and by using values taken from the main body of the paper, it can be shown that the mass of crystals precipitated is approximately one quarter of the mass of nodules, assuming that $T \approx T_M$. As the crystals and nodules have different densities, it is to be expected that differential settling will occur during the ascent from 50 km or so; hence a correlation in every lava flow may be difficult to establish. There could be occasions where only the megacrysts arrive on the surface, or alternatively if by chance the nodule temperature is close to the magma temperature, there may be no precipitation. Certainly many nodules show signs of reaction with the enclosing magma.

To reply to Professor O'Hara's compound questions and statements would take more space than we are allowed. We have not yet been able to measure sufficient compositions to obtain values for the partial molar enthalpies, and give only the partial molar heat capacities, of the common oxide components in magmas. However, the pressure derivatives of both enthalpy and heat capacity are accounted for in the contribution to the free energy through the $V\mathrm{d}P$ terms, i.e. G is a state function. Furthermore, in the ideal range, our data will be unaffected by H_2O or CO_2. The errors involved in our approach were determined by using experimental phase equilibria; unfortunately there is a dearth of reversed experiments from 1 bar to 20–50 kbar in which the compositions of the liquid and solids are known. The method is based on, can be tested by, and doubtless will be revised by, well designed experiments which seem all too scarce, and often internally inconsistent; thermodynamic quantities are necessarily anchored in experiment.

Lastly, the calculated olivine composition in basanite composition at P and T with 2 % water and with f_{O_2} close to the fayalite–magnetite–quartz buffer, is $Fa_{15} \pm 1$ %; whether or not this is so can easily be resolved by experiment. If the prediction is in error, then it seems likely that for components whose ideal contribution to the activity is dependent on $FeO:Fe_2O_3$, as in Fe_2SiO_4, there will be both a temperature and pressure dependence of that quantity. This seems likely as f_{O_2} (in a closed system) will depend on $\bar{V}_{Fe_2O_3}$ and $\bar{V}_{FeO}$ as a function of pressure, and the former also seems likely to be a function of the concentration of Fe_2O_3. Alternatively the predictions and experiment may agree within reasonable limits, so that the basanite magmas may have had a complex history prior to the engulfment of nodules. If the composition of the olivine in the source region is more magnesian than Fa_{15} and O'Hara's estimates of this have an uncertainty of 50–100 % by his method of calculation, then in the stage between generation and ascent towards the top of the mantle a significant change in composition may have occurred. This will be contributed to by a variety of factors, including mass flux (note the opposite sign of Fe and Mg in table 17), and possibly crystal fractionation; but to ascribe such a change, if substantiated, solely to one mechanism traditionally crystal fractionation, is to imply that a great deal is known about the rates of nucleation, crystal growth, heat loss and the dynamic régime of an ascending magma. The point of this paper is that these are often ignored by petrologists, and to focus on only one mechanism may be conceptually simple, but it is scientifically inchoate.

PHILOSOPHICAL TRANSACTIONS OF THE ROYAL SOCIETY A MATHEMATICAL, PHYSICAL & ENGINEERING SCIENCES